

A STUDY ON THE ION TEMPERATURE
GRADIENT DRIVEN TURBULENCE
TRANSPORT IN TOKAMAK PLASMAS

Von der Universität Bayreuth
zur Erlangung des Grades eines
Doktors der Naturwissenschaften (Dr. rer. nat.)
genehmigte Abhandlung

von

Pierluigi Migliano

aus Mailand

April 2015

Abstract

The continuous growth of the energy worldwide consumption is one of the most important challenges to our civilization. New kinds of energy resources are without doubt needed. Nuclear fusion promises to supply large amounts of energy, with minimal environmental impact. This has motivated at least sixty years of research in which substantial progress has been achieved, but without breakthrough result.

Nuclear fusion can occur at temperatures of the order of 150 million degrees Celsius (thermonuclear fusion). At these temperatures atoms are completely ionized, the fuel is then in the state of matter called a plasma, a gas of ions and electrons.

The most promising approach towards the goal of using thermonuclear fusion for large scale energy production is to confine the plasma using magnetic fields. The tokamak is the device that produces the best results concerning plasma magnetic confinement to date.

One of the main tasks of fusion research is the understanding of plasma confinement. The energy confinement must be sufficiently good such that a large amount of reactions take place, this in order to make the process economically convenient. This translates in the necessity of minimizing the heat fluxes out of the plasma.

The heat fluxes observed experimentally in tokamak plasmas are much higher than those that can be ascribed to collisions. This so called anomalous transport is largely controlled by the destabilization of low frequency drift wave fluctuations, resulting in turbulence in the plasma on small scales compared to the tokamak size.

The drift waves are collective modes of plasma oscillations that propagate through the plasma, arising as a result of the independent dynamics of ions and electrons in the presence of gradients of quantities describing the plasma (temperature, density, etc.).

In this thesis, physical phenomena connected with the global description of turbulence in tokamak plasma have been analysed. Quasi-local simulations of electrostatic Ion Temperature Gradient (ITG) modes instabilities, i.e. electrostatic microinstabilities driven in the plasma by the presence of an ion temperature gradient, have been performed. Quasi-local refers to the case in which background quantities are assumed constant throughout the simulation domain, but inhomogeneities in the profiles of the turbulent quantities are taken into account. The work consists of two main parts.

In the first part of the thesis, the electrostatic linear ITG modes growth rate (γ) spectrum is numerically calculated. It is observed that γ as a function of the poloidal wave vector (k_θ) is given by a double-humped curve. In particular, it is observed that modes with high value of k_θ have a maximum

amplitude at a position that is shifted away from the low field side. The physical mechanism responsible for this behaviour is clarified through the use of a fluid model. It is shown that the shift of the mode away from the low field side reduces the effective drift frequency which allows for the instability to develop. Numerical tests using the gyro-kinetic model confirm this physical mechanism.

The second part of the thesis is dedicated to the study of Turbulence Spreading (TS), i.e. the turbulent transport of turbulence.

Gyro-kinetic simulations predict that, when increasing the size of the reactor, the heat conduction coefficient (χ) undergoes a scaling transition from Bohm ($\chi \propto \chi_B$, with χ_B the Bohm diffusion coefficient) to gyro-Bohm ($\chi \propto \rho_* \chi_B$, with ρ_* the normalized Larmor radius $\rho_* = \rho/R$ where ρ is the ion Larmor radius and R is the tokamak size). This transition is ascribed to non-local phenomena. Non-local refers to situations in which the fluxes do not depend just on the local gradients.

In the literature, TS has been proposed as the mechanism responsible for this transition. Up to now, TS has been analytically described applying an ad hoc conservation equation for the evolution of the local intensity of the turbulence, defined as the squared modulus of the electrostatic potential. The conservation equation is given in the form of a Fisher-Kolmogorov (FK) equation with inhomogeneous diffusion coefficient. Although physically motivated, the FK equation proposed to describe TS is not derived from first principles. No explicit expression for the transport flux of turbulence exists, and this flux can therefore not be directly calculated in numerical simulations of plasma turbulence.

In this thesis, a conservation equation is derived for the radially dependent entropy in toroidal geometry using the local approximation of the gyro-kinetic equation. This naturally leads to an operative definition for the turbulence intensity. The treatment provides an operative tool for both analytic as well as numeric studies of the radial propagation of turbulence in tokamak plasmas. In fact, explicit expressions for the turbulence intensity and the turbulence intensity flux, that allow direct numerical evaluation, are derived.

A carefully designed numerical experiment is used to determine the turbulence diffusion coefficient for the first time. This is found to be smaller than the heat conduction coefficient, and a spreading length is found to be of the order of the turbulence correlation length. The results show that turbulence spreading can play a role in the non-local flux gradient relation, or in the scaling of transport coefficients with the normalized Larmor radius, only over length scale of the order of the turbulence correlation length.

Finally, the turbulence convection through the drift connected with the magnetic field inhomogeneities is investigated. The convective flux integrates to zero under the flux surface average unless there is an up-down (in the poloidal plane) asymmetry in the turbulence intensity. The latter asym-

metry can be generated through a radial inhomogeneity or plasma rotation. It is shown that the turbulence convection can lead to a spreading of the order of the correlation length under some circumstances.

Contents

1	Introduction	2
1.1	Motivation	2
1.2	The Tokamak	5
1.2.1	Confinement mechanism	5
1.2.2	Ignition and the triple product criterion	7
1.3	Single particle motion	8
1.3.1	Gyro-motion	8
1.3.2	Particle drifts	10
1.4	Equilibrium magnetic configurations	13
1.4.1	Ideal MHD equilibrium	13
1.4.2	Safety factor, magnetic shear and beta	16
1.5	Drift waves	17
1.5.1	The Vlasov-Maxwell equations	18
1.5.2	Landau damping	20
1.5.3	Drift waves instability	24
1.6	The gyro-kinetic model	30
1.6.1	The gyro-kinetic ordering	30
1.6.2	The local limit approximation	32
1.6.3	The gyro-kinetic equations	33
1.6.4	The GKW code	36
2	ITG instability at sub-Larmor radius scales with non-zero ballooning angle	44
2.1	Introduction	44
2.2	High k_θ ITG	45
2.3	Physical mechanism	48
2.4	Comparison with previous work	54
2.5	Conclusion	54
3	On the radial propagation of turbulence in gyro-kinetic toroidal systems	56
3.1	Introduction	56
3.2	Turbulence intensity balance in gyro-kinetic theory	58

3.3	Conclusion	65
4	Turbulence spreading in gyro-kinetic theory	66
4.1	Introduction	66
4.2	Analytical analysis of turbulence spreading	69
4.3	Turbulence spreading measurement	71
4.4	Turbulence convection measurement	78
	4.4.1 Radially inhomogeneous heat source	78
	4.4.2 Background toroidal rotation	80
4.5	Conclusion	81
5	Conclusion and outlook	84
	Bibliography	87

Chapter 1

Introduction

1.1 Motivation

The continuous growth of the energy worldwide consumption is one of the most important challenges to our civilization. New kinds of energy resources are without doubt needed.

Nuclear fusion promises to supply large amounts of energy, with minimal environmental impact. This has motivated at least sixty years of research in which substantial progress has been achieved, but without breakthrough result.

Nuclear fusion occurs only under extreme conditions. It is necessary for the nuclei involved in the reaction to have energies of the order of at least tens of keV to overcome their Coulomb repulsion. The nuclei can reach these energies at high temperatures (of the order of 150 million degrees Celsius), speaking in this case of thermonuclear fusion. At these temperatures atoms are completely ionized, the fuel is then in the state of matter called a plasma, a gas of ions and electrons at ultra high temperature.

The most advantageous fusion reactions occur when using as fuel a plasma of deuterium and tritium. Obtaining the energy confinement necessary to ensure that such reactions occur, presents many technical as well as scientific difficulties. The most promising approach towards this goal is to confine the plasma using magnetic fields. The tokamak is the device that produces the best results concerning plasma magnetic confinement to date, showing the possibility of obtaining controlled thermonuclear fusion [1].

One of the main tasks of fusion research is the understanding of plasma confinement. The energy confinement must be sufficiently good such that a large amount of reactions take place and $Q = P_{th}/P_{in} > 1$, where P_{th} is the thermonuclear power, obtained as output from the reactor, released by the fusion reactions, and P_{in} the input power required to keep it running.

The next step in the development of tokamak fusion reactors is the construction of ITER (International Thermonuclear Experimental Reactor), an

international project aimed at demonstrating the possibility of a fusion reactor on the scale needed for a commercial powerplant; the goal is to produce energy from nuclear fusion with a Q factor of ten. If the goal is reached the results of ITER will be used for the construction of the first fusion power plant (DEMO).

Among the physical and technological problems still open, understanding and controlling heat transport is of primary importance for the optimization of the ITER operational scenarios, since the achievement of the high temperatures required in the center of the plasma for a significant production of fusion power depends on the possibility of obtaining low values of heat diffusivity. Given the extreme complexity of plasma transport processes, despite the significant progress made in half a century of study, a comprehensive theoretical formulation and numerical models suitable for the complete simulation of a tokamak discharge are not yet available. The research on thermal transport is therefore still the subject of intense work.

The heat fluxes observed experimentally in tokamak plasmas are much higher than those that can be ascribed to collisions. The past 30 years of research in plasma confinement has shown that anomalous transport across the magnetic field is largely controlled by the destabilization of low frequency drift wave fluctuations [2]. These result in turbulence in the plasma on small scales compared to the tokamak size. The drift waves are collective modes of plasma oscillations that propagate through the plasma, arising as a result of the independent dynamics of ions and electrons. These interact through the electrostatic force to ensure the quasi-neutrality of the plasma. While ions and electrons are free to move independently in the plasma, a charge separation on a large scale is prevented by the generation of strong electric fields acting against it. The different motion of ions and electrons in the presence of gradients (density, temperature, etc.) gives origin to the drift waves. The destabilization of drift waves causes a turbulent flux of energy from the plasma center to the edge.

The drift waves destabilization problem is therefore a fundamental subject concerning thermonuclear fusion research. The development of its analytical and numerical description makes it nowadays possible to treat this problem in many different scenarios both linearly and non-linearly. In the linear regime the various modes do not interact, their evolution is considered in its interaction with the background system, the energy exchange between the modes and the background makes the modes frequency to develop an imaginary part (growth rate γ) and, according to its sign, the mode amplitude can grow exponentially (the mode continuously acquires energy from the background, this is known as linearly unstable mode) or be damped (the mode energy is dissipated, this is known as linearly stable mode). Focusing on the instability due to the presence of an ion temperature gradient (ITG), it is found that γ depends on this gradient, and there is a critical value (ITG threshold) of the normalized inverse ion temperature gradient

length $R/L_T = R\nabla T/T$ (with R the tokamak size), above which ITG modes become linearly unstable. In the non-linear regime, the dynamics is much more complex, many modes evolve together interacting with each other and with the background system, the energy exchanges make the system to reach a quasi-steady state, then the ITG threshold is determined by the value of R/L_T when the ion heat flux is close to zero.

Many numerical models have been developed up to date, which can simulate drift waves turbulence in a small region of the plasma spatial domain, these are called local simulations. Their reliability has been widely tested, however their spectrum of applicability is limited. At first because of the restricted size of the simulation domain. Secondly, in this kind of approach background quantities are assumed constant and turbulent quantities turn out to be homogeneous throughout the simulation domain, not allowing the study of turbulent transport processes due to profiles effects. During the last two decades, experimental observations accompanied by theoretical studies [3] have pointed out that non-local phenomena (phenomena which do not depend just on the local plasma parameters) could play an important role in transport processes. It is therefore necessary to be able to simulate larger plasma domains, taking into account background and turbulence profiles, these are called global simulations.

The work presented in this thesis is a contribution to the development of this research field. It is placed in the gap between local and global simulations. In particular, the study focuses on quasi-local simulations of electrostatic ITG modes instabilities, i.e. electrostatic microinstabilities driven in the plasma by the presence of an ion temperature gradient. Quasi-local refers to the case in which background quantities are assumed constant throughout the simulation domain, but inhomogeneities in the profiles of the turbulent quantities are taken into account.

Three years ago I joined the plasma research group at Bayreuth University as a PhD student under the supervision of Prof. A.G. Peeters. The main task of the group is the understanding of plasma phenomena in connection to the development of the code GKW [4, 5, 6], the purpose of which is to model drift waves turbulence in a magnetically confined tokamak plasma.

My first assignment was to perform a series of benchmarks comparing two different code implementations (local and quasi-local) when calculating the electrostatic linear ITG modes growth rate. The numerical calculations gave some peculiar results which turn out to be similar to the ones obtained by many other numerical models reported in the literature. In the first part of this thesis (chapter 2) these benchmarks are presented and a physical mechanism, based on a fluid model of the plasma, is proposed in order to give a qualitative explanation of the numerical results obtained.

The second part of this thesis (chapters 3 and 4) deals with the non-linear behaviour of the ITG modes. In this case the guiding motivation has been the study of the phenomenon called turbulence spreading, i.e. the

transport of turbulence intensity. A fundamental issue, when dealing with the description of anomalous transport in magnetically confined plasmas is the scaling of its properties with respect to the size of the reactor. In this regard it is important to understand to what extent the transport is determined by non-local effects. Turbulence spreading has been reported in the literature as one of the physical mechanism responsible for the non-local behaviour of the turbulence. In this thesis a proper consistent definition of the turbulence intensity is given in connection to the entropy of the system, then an analytical description of its evolution is presented and finally numerical quasi-local simulations are performed, for the case of electrostatic non-linear ITG driven turbulence, in order to quantitatively measure the impact of turbulence spreading on the non-local behaviour of turbulent transport processes.

Part of the work reported in this thesis has been published in peer reviewed journals as

- a) P. Migliano, Y. Camenen, F.J. Casson, W.A. Hornsby and A.G. Peeters. *ITG instability at sub-Larmor radius scales with non-zero ballooning angle*. Phys. Plasmas **20**, 022101 (2013)
- b) P. Migliano, R. Buchholz, S.R. Grosshauser, W.A. Hornsby and A.G. Peeters. *The radial propagation of turbulence in gyro-kinetic toroidal systems*. PPCF **57**, 054008 (2015)

Publication a) is the basis of chapter 2, publication b) is the basis of chapter 3. Chapter 4 is based on a paper in preparation for submission to Phys. Plasmas.

The rest of this chapter introduces the fundamental concepts necessary to understand this thesis.

1.2 The Tokamak

The tokamak is today's most advanced and best investigated fusion device. It is a torus-shaped vacuum chamber surrounded by magnetic coils, which create a magnetic field that confines the plasma (Fig. 1.1).

1.2.1 Confinement mechanism

The electric current passing through the toroidal field coils generates the toroidal magnetic field, this field alone does not allow to confine the plasma. In fact, solution of Ampere's law for a toroidal solenoid shows that the toroidal magnetic field has a radial variation of the form $B \approx 1/R$ (where R is the radial distance from the torus vertical axis of symmetry) inside the solenoid. The resulting radial component of the magnetic field gradient

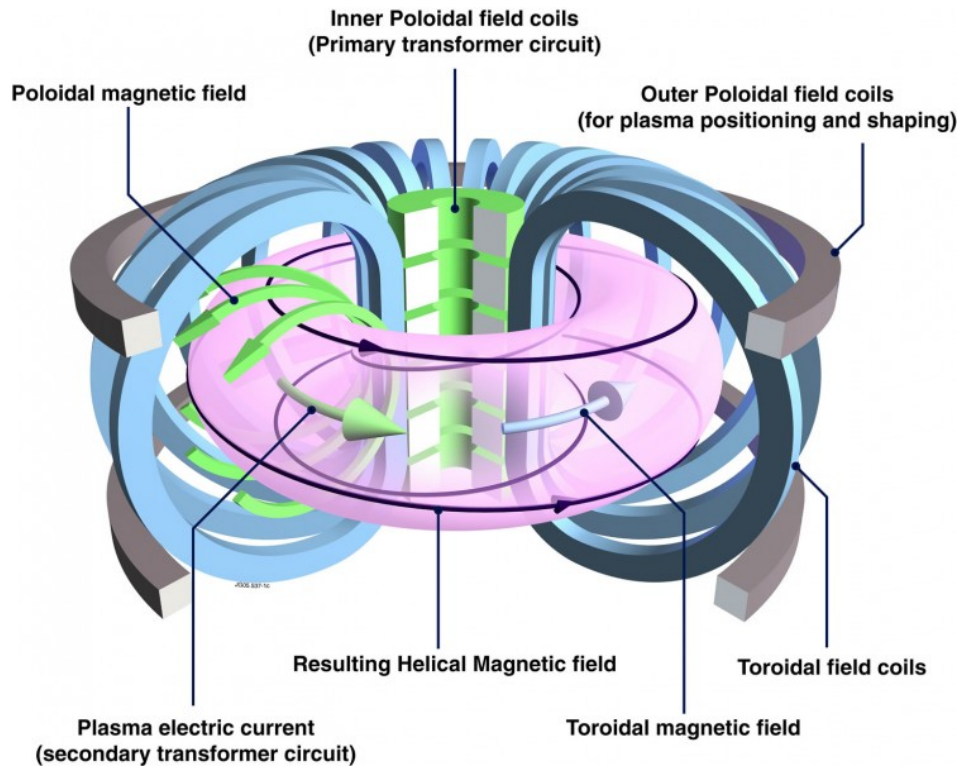


Figure 1.1: Schematic representation of a tokamak illustrating the arrangement of magnetic field coils and the resulting helical magnetic field that confines the plasma. Image: www.euro-fusion.org.

generates a particles drift in the vertical direction (positive or negative depending on the particles charge). The consequent up-down vertical charge separation gives rise to an electric field in the vertical direction. The presence of the toroidal magnetic field causes the particles to drift in the outwards radial direction, making the plasma hit the surrounding walls (particles drifts will be discussed in more details later in section 1.3).

The plasma confinement is then achieved introducing a poloidal magnetic field. The poloidal magnetic field is generated by driving a toroidal electric current in the plasma. The plasma current is produced by the inner poloidal field coils, they are used to generate a vertical magnetic field which can be modulated in order to create a variation of the magnetic flux through a circular surface perpendicular to the torus vertical axis. This variation induces a current flowing along the circular surface boundary line. The current radial profile peaks roughly in the middle of the torus poloidal cross section. This is the main plasma electric current inducing the poloidal magnetic field.

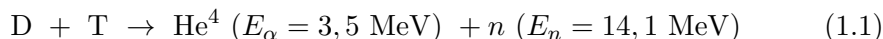
The superposition of the poloidal and toroidal magnetic fields results in

helical magnetic field lines that wind around the torus. These circulate the charged particles that have drifted towards the outside of the ring back into the center, preventing the plasma from escaping.

1.2.2 Ignition and the triple product criterion

The ultimate goal of tokamak research is to obtain a plasma of deuterium and tritium, adequately confined such that the high temperature needed for fusion is sustained, against the energy losses, only through the heating due to the fusion products. This event is called ignition.

The deuterium-tritium (D-T) nuclear reaction gives as products an alpha particle (He^4) and a neutron (n). The mass defect involved in the process $\delta m = 17.6 \text{ MeV}/c^2$, with c the speed of light, results in an energy gain of the products in the form of kinetic energy. Since an alpha particle is approximately four times heavier than a neutron,



where the kinetic energy of the products has been indicated. The thermonuclear power P_{th} produced by the reactions (1.1) in a D-T plasma of total ion density $n = n_D + n_T$, confined in a volume V , can be written as [7]

$$P_{th} = \int_V n_D n_T \sigma E d^3x = \int_V \frac{1}{4} n^2 \sigma E d^3x \quad (1.2)$$

where $n_D = n_T$ has been assumed, $E = E_\alpha + E_n$ is the energy released per reaction and σ is the reaction rate, which in the temperature interval between 10 and 20 keV/ k_B , with k_B the Boltzmann's constant, can be approximated by the formula [7]

$$\sigma \approx 1.1 \cdot 10^{-24} [k_B T \text{ in keV}]^2 \text{ m}^3 \text{ s}^{-1} \quad (1.3)$$

where $[k_B T \text{ in keV}]$ indicates that the energy $k_B T$ is expressed in the unit keV.

The neutrons leave the plasma and are absorbed by the blanket surrounding the toroidal chamber, transferring their energy in the form of heat. The alpha particles, being charged, are confined by the magnetic field and contribute to the heating of the plasma, transferring their energy to the plasma through collisions. The power delivered to the plasma from the alpha particles is

$$P_\alpha = \int_V \frac{1}{4} n^2 \sigma E_\alpha d^3x . \quad (1.4)$$

In steady state, the continuous loss of power P_L from the plasma must be balanced by the sum of the fusion power (P_α) due to the alpha particles and the input power (P_{in}) provided from outside the plasma, i.e.

$$P_L = P_{in} + P_\alpha . \quad (1.5)$$

The mean energy per particle at a temperature T is $\frac{3}{2}k_B T$. Assuming for simplicity that ions and electrons are at the same temperature, the energy per unit volume is $3nk_B T$, the total plasma energy is then given by

$$W = \int_V 3nk_B T d^3x \approx 3nk_B TV \quad (1.6)$$

where in the last step n and T have been taken constant for simplicity. The loss of power P_L defines a parameter τ_E called energy confinement time in the form

$$P_L = \frac{W}{\tau_E} = \frac{3nk_B TV}{\tau_E}, \quad (1.7)$$

τ_E is not the life time of the plasma, it strictly characterizes the ability of the plasma to sustain itself, it measures the rate at which the plasma loses energy to its environment.

Ignition is obtained when $P_{in} \leq 0$. Eqs. (1.3)-(1.7) with n and T constants give

$$nk_B T \tau_E \geq 3 \cdot 10^{21} \text{ m}^{-3} \text{ keV s} \quad (1.8)$$

this is the triple product criterion setting a condition on density, temperature and confinement time.

1.3 Single particle motion

A tokamak plasma is an ionized gas in interaction with curvilinear non homogeneous electromagnetic fields. In this section the single particle motion is considered in the case of strong static magnetic field (a detailed treatment can be found in [8]).

1.3.1 Gyro-motion

Consider a static uniform magnetic field, the equation of motion for a particle of mass m and charge q is

$$m \frac{d\mathbf{v}}{dt} = q\mathbf{v} \times \mathbf{B}. \quad (1.9)$$

The solution of this equation shows that the motion constitutes a helix along the magnetic field line, i.e. the particle travels at constant speed along the magnetic field line, and undergoes a uniform circular motion in the plane perpendicular to the magnetic field line with gyration frequency ω_c and radius ρ given by

$$\omega_c = \frac{|q|B}{m} \quad \rho = \frac{v_{\perp}}{\omega_c} \quad (1.10)$$

where v_{\perp} is the initial perpendicular (to the magnetic field) velocity. The frequency ω_c is called the cyclotron frequency or Larmor frequency and the

length ρ is called the Larmor radius. The Larmor motion of the electron is a right-handed rotation, while for the ion is a left-handed rotation (with respect to the magnetic field direction). Given v_{\perp} and B , the size of the orbit depends on the particle mass, heavier particles have larger orbits.

The Larmor frequency and the Larmor radius provide fundamental spatio-temporal scales in magnetized plasma. In a tokamak plasma, the equilibrium fields vary on length scales large compared to the Larmor radius, and vary slowly in time compared to the Larmor frequency. This scale separation allows single particle motion to be accurately decomposed into the fast cyclotron rotation around the magnetic field line, and a slower motion of the center of its gyro-orbit along the magnetic field line. The center of the gyro-orbit is called guiding center (\mathbf{x}_{gc}), it is related to the particle's position (\mathbf{x}) by the Larmor radius vector ($\boldsymbol{\rho}$), a vector of magnitude ρ pointed from the guiding center to the particle's position at any given time instant. The relation is given by

$$\mathbf{x} = \mathbf{x}_{gc} + \boldsymbol{\rho} \quad \text{with} \quad \boldsymbol{\rho} = \pm \frac{\mathbf{b} \times \mathbf{v}}{\omega_c} . \quad (1.11)$$

where the \pm refers to the sign of q and \mathbf{b} is a unit vector in the \mathbf{B} direction. The motion of the guiding center is determined by time-averaging the equations of motion over the gyro-period, this procedure is called gyro-average.

Gyro-averaged fields

Consider the magnetic configuration described above, with the magnetic field in the z -direction of a cartesian coordinate system. The gyro-motion will take place in the xy -plane, and in particular for the y -direction it is $y(t) = y_{gc} + \rho \cos(\zeta - \omega_c t)$ where ζ indicates the initial condition. Furthermore, assume that the particle experiences an electric field $E(y, t)$ which can be represented in a wave-like form as

$$E(y, t) = E_k \cos(ky - \omega t) \quad (1.12)$$

where E_k is the amplitude of the wave. The gyro-averaged field $\langle E \rangle$ acting on the particle, i.e. the average of E over a gyro-period $T = 2\pi/\omega_c$, is then given by

$$\langle E \rangle = \frac{1}{T} \int_0^T E_k \cos[k(y_{gc} + \rho \cos(\zeta - \omega_c t)) - \omega t] dt . \quad (1.13)$$

In order to evaluate the integral we use the identity

$$\exp(i\alpha \sin \theta) = \sum_{n=-\infty}^{+\infty} J_n(\alpha) \exp(in\theta) \quad (1.14)$$

where J_n is the n -th order Bessel function of the first kind. Using the real part of this identity, and assuming $\omega \ll \omega_c$ (which means that the term ωt in Eq. (1.13) remains approximately constant during a gyro-period, and therefore it does not need to be integrated), Eq. (1.13) becomes

$$\langle E \rangle = J_0(k\rho)E_k \cos(ky_{gc} - \omega t) . \quad (1.15)$$

Thus, for a wave-like field, the gyro-averaged can be expressed evaluating the field at the guiding center position with its amplitude reduced by a factor equal to the zeroth order Bessel function of the first kind. In the case where the field spatial variation is much larger than the Larmor radius ($k\rho \ll 1$), then $J_0(k\rho) \approx 1$ and the gyro-averaged field is just the field evaluated at the guiding center position. In the case of fields which can not be represented in a wave-like form, the gyro-average is an integral operation over the gyro-phase angle ($\omega_c t$), which has to be explicitly performed.

1.3.2 Particle drifts

In a tokamak, in order to describe the particle motion, one needs to take into account the electric field, as well as the inhomogeneity and curvature of the magnetic field. The particle's non-relativistic equation of motion is given by

$$m \frac{d\mathbf{v}}{dt} = q(\mathbf{E} + \mathbf{v} \times \mathbf{B}) . \quad (1.16)$$

The gyro-averaged solution of this equation describes the guiding center motion. The presence of the electric field and the magnetic field inhomogeneity and curvature, generate accelerations in both parallel and perpendicular (to the magnetic field) directions, which modify the simple gyro-motion described above. In particular, the perpendicular acceleration modifies the particle gyro-orbit such that the guiding center is forced to move across the magnetic field lines. This particular motion of the guiding center is called drift motion. In the following, the drifts that will be used in this thesis are presented.

The $\mathbf{E} \times \mathbf{B}$ drift

Consider a plasma configuration with uniform magnetic and electric field. The gyro-averaged solution of Eq. (1.16) gives the guiding center velocity as

$$\mathbf{v}_{gc} = v_{\parallel} \mathbf{b} + \mathbf{v}_E \quad \text{with} \quad v_{\parallel} = v_{\parallel i} + \frac{qE_{\parallel}}{m} t \quad (1.17)$$

where v_{\parallel} describes the motion of the guiding center along the field line, and \mathbf{v}_E represents the guiding center motion across the field line given by

$$\mathbf{v}_E = \frac{\mathbf{E} \times \mathbf{B}}{B^2} \quad (1.18)$$

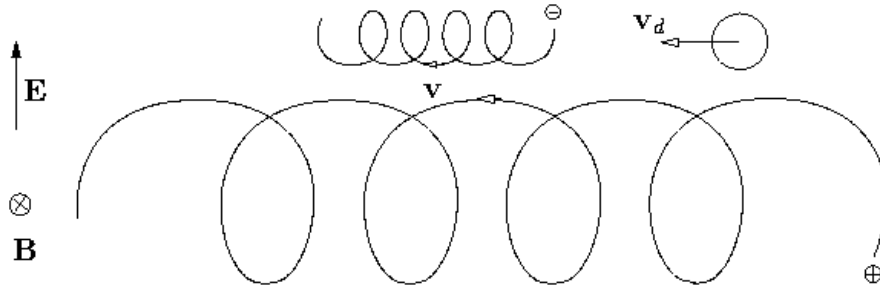


Figure 1.2: $\mathbf{E} \times \mathbf{B}$ drift motion. The ion (electron) half orbit on the upper (lower) side is larger than that one on the lower (upper) one, because the ion (electron) has been accelerated by the force due to the electric field. This causes the guiding center drift. The magnetic field faces into the page. Image: www.psfc.mit.edu.

it is therefore called the $\mathbf{E} \times \mathbf{B}$ drift velocity. The presence of the electric field causes the guiding center to accelerate along the field lines and to drift across the field lines. The $\mathbf{E} \times \mathbf{B}$ drift has the same magnitude and direction for both ions and electrons, so it does not give rise to net currents, it generates a motion of plasma particles in the $\mathbf{E} \times \mathbf{B}$ direction (Fig. 1.2 shows the effect of a perpendicular to \mathbf{B} electric field).

The grad-B and curvature drifts

Consider a plasma configuration with no electric field and an inhomogeneous curved magnetic field. As already mentioned, the Larmor radius ρ is much smaller than the typical scale-length variation of the magnetic field. If $1/k$ is a characteristic magnetic field gradient scale-length (for example if $B \propto \cos(kx)$), then $k\rho \ll 1$, and the quantity $k\rho$ can be treated as an expansion parameter in studying the equation of motion. Therefore an asymptotic expansion procedure can be used in order to express the particle velocity in the form

$$\mathbf{v} = \mathbf{v}_0 + \mathbf{v}_1 + \mathbf{v}_2 + \dots \quad (1.19)$$

where each successive term in the series is assumed to be one order smaller in $k\rho$ than the previous one. In this section only the solutions to the zeroth and first order will be discussed.

The zeroth order gyro-averaged solution is simply the particle's parallel (to the magnetic field) velocity ($v_{\parallel} \mathbf{b}$). In the case the magnetic field gradient has a component parallel to \mathbf{B} , this component generates an acceleration in the \mathbf{B} direction.

The components of the magnetic field gradient perpendicular to \mathbf{B} and the magnetic field curvature can be treated as first order effects. They give rise to accelerations in the direction perpendicular to \mathbf{B} making the

guiding center to drift across the magnetic field lines, modifying the gyro-orbit similarly to the case of the $\mathbf{E} \times \mathbf{B}$ drift. The first order gyro-averaged solution of the equation of motion (the time average of \mathbf{v}_1 over the gyro-period), which we denote with \mathbf{v}_D , gives the guiding center drift motion, and it can be expressed as

$$\mathbf{v}_D = \mathbf{v}_{grad} + \mathbf{v}_{curv} . \quad (1.20)$$

The first term \mathbf{v}_{grad} is due to the magnetic field gradient, it is called the grad-B drift, it is given by

$$\mathbf{v}_{grad} = \pm \frac{v_{\perp}^2}{2\omega_c} \frac{\mathbf{B} \times \nabla B}{B^2} . \quad (1.21)$$

The second term \mathbf{v}_{curv} is caused by the magnetic field curvature, it is called the curvature drift¹, it is given by

$$\mathbf{v}_{curv} = \pm \frac{v_{\parallel}^2}{\omega_c} \frac{\mathbf{B} \times (\mathbf{b} \cdot \nabla) \mathbf{b}}{B^2} . \quad (1.22)$$

The grad-B and curvature drifts depend on the sign of the particle charge, so they give rise to net currents, which in turn lead to charge separation and therefore to the generation of electric fields. The total guiding center velocity is then given by

$$\frac{d\mathbf{x}_{gc}}{dt} = \mathbf{v}_{gc} = v_{\parallel} \mathbf{b} + \mathbf{v}_E + \mathbf{v}_{grad} + \mathbf{v}_{curv} . \quad (1.23)$$

The \mathbf{v}_E can be treated, provided that the electric field is small enough, as a first order contribution to the drifts. It is interesting to notice that these drifts do not interfere with each other, they simply add up and each one can be treated separately.

The polarization drift

The polarization drift velocity \mathbf{v}_p is due to a time varying electric field. In the case of a time dependent electric field, the second order² gyro-averaged solution of the equation of motion gives

$$\mathbf{v}_p = \frac{m}{qB^2} \frac{d\mathbf{E}_{\perp}}{dt} . \quad (1.24)$$

The direction and the magnitude of \mathbf{v}_p are different for ions and electrons, therefore a net current is driven in the plasma. This current is analogous

¹In the low beta (see section 1.4) limit the approximation $\mathbf{b} \times (\mathbf{b} \cdot \nabla) \mathbf{b} \approx \mathbf{b} \times \nabla B/B$ is valid and will be used later in this thesis.

²Note that Eq. (1.24) states $|\mathbf{v}_p| \approx (\omega/\omega_c)(E/B)$, where $\omega/\omega_c \ll 1$ and the electric field E is assumed to be a perturbation of the first order. Therefore, the polarization drift \mathbf{v}_p is a second order effect.

to the polarization current in dielectric materials. The polarization drift effect, because of the mass dependence, is dominated by ions compared to electrons. Indeed, it is usually necessary to include this second order effect in the description of the ions dynamics, while it can be neglected in the electrons case.

1.4 Equilibrium magnetic configurations

In the previous section we discussed the situation in which the field is unaffected by the presence of the plasma particles. However, in a real plasma, the large number of particles can make the plasma currents to become large enough to modify the externally created magnetic field. The plasma equilibrium must be then determined self consistently.

1.4.1 Ideal MHD equilibrium

The problem of finding equilibrium magnetic configurations for a tokamak plasma can be tackled in the framework of the magnetohydrodynamic model (MHD: a single fluid model of a fully ionized plasma, in which the plasma is treated as an ideal hydrodynamic fluid acted upon by the Lorentz force [8]). The plasma equilibrium, in the absence of plasma flow (the plasma fluid velocity is zero) and isotropic pressure tensor (the pressure p is a scalar) obeying an equation of state (such as the adiabatic gas law), is governed by the balance between the Lorentz force ($\mathbf{J} \times \mathbf{B}$) and the thermal pressure force (∇p). Therefore the MHD force balance equation is

$$\mathbf{J} \times \mathbf{B} = \nabla p . \quad (1.25)$$

In the tokamak the magnetic field is axisymmetric, i.e. its components do not vary along the toroidal direction. Define a cylindrical coordinate system (z, R, ϕ) , where the z -axis is the torus vertical axis of symmetry, R is the distance from the z -axis (radial direction) and ϕ is the counterclockwise revolution angle around the z -axis (toroidal direction). Then a general axisymmetric magnetic field \mathbf{B} , which is not necessarily an equilibrium magnetic field, can be expressed in term of its vector potential \mathbf{A} as $\mathbf{B} = \nabla \times \mathbf{A}$ and written in the form [9]

$$\mathbf{B} = \nabla \Psi \times \nabla \phi + g \nabla \phi \quad (1.26)$$

with the definitions $\Psi(z, R) = RA_\phi(z, R)$ and $g(z, R) = RB_\phi(z, R)$, where A_ϕ and B_ϕ are the toroidal components of the vector potential and the magnetic field respectively.

The axial symmetry of a vector field allows to introduce a surface of revolution that is generated by rotating the projection of a vector field line on the (R, z) plane (poloidal plane) around the axis of symmetry, z -axis.

The property which characterizes this revolution surface is that if a field line intersects it at one point, then the whole field line will lie on the surface. In the case of axisymmetric magnetic field, these revolution surfaces are called magnetic surfaces.

A direct consequence of Eq. (1.26) is that $\mathbf{B} \cdot \nabla \Psi = 0$, indicating that Ψ is constant along a magnetic field line. Because Ψ is constant along a magnetic field line and Ψ is independent of ϕ , it follows that Ψ is constant on a flux surface. The physical relevance of this property is understood looking at the relation between Ψ and the poloidal magnetic flux Ψ_p . Consider an annular surface enclosed between two radii R_1 and R_2 contained in the plasma, lying on a plane perpendicular to the z -axis which includes the origin $z = 0$, then the poloidal magnetic flux through this surface is given by

$$\Psi_p = 2\pi [\Psi(R_2) - \Psi(R_1)] \quad (1.27)$$

that is, the difference of Ψ between two locations determines the poloidal magnetic flux. For this reason the magnetic surfaces are called flux surfaces in the tokamak literature, and they can be labeled by the value Ψ takes on each particular surface.

It is clear from Eq. (1.25) that $\mathbf{B} \cdot \nabla p = 0$, which is equivalent to $p = p(\Psi)$, and that $\mathbf{J} \cdot \nabla p = 0$, indicating that the current density vector must be tangent to the flux surfaces. Therefore the current flows on the flux surface even though the single particle trajectory does not during a revolution around the torus, because of the drift motion of its guiding center. Furthermore Eq. (1.25) imposes additional constraints on the expression given in Eq. (1.26) for a general axisymmetric magnetic field. In particular, considering the toroidal component of Eq. (1.25) together with Ampere's law, one finds $\mathbf{B} \cdot \nabla g = 0$, which implies that g is constant along a magnetic field line, i.e. $g = g(\Psi)$ (the function g is usually called the "poloidal current function" because using Ampere's law it can be directly related to the poloidal current density³). The radial component of Eq. (1.25) is known as the Grad-Shafranov equation⁴, it is a partial differential equation for Ψ which has to

³The R and z components of Ampere's law $\nabla \times \mathbf{B} = \mu_0 \mathbf{J}$ with \mathbf{B} given by Eq. (1.26) can be written as

$$\mu_0 J_R = -\frac{1}{R} \frac{\partial g}{\partial z} \quad \mu_0 J_z = \frac{1}{R} \frac{\partial g}{\partial R}$$

with J_R and J_z respectively the R and z component (the poloidal components) of the current density vector. The toroidal component of Eq. (1.25) is $J_z B_R - J_R B_z = 0$, therefore $\mathbf{B} \cdot \nabla g = 0$.

⁴The radial component of Eq. (1.25), using the toroidal component of Ampere's law $\nabla \times \mathbf{B} = \mu_0 \mathbf{J}$, with \mathbf{B} given by Eq. (1.26), and the fact that p and g are functions of Ψ only, can be written as

$$\frac{\partial^2 \Psi}{\partial z^2} + R \frac{\partial}{\partial R} \left(\frac{1}{R} \frac{\partial \Psi}{\partial R} \right) = -\mu_0 R^2 \frac{dp}{d\Psi} - g \frac{dg}{d\Psi}$$

this is the Grad-Shafranov equation.

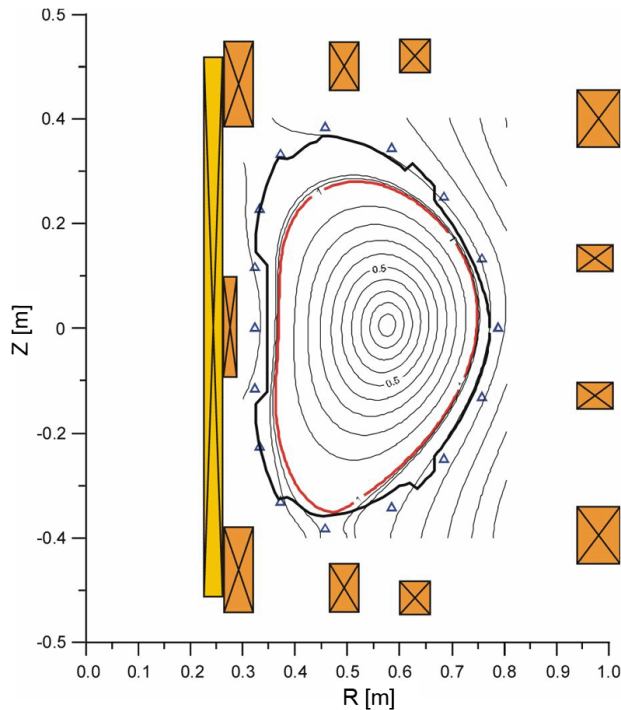


Figure 1.3: Example of EFIT [10] reconstruction of flux surfaces (tokamak COMPASS-D, UKAEA, Culham, shot 30866). Image: www.ipp.cas.cz.

be solved given the pressure $p(\Psi)$ and the poloidal current function $g(\Psi)$ for specified boundary conditions. A part from a limited amount of simplified cases which can be analytically solved, the Grad-Shafranov equation is in general numerically solved employing codes specifically designed for the reconstruction of magnetic equilibrium configurations, starting from experimental data sets. An equilibrium axisymmetric magnetic field can thus be expressed in the general form given in Eq. (1.26) with the additional requirements for Ψ to satisfy the Grad-Shafranov equation, and for g to be a function of Ψ only (a detailed treatment can be found in [7]).

Equilibrium magnetic configurations for a tokamak plasma consist of nested closed magnetic surfaces labeled by the value Ψ takes on each particular surface (Fig. 1.3 shows an example of the reconstruction of flux surfaces performed with the equilibrium fitting code EFIT [10]). The innermost magnetic surface is actually a line, which is usually called the magnetic axis, the magnetic field has only toroidal component on this line. A flux surface must be a surface of constant pressure with the current density vector be-

ing tangent to the surface. Equilibrium (thermalised) plasma quantities (like temperature, density, etc.) are also constant on a flux surface due to the fast thermal motion of particles over the flux surfaces, ensuring the equilibrium to be axisymmetric.

In this thesis, as it is common in tokamak literature, the geometric distance ψ will be used to label the surface, it is defined as

$$\psi = \frac{R_{max} - R_{min}}{2} \quad (1.28)$$

where R_{max} (R_{min}) is the maximum (minimum) major radius of the flux surface. It scales as the square root of the poloidal magnetic flux ($\psi \approx \sqrt{\Psi}$). In the simplified case of circular concentric flux surfaces, centered at the magnetic axis, the minor radius ψ will coincide with the radius of the circular poloidal cross section of a flux surface.

1.4.2 Safety factor, magnetic shear and beta

The safety factor q is an indicative parameter of the plasma configuration stability, it must be larger than one to avoid macroscale instabilities [11]. It is a flux function $q = q(\psi)$ which characterizes the pitch angle of magnetic field lines on closed magnetic surfaces. It is defined as the number of toroidal turns a magnetic field line needs to complete one loop in the poloidal direction, and can be expressed in the form

$$q = \frac{\Delta\phi}{2\pi} , \quad (1.29)$$

where $\Delta\phi$ is the change of the toroidal angle when a magnetic field line travels a full loop (2π) in the poloidal direction. In the case of axisymmetric equilibrium a value of q is attached to each field line. If $q = m/n$ is a rational number, then the corresponding field line will close on itself after m toroidal turns and n poloidal turns. On the other hand, if q is given by a irrational number, then the field line will ergodically cover the flux surface. The radial profiles of q have also a crucial role in the description of the plasma behaviour, in fact a quantity called magnetic shear \hat{s} is defined in connection to the q radial derivative as

$$\hat{s} = \frac{\psi}{q} \frac{dq}{d\psi} \quad (1.30)$$

it has a strong influence on the plasma stability. High values of the magnetic shear help preventing the formation of large structures elongated in the radial direction, these can contribute in destroying the equilibrium configurations. Therefore more stable configurations are those with higher values of the magnetic shear.

Consider now Eq. (1.25) together with Ampere's law $\nabla \times \mathbf{B} = \mu_0 \mathbf{J}$, one obtains

$$\nabla \left(p + \frac{B^2}{2\mu_0} \right) = (\mathbf{B} \cdot \nabla) \frac{\mathbf{B}}{\mu_0} \quad (1.31)$$

which expresses the balance between pressure and magnetic field tension, i.e. the first term on the left hand side (p) is the thermal pressure, the second term ($B^2/2\mu_0$) gives the magnetic pressure, the term on the right hand side is the magnetic field tension. The parameter β is defined as the ratio between thermal and magnetic pressure

$$\beta = \frac{p}{B^2/2\mu_0} . \quad (1.32)$$

This quantity is a measure of the efficiency of the magnetic field in confining the plasma. The tokamak is a low β magnetic configuration. It is expected to have $\beta \approx 1 - 3\%$ for an operative reactor.

1.5 Drift waves

The fluid model is very successful in describing large scale plasma phenomena. In fluid theory, the macroscopic quantities (density, temperature, etc.) are a function of \mathbf{x} and t only, they do not depend on the velocities. The particles velocity distribution is assumed to be close to a Maxwellian, because of the high interparticle collisionality. In hot plasmas, the interparticle collisionality can be relatively small (zero in ideal cases), and deviation from local thermodynamic equilibrium (deviation from Maxwellian distribution) can be maintained for long times. Even in low collisionality plasmas the fluid picture is sometimes valid, for example in the presence of strong magnetic fields and for phenomena with typical time and length scales larger compared to the Larmor motion.

There are situations, however, in which the fluid description is not applicable. In general, this is the case when treating problems involving motion of particles along the magnetic field with a mean free path (the mean path between collisions) larger than the length scale of the field gradient along the field, and also cases in which the perturbations vary, in the direction perpendicular to the magnetic field, over scales of the Larmor radius. In these cases one needs to work directly with the phase space distribution function for each of the particle species. This is the plasma kinetic theory.

Drift waves are collective low frequency ($\omega \ll \omega_c$) modes of plasma oscillations that propagate through the plasma. They arise in spatially non uniform plasmas as a result of the independent dynamics of ions and electrons. The charged particles interact through the electrostatic force to ensure the quasi-neutrality of the plasma. While ions and electrons are free to move independently in the plasma, a charge separation on a large scale is

prevented by the generation of strong electric fields acting against it. The different motion of ions and electrons gives origin to the drift waves. The single fluid MHD model is thus not appropriate in this context, and at least a two fluid representation is required. In fact, many drift waves features are actually found only in a kinetic description.

A plasma in thermodynamic equilibrium is described by a homogenous Maxwellian distribution for each particle species. Deviation from this equilibrium can be the source of free energy which can lead to instabilities. This mechanism can be observed both in homogenous and inhomogeneous plasmas. In homogenous plasmas, deviation from the Maxwellian are given only by the velocity dependence of the distribution. In the inhomogeneous case, both velocity and spatial dependences give a contribution.

Inhomogeneities can be maintained by confining the plasma with magnetic fields. Such a plasma will develop mechanisms to relax to the thermodynamic equilibrium. Particles collisions, for example, can bring a plasma back to a homogeneous equilibrium configuration. However, there are much more efficient mechanisms which provide a way to deteriorate the confinement of inhomogeneous plasmas, these are the drift waves instabilities. Indeed, instabilities arising in inhomogeneous plasmas are the origin of a turbulent state characterised by a certain level of fluctuations. The electromagnetic fields associated with these fluctuations can cause stochastic motion of the plasma particles. This motion leads to the so called anomalous transport, and results in the escape of particles and energy from the system. The heat and particle loss observed in most plasma confinement experiments are mainly attributed to this mechanism of plasma turbulence.

In this section we will study linear plasma instabilities arising from both velocity and spatial dependence of the distribution function. starting from the presentation of the equations needed for a kinetic description of plasma, i.e. the Vlasov-Maxwell equations.

1.5.1 The Vlasov-Maxwell equations

Consider a plasma composed by $N = \sum_{\alpha} N_{\alpha}$ charged particles (where α indicates the particle species), with positions \mathbf{x}_i and velocities \mathbf{v}_i ($i = 1, \dots, N$). The system is described by the many-body phase space distribution function $F(\mathbf{x}_1, \dots, \mathbf{x}_N, \mathbf{v}_1, \dots, \mathbf{v}_N, t)$. It is a function of all the particles coordinates, and $\int F d\mathbf{x}_1 \dots d\mathbf{x}_N d\mathbf{v}_1 \dots d\mathbf{v}_N = 1$. For a plasma of $N/2$ ions and $N/2$ electrons in thermodynamic equilibrium, F is the Gibbs distribution [12]. If the plasma is not in thermodynamic equilibrium, F must in principle be calculated from the dynamics of the N particles. This distribution obeys the Liouville equation [13]

$$\frac{\partial F}{\partial t} + \sum_i \left(\frac{\partial F}{\partial \mathbf{x}_i} \cdot \mathbf{v}_i + \frac{\partial F}{\partial \mathbf{v}_i} \cdot \mathbf{a}_i \right) = 0 \quad (1.33)$$

where \mathbf{a}_i is the total acceleration of particle i due to external and interparticle forces. The interparticle forces can be divided into two parts: one part is the average force on a particle due to a large number of relatively distant particles, and the other part is the force due to the nearest-neighbor particles, i.e. collisions. In this thesis only collisionless plasmas will be treated, in this case the average force of the many distant particles is the dominant one, and the nearest-neighbor force is neglected. The total acceleration is then given by the combination of the acceleration due to externally applied forces (\mathbf{a}_i^{ext}) and the acceleration arising from internal average forces due to distant plasma particles (\mathbf{a}_i^{av}), i.e.

$$\mathbf{a}_i = \mathbf{a}_i^{ext} + \mathbf{a}_i^{av} . \quad (1.34)$$

In practice, the problem of calculating or even estimating F is not tractable. In order to be able to operatively describe the plasma, the one particle distribution for particles of type α is used, i.e.

$$\begin{aligned} f_\alpha(\mathbf{x}_i, \mathbf{v}_i, t) \\ = N_\alpha \int F d\mathbf{x}_1 \dots d\mathbf{x}_{i-1} d\mathbf{x}_{i+1} \dots d\mathbf{x}_N d\mathbf{v}_1 \dots d\mathbf{v}_{i-1} d\mathbf{v}_{i+1} \dots d\mathbf{v}_N . \end{aligned} \quad (1.35)$$

The quantity $f_\alpha d\mathbf{x}_i d\mathbf{v}_i$ is the number of particles of type α contained in the phase space volume element $d\mathbf{x}_i d\mathbf{v}_i$ centered at $\mathbf{x}_i, \mathbf{v}_i$ at time t . For a plasma in thermal equilibrium, f_α is a maxwellian distribution. The macroscopically observable quantities (mass and charge density, currents, fluxes, etc.) are found from the velocity moments of f_α . The equations that are satisfied by these variables are obtained taking the velocity moments of the evolution equation for f_α (1.36). From now on, only the one particle distribution will be treated, so the i -index for the coordinates will be dropped.

The equation for the one particle distribution function, for a plasma whose particles are acted upon by electric and magnetic forces is given by

$$\frac{\partial f_\alpha}{\partial t} + \mathbf{v} \cdot \nabla f_\alpha + \frac{q_\alpha}{m_\alpha} (\mathbf{E} + \mathbf{v} \times \mathbf{B}) \cdot \frac{\partial f_\alpha}{\partial \mathbf{v}} = 0 \quad (1.36)$$

where q_α is the particle charge, m_α the particle mass, \mathbf{E} and \mathbf{B} are the sum of external and average internal fields. Thus the electric and magnetic fields have to be calculated self-consistently from the Maxwell equations, i.e.

$$\begin{aligned} \nabla \cdot \mathbf{E} &= \frac{\sigma}{\epsilon_0} & \nabla \times \mathbf{B} &= \mu_0 \mathbf{J} + \frac{1}{c^2} \frac{\partial \mathbf{E}}{\partial t} \\ \nabla \cdot \mathbf{B} &= 0 & \nabla \times \mathbf{E} &= -\frac{\partial \mathbf{B}}{\partial t} \end{aligned} \quad (1.37)$$

where c is the speed of light, the curl of \mathbf{E} is zero due to the electrostatic limit, the charge density σ and the current density \mathbf{J} have to be obtained

from the sum between the externally imposed sources (σ^{ext} and \mathbf{J}^{ext}) and the integrals of f_α (average internal sources) as

$$\sigma = \sigma^{ext} + \sum_{\alpha} q_{\alpha} \int f_{\alpha} d^3v \quad \mathbf{J} = \mathbf{J}^{ext} + \sum_{\alpha} q_{\alpha} \int \mathbf{v} f_{\alpha} d^3v . \quad (1.38)$$

Equations (1.36)-(1.38) are the Vlasov-Maxwell equations.

In the rest of this thesis, only the electrostatic limit will be treated, which means that Maxwell equations reduce to

$$\nabla \cdot \mathbf{E} = \frac{\sigma}{\epsilon_0} \quad \nabla \times \mathbf{E} = 0 \quad \mathbf{E} = -\nabla\phi \quad (1.39)$$

with ϕ the electrostatic scalar potential, i.e. perturbations of the magnetic field are neglected.

1.5.2 Landau damping

As an example of instability due to the velocity dependence of the distribution function, we present the kinetic study of the electron plasma (Langmuir) waves. The detailed treatment can be found in [8].

If electrons in an unmagnetized plasma are displaced from their equilibrium position, leaving the ions unmoved (the approximation holds in the case of small electron displacement due to the ions inertia), the electric field that is created will act as a restoring force, pulling the electrons back to neutralize the ions charge. The energy initially stored in the electric field will be converted into electrons kinetic energy, and when the electrons arrive again at their initial position (before they have been displaced), the acquired kinetic energy will cause the electrons to pass through the unmoved ions, until the pulling back electric field will be restored and will make them to stop and repeat the process. These oscillations are called electrostatic Langmuir oscillations. A linear fluid treatment, in which the perturbations are assumed to vary as $\exp(ikx - i\omega t)$, gives the frequency of the Langmuir waves in the form

$$\omega^2 = \omega_{pe}^2 + 3k^2 v_{th,e}^2 \quad (1.40)$$

where ω_{pe} is the electron plasma frequency given by

$$\omega_{pe}^2 = \frac{n_e e^2}{\epsilon_0 m_e} \quad (1.41)$$

it describes oscillations without considering thermal effect. The second term, with $v_{th,e} = (k_B T / m_e)^{1/2}$ the electron thermal velocity, gives the finite temperature effect. Thermal effects are important since they allow the wave to have a non zero group velocity $d\omega/dk$ and therefore propagate energy from one part of the plasma to another.

Below the kinetic treatment is discussed. Referring only to the electron species, the e -subscript will be dropped. Consider the case of an unmagnetized plasma, with uniform background equilibrium quantities. The equilibrium distribution function f_0 can be considered to be a function of \mathbf{v} only. There is no electric field in the equilibrium state, it will arise as a perturbation. We consider the one dimensional problem in the x -direction. Writing the distribution function as $f = f_0 + f_1$, where f_1 is a small perturbation to the equilibrium, the linearized Vlasov equation is given by

$$\frac{\partial f_1}{\partial t} + v \frac{\partial f_1}{\partial x} - \frac{e}{m} E \frac{\partial f_0}{\partial v} = 0 \quad (1.42)$$

where v is the velocity in the x -direction and E is the perturbed electric field. The magnetic field plays no role, thus the only Maxwell equation needed is the Poisson equation, which in this case is given by

$$\frac{\partial E}{\partial x} = -\frac{e}{\epsilon_0} \int f_1 dv . \quad (1.43)$$

Eqs. (1.42) and (1.43) have to be simultaneously solved.

The correct mathematical treatment was first given by Landau. In order to consistently solve the problem, Landau used the Laplace transform approach in solving the linear differential equation (1.42), then the physical conclusions come from the analysis of the singularities when inverting the Laplace transformation.

The treatment goes as follow, assume a wave-like form of the perturbations only in space, thus

$$\psi(x, v, t) = \psi(v, t) \exp(ikx) \quad (1.44)$$

and then solve the initial value problem using the Laplace method. This procedure allows the frequency ω to be a complex number, entering the equations as the Laplace transformation variable. The initial conditions for ψ are included in the problem through the definition of the Laplace transform of a time derivative. In fact, the Laplace transforms $\tilde{\psi}(v, \omega)$ and $\dot{\tilde{\psi}}(v, \omega)$ of the functions $\psi(v, t)$ and $\dot{\psi}(v, t)$ are given by

$$\tilde{\psi}(v, \omega) = \int_0^{+\infty} \psi(v, t) e^{i\omega t} dt \quad \dot{\tilde{\psi}}(v, \omega) = \omega \tilde{\psi}(v, \omega) - \psi(v, 0) \quad (1.45)$$

defined for $\text{Im}(\omega) > 0$ and large enough to ensure the convergence of the integral. The system of eqs. (1.42) and (1.43), after Laplace transform, is reduced to

$$D(k, \omega) \tilde{E}(\omega) = N(k, \omega) \quad (1.46)$$

whith the functions $D(k, \omega)$ and $N(k, \omega)$ given by

$$\begin{aligned} D(k, \omega) &= 1 + \frac{e^2}{mk\epsilon_0} \int \frac{\partial f_0 / \partial v}{\omega - kv} dv \\ N(k, \omega) &= -\frac{e}{k\epsilon_0} \int \frac{f_1(v, 0)}{\omega - kv} dv \end{aligned} \quad (1.47)$$

where $f_1(v, 0)$ is the initial condition, at $t = 0$, for the perturbed distribution function. In principle, given $f_0(v)$ and $f_1(v, 0)$ the solution $\tilde{E}(\omega)$ for the Laplace transform of the electric field can be obtained. Then, the physical field $E(t)$ must be calculated inverting the Laplace transformation as

$$E(t) = \frac{1}{2\pi i} \int_C \tilde{E}(\omega) e^{-i\omega t} d\omega = \frac{1}{2\pi i} \int_C \frac{N(k, \omega)}{D(k, \omega)} e^{-i\omega t} d\omega \quad (1.48)$$

where C must be a closed contour in the complex plane composed by an horizontal line running from $-\infty$ to $+\infty$ parallel to the real axis and intersecting the imaginary axis at some point $i\omega_0$ with $\omega_0 > 0$ (because the Laplace transform is defined for $\text{Im}(\omega) > 0$), and since $t > 0$ the contour is then closed by an arc of infinite radius enclosing the negative imaginary axis ($\text{Im}(\omega) < 0$), which therefore does not contribute to the integral. The value of ω_0 has to be taken large enough to include inside C all the existing singularities of the $\tilde{E}(\omega)$ function. The integral around such a closed contour is given by the sum of the residues of the integrand at each singularity within the closed contour. Therefore we can write

$$E(t) = \text{Res}_{\omega=\omega_1} [\tilde{E}(\omega) e^{-i\omega t}] + \frac{1}{2\pi i} \int_{C'} \tilde{E}(\omega) e^{-i\omega t} d\omega \quad (1.49)$$

where the first term on the right is the residue at ω_1 of the function in square brackets, ω_1 is the singularity of $\tilde{E}(\omega)$ with the largest imaginary part and C' is a closed contour shaped as C but not including ω_1 . Using the residues formula we find

$$\text{Res}_{\omega=\omega_1} [\tilde{E}(\omega) e^{-i\omega t}] \propto e^{-i\omega_1 t} \quad (1.50)$$

therefore, being ω_1 the singularity with the largest imaginary part, it is also the one that gives the main contribution to the time dependence as $t \rightarrow +\infty$ of the electric field perturbation.

To solve the problem, the singularities of $\tilde{E}(\omega)$ have to be determined. Assuming the right hand side of Eq. (1.46) not singular, all singularities of $\tilde{E}(\omega)$ are zeros of $D(k, \omega)$. Therefore the equation to be solved to find the singular values of the frequency is

$$D(k, \omega) = 1 + \frac{e^2}{mk\epsilon_0} \int \frac{\partial f_0 / \partial v}{\omega - kv} dv = 0 \quad (1.51)$$

which gives the dispersion relation $\omega = \omega(k)$. In fact the function $D(k, \omega)$ is called the plasma dispersion function. The velocity integral appearing in this formula has to be performed in the complex velocity plane, on a contour running from $-\infty$ to $+\infty$ over the real axis.

If the singularity is such that $\text{Im}(\omega) > 0$ then the integral can be performed, since there are no singularities on the real axis, without changing the contour of integration in the complex velocity plane, the result is a

frequency with positive imaginary part and therefore a wave with an exponentially growing amplitude representing an instability.

The physically most relevant case is the one with a singularity in which the imaginary part of the frequency can be treated as a small correction to its real part. Assume that $\omega = \omega_r + i\gamma$ where $\text{Re}(\omega) = \omega_r$, $\text{Im}(\omega) = \gamma$ with $\gamma \ll \omega_r$ and $\gamma > 0$. Consider then the limit $\gamma \rightarrow 0$. In this case, while ω is approaching the real axis, the singularity will lie closer and closer to the integration contour in the complex velocity plane. Therefore, in the vicinity of ω , as $\gamma \rightarrow 0$, the velocity contour has to be deformed in order to avoid the singularity. Landau's prescription states that the contour needs to be deformed in such a way that the singularity always lies on the same side of the contour. This choice makes possible to define the function $D(k, \omega)$ in the negative imaginary half of the complex plane by analytic continuation. In this case the singularity is approaching the real axis from above, thus the velocity contour passes below the singularity. In the limit $\gamma \rightarrow 0$ the velocity contour will then be composed by two straight lines running on the real axis, one from $-\infty$ to $\omega_r - \epsilon$ and the other from $\omega_r + \epsilon$ to $+\infty$, connected by a half circle of radius ϵ centered at ω_r passing below the singularity, where ϵ is an infinitesimal length. The integral in $D(k, \omega)$ is then given by

$$\int \frac{\partial f_0 / \partial v}{\omega - kv} dv = \text{Pr} \int \frac{\partial f_0 / \partial v}{\omega - kv} dv - \frac{i\pi}{k} \frac{\partial f_0}{\partial v} \Big|_{v=\omega/k} \quad (1.52)$$

where Pr denotes the principal value of the integral and the second term is the contribution from the half circle around the pole. The principal part can be evaluated assuming that f_0 is given by a Maxwellian everywhere except in the vicinity of the singularity, then under the approximation $kv \ll \omega$ expanding the integrand to 3-rd order in kv/ω , the dispersion relation takes the form

$$1 - \frac{\omega_p^2}{\omega^2} - \frac{3k^2 v_{th}^2 \omega_p^2}{\omega^4} - \frac{i\pi e^2}{mk^2 \epsilon_0} \frac{\partial f_0}{\partial v} \Big|_{v=\omega/k} = 0. \quad (1.53)$$

This equation can be evaluated substituting $\omega = \omega_r + i\gamma$, using $\gamma \ll \omega_r$ to write $\omega^2 = \omega_r^2 + 2i\omega_r\gamma$ and $\omega^4 = \omega_r^4 + 4i\omega_r^3\gamma$, treating the term due to the contribution of the pole as a small correction, and assuming $kv_{th} \ll \omega$ in evaluating the contribution of the principal part of the integral. Then, equating the real and the imaginary part of Eq. (1.53) separately to zero we obtain

$$\omega_r^2 = \omega_p^2 + 3k^2 v_{th}^2 \quad \gamma = \frac{\pi e^2}{2mk^2 \epsilon_0} \frac{\partial f_0}{\partial v} \Big|_{v=\omega/k} \quad (1.54)$$

the real part of the frequency recovers the result obtained in Eq. (1.40) with the fluid theory, while the imaginary part is of course the new result coming from the kinetic treatment. It shows explicitly the influence of the velocity dependence of the distribution function, for velocities next to the phase velocity of the wave. It is clear that the sign of γ depends on the sign

of the velocity derivative of the background distribution function. Therefore, even though the Laplace transform has been defined for $\text{Im}(\omega) > 0$, Landau's treatment shows that also solution with $\text{Im}(\omega) < 0$ are allowed, provided that the function $D(k, \omega)$ is defined in the negative imaginary half of the complex plane by analytic continuation, properly deforming the contour of the velocity integral. According to the sign of γ the wave can be damped, i.e. $\gamma < 0$ which corresponds to the mechanism called Landau damping (this is the case of a Maxwellian distribution), or it can go unstable growing exponentially, i.e. $\gamma > 0$ called inverse Landau damping (this can be the case for a non-monotonously decreasing distribution function).

Landau damping is associated with those particles that have a velocity nearly equal to the phase velocity of the wave, the resonant particles. The resonant particles see an almost static electric field, and can efficiently exchange energy with the wave. They can be either accelerated or decelerated by the wave, depending on their relative phase relation. If, in the velocity interval around $v = \omega/k$, the distribution function has more particles slower than the phase velocity compared with particles that are faster than the phase velocity (like it happens for a Maxwellian distribution) then more particles are accelerated by the wave than decelerated, resulting in a net transfer of energy from the wave to the particle, and therefore the wave is damped. In the opposite case there is an energy transfer from the particles to the wave, which result in the growth of an instability.

1.5.3 Drift waves instability

Kinetic and hydrodynamic effects can both lead to non dissipative destabilization of drift waves in spatially inhomogeneous plasmas. A detailed treatment about drift waves instability can be found in [14] and references therein. Only the main results useful for the purpose of understanding this thesis are presented here.

Dispersion relation for the plane plasma slab

The simplest possible configuration involving a spatially non uniform plasma is used here: the plane plasma slab. In this configuration the plasma can be treated in a cartesian coordinates system. The equilibrium is maintained by a strong uniform magnetic field, taken to be in the z -direction. The plasma is considered to be non uniform in one direction only: the x -direction. The typical length scale over which the plasma is non uniform is assumed to be much larger than the Larmor radius. Since the particles can travel along the x -direction only for distances of the order of the Larmor radius, it is thus possible to consider perturbations localized at the surface $x = 0$ and consider all quantities (magnetic field, density, temperature and their gradients) as

evaluated on this surface. All perturbations can then be written as

$$\psi(\mathbf{x}, \mathbf{v}, t) = \psi(\mathbf{v}, t) \exp(ik_y y + ik_z z) . \quad (1.55)$$

Furthermore the following ordering, which is generally valid for the plasma phenomena here considered, is applied

$$\rho_e \ll \rho_i \ll L \quad \lambda_{De,i} \ll \rho_i \quad \omega \ll \omega_{ce,i} \quad (1.56)$$

where L is a characteristic gradient length of background quantities, and $\lambda_{De,i}$ is the Debye length⁵. The background Maxwellian distributions (one for the ions and one for the electrons) can be written as

$$f_{0s} = n_{0s} \left(\frac{m_s}{2\pi k_B T_{0s}} \right)^{3/2} \exp \left(-\frac{mv^2}{2k_B T_{0s}} \right) \quad (1.57)$$

where $s = i, e$ is the subscript referring to the particle species, n_{0s} and T_{0s} are the equilibrium density and temperature, and $v^2 = v_\perp^2 + v_z^2$. The linearized Vlasov equation, in this case, is given by [14]

$$\frac{\partial f_{1s}}{\partial t} + \mathbf{v} \cdot \frac{\partial f_{1s}}{\partial \mathbf{x}} + \frac{1}{m_s} (q_s \mathbf{v} \times \mathbf{B} + \mathbf{F}_s) \cdot \frac{\partial f_{1s}}{\partial \mathbf{v}} + \frac{q_s}{m_s} \mathbf{E} \cdot \frac{\partial f_{0s}}{\partial \mathbf{v}} = 0 \quad (1.58)$$

where \mathbf{F}_s indicates an externally imposed force. Solving this equation, together with the Poisson equation, gives the dispersion relation $D(\mathbf{k}, \omega) = 0$ with the dispersion function given by

$$D(\mathbf{k}, \omega) = 1 + \sum_s \frac{1}{(k\lambda_{Ds})^2} \frac{\omega - \omega'_{ds}}{\omega - \omega_{Fs}} \left[W \left(\frac{\omega - \omega_{Fs}}{|k_z|v_{ths}} \right) - 1 \right] \Lambda_0(k_y \rho_s) \quad (1.59)$$

where only low frequency waves have been considered ($\omega \ll \omega_{cs}$), k is the modulus of the wave vector, ω'_{ds} is the drift frequency operator given by

$$\omega'_{ds} = \frac{T_{0s} k_y}{q_s B} \left(\frac{d \ln(n_{0s})}{dx} + \frac{dT_{0s}}{dx} \frac{\partial}{\partial T_{0s}} - \frac{F_s}{T_{0s}} \right) = \omega_{ns} + \omega'_{Ts} + \omega_{Fs} , \quad (1.60)$$

with F_s modulus of the applied external force and the derivative towards the temperature acts on both W and Λ_0 through their dependence on the thermal velocity, the function $W(z)$ takes into account the wave-particle resonances along the magnetic field lines, it is given by

$$W(z) = \frac{1}{\sqrt{2\pi}} \int_C \frac{v_z}{v_z - z} e^{-v_z^2/2} dv_z \quad (1.61)$$

where C is a contour running on the real v_z axis avoiding the singularity according to the Landau prescription described in the previous section, the function $\Lambda_0(z) = e^{-z} I_0(z)$, with $I_0(z)$ the zeroth order modified Bessel function, expresses the integral over v_\perp and therefore it takes into account the FLR effects due to the gyro-average procedure (as shown in section 1.3.1).

⁵The Debye length of the s -species $\lambda_{Ds} = \sqrt{(\epsilon_0 T_s)/(n_s e^2)}$ is a measure of the sphere of influence of a given charge in a plasma. In fact, the electrostatic potential of an isolated charge q is $\phi \approx q/r$, while for a charge at rest in a plasma it is $\phi \approx (q/r) \exp(-r/\lambda_D)$.

Inhomogeneous ion and electron density

The simplest case in which an instability can arise consists of a plasma configuration in which $\mathbf{F}_s = 0$ and $dT_{0s}/dx = 0$ and the inhomogeneity is given by the density gradients only. The wave propagation is considered to be mainly in the perpendicular to the magnetic field direction ($k_z/k_y \ll 1$). For the electrons, it is appropriate to assume that $\omega/(k_z v_{th,e}) \ll 1$ i.e. the wave phase velocity along the magnetic field can be considered much smaller than the electron thermal velocity, the electrons therefore are described by an adiabatic response (the electron density perturbation is proportional to the perturbed electrostatic potential). For the ions, instead, it can be assumed $\omega/(k_z v_{th,i}) \gg 1$ (cold ions approximation). Furthermore, because of the different sizes of their gyro-orbits, it is possible to neglect finite Larmor radius (FLR) effects when performing the gyro-average in the electron case ($k_y \rho_e \ll 1$), while the FLR has to be retained in the ion case. The dispersion relation, under these assumptions, takes the form

$$1 + \frac{1}{(k\lambda_{De})^2} \left\{ 1 + \left(1 - \frac{\omega_{ne}}{\omega}\right) i\sqrt{\frac{\pi}{2}} z_e \right\} + \frac{1}{(k\lambda_{Di})^2} \left\{ 1 + \left(1 - \frac{\omega_{ni}}{\omega}\right) \left[i\sqrt{\frac{\pi}{2}} e^{-\frac{z_i^2}{2}} - \frac{1}{z_i^2} - 1 \right] \Lambda_0(k_y \rho_i) \right\} = 0 \quad (1.62)$$

where we defined $z_s = \omega/(|k_z|v_{th,s})$. Equating then separately to zero the real and the imaginary part of this equation, and neglecting the exponentially small ions contribution to the imaginary part, one finds the frequency $\omega = \omega_r + i\gamma$ with

$$\omega_r = \omega_{ne} \frac{\Lambda_0(k\rho_i)}{1 + (T_{0e}/T_{0i}) [1 - \Lambda_0(k\rho_i)] + (k\lambda_{De})^2} \quad (1.63)$$

$$\gamma = \sqrt{\frac{\pi}{2}} \frac{\omega_r^2}{\Lambda_0(k\rho_i)} \left(\frac{\omega_r}{\omega_{ne}} - 1 \right) \frac{1}{|k_z|v_{th,e}}.$$

Therefore, the solution is a wave propagating in the direction perpendicular to the magnetic field with frequency ω_r of the order of the electron drift frequency $\omega_{ne} = (T_{0s}k_y)/(q_s B) d \ln(n_{0s})/dx$ (in fact $\omega_r \approx \omega_{ne}$ if $k_y \rho_i \ll 1$). The wave can be destabilized by the resonant interaction between the wave and the particles (electrons in this case). In fact, note how the contribution to γ representing the resonant effect is proportional to $(\omega_r/\omega_{ne} - 1)$. The term "−1" represents the Landau damping mechanism due to the resonant particles (particles with $v_z = \omega_r/k_z$) driven along the magnetic field by the parallel component of the electric field. The term " ω_r/ω_{ne} " is related to the plasma inhomogeneity, it can be positive and therefore give an instability. It represents the $\mathbf{E} \times \mathbf{B}$ convection along or against the density gradient, so perpendicular to \mathbf{B} , of resonant particles. This results in a reinforcement of the density perturbation. In fact, particles with velocity far away from

the wave phase velocity, experience an oscillating electric field and bounce back and forth in the passing wave, in both the parallel (due to the parallel component of the electric field) and perpendicular direction (due to the $\mathbf{E} \times \mathbf{B}$ velocity). Resonant particles, travelling at the wave phase velocity, undergo a drive due to the electric field perturbation whose orientation does not change (since the electric field is not oscillating in their reference system). The drive along \mathbf{B} leads to Landau damping. The $\mathbf{E} \times \mathbf{B}$ convection, perpendicular to \mathbf{B} , results in an enhancement of the density perturbation. If this latter mechanism is stronger than the Landau damping, it leads to a destabilization of the wave.

This instability can not be found within the fluid theory, unless one introduces some kind of dissipation (plasma resistivity for example). A two-fluid description can be given in terms of a continuity equation for the cold ion fluid, i.e.

$$\frac{\partial n_i}{\partial t} + \nabla \cdot (n_i \mathbf{u}_i) = 0 \quad (1.64)$$

where \mathbf{u}_i is the ion fluid velocity (i.e. the $\mathbf{E} \times \mathbf{B}$ velocity), and considering adiabatic electrons

$$n_e = n_{0e} \exp(e\phi/T_{0e}) . \quad (1.65)$$

Solving then the linear problem, and imposing the quasi-neutrality condition ($n_e = n_i$), one finds the solution $\omega = \omega_{ne}$, i.e. a wave travelling at the electron drift velocity without damping or growth. The reason is that, in the absence of dissipation mechanisms, the requirement about the electrons adiabatic response, forces the density perturbation to be always in phase with the electrostatic potential perturbation. This will cause the $\mathbf{E} \times \mathbf{B}$ velocity and the density perturbation to be $\pi/2$ out of phase (since $\mathbf{v}_E \propto \nabla\phi$). Therefore, given an initial density perturbation in the presence of a density gradient, the $\mathbf{E} \times \mathbf{B}$ convection will cause the density perturbation to be shifted rather than growing or decaying. The result is a wave propagating at the electron drift frequency. However, in the case of non zero resistivity, a phase shift between density and potential perturbations is introduced, which lead to an enhancement of the density perturbation and thus to the destabilization of the wave.

Inhomogeneous ion temperature

Assume again adiabatic electrons and zero ion density gradient. If the inhomogeneity is given only by the ion temperature gradient (ITG), also in this case an instability can arise. This is called the slab-ITG drift wave instability.

Consider, at first, the fluid limit (neglecting FLR effects, i.e. $k_y \rho_i \ll 1$) with the ions treated as a cold fluid ($\omega/(k_z v_{th,i}) \gg 1$), then with a similar procedure to the one described above, starting from the general expression

of the dispersion function given in Eq. (1.59), the dispersion relation can be written as [14]

$$1 - \left(\frac{k_z c_s}{\omega}\right)^2 \left(1 - \frac{\omega_{Ti}}{\omega}\right) = 0 \quad (1.66)$$

where c_s is the sound speed and $\omega_{Ti} = (T_{0i} k_y / eB)(d \ln T_{0i} / dx)$. It is interesting to notice that without a temperature gradient, one obtains $\omega = \pm k_z c_s$, i.e. the two sound wave branches, which means that the slab-ITG drift wave is a deformation of one of the sound wave branches due to the presence of an ion temperature gradient. The dispersion relation is cubic in ω , it admits therefore two complex conjugate solutions, one of which leads to an instability. In particular, solving Eq. (1.66) for $|k_z c_s| \ll |\omega_{Ti}|$ and then evaluating the solution in the limit of applicability of this formula ($|k_z c_s| \rightarrow |\omega_{Ti}|$), it is found that the unstable ITG mode is given by $\omega_r \approx \gamma \approx \omega_{Ti}$, showing that the solution describes a propagating wave which can be destabilized because of the presence of an ion temperature gradient. This result is also recovered in the context of a two-fluid model, in which the electrons are treated adiabatically

$$n_e = n_{0e} \exp(e\phi / T_{0e}) \quad (1.67)$$

and the ions are described by a continuity equation, a momentum equation and a heat equation representing $\mathbf{E} \times \mathbf{B}$ convection in the flow, i.e. respectively

$$\begin{aligned} \frac{\partial n_i}{\partial t} + \nabla \cdot (n_i \mathbf{u}_i) &= 0 \\ m_i n_i \left[\frac{\partial \mathbf{u}_i}{\partial t} + \mathbf{u}_i \cdot (\nabla \mathbf{u}_i) \right] &= e n_i (\mathbf{E} + \mathbf{u}_i \times \mathbf{B}) - \nabla (n_i T_i) \\ \frac{\partial (n_i T_i)}{\partial t} + \nabla \cdot (n_i T_i \mathbf{v}_E) &= 0 \end{aligned} \quad (1.68)$$

where \mathbf{u}_i is the ion fluid velocity and $T_i = T_{0i} + \delta T_i$ with δT_i ion temperature perturbation. The dispersion relation given in Eq. (1.66) is then found linearizing the system of eqs. (1.68) and imposing the quasi-neutrality condition ($n_e = n_i$).

The reason for this instability, even in a fluid treatment without dissipation, is that the ion temperature perturbation (δT_i) does not have any constraints concerning its relative phase with respect to the electrostatic potential perturbation. Therefore, the $\mathbf{E} \times \mathbf{B}$ convection, in the presence of a temperature gradient, can be such that hotter plasma is brought in region of higher temperature perturbation and colder plasma in region of lower temperature perturbation, which results in an enhancement of the perturbation. The ITG instability, in slab geometry, is therefore dominantly of hydrodynamic type, the underlying mechanism being the result of $\mathbf{E} \times \mathbf{B}$ heat convection in the presence of an ion temperature gradient.

The toroidal-ITG instability

In the case of a tokamak, the inhomogeneities due to the magnetic field configuration (grad-B and curvature) have to be included. Referring to the general treatment given in Eq. (1.59), these effects will enter the equations as external forces (the \mathbf{F}_i term). The slab-ITG is then modified, acquiring an interchange-like character, i.e. the presence of the instability depends on the combined action of a force (the one related to the grad-B) and the temperature gradient of the plasma (similarly to the Rayleigh-Taylor or Interchange instability, where the instability arises from a force, such as a gravitational field, acting against the density gradient). This is the so called toroidal-ITG drift wave instability, and it is the one which will be studied in the rest of this thesis. The dispersion relation, in this case, has the form

$$\frac{1}{(k\lambda_{De})^2} + \frac{1}{(k\lambda_{Di})^2} \left[1 + (\omega - \omega'_{Ti}) \int \frac{f_{0i}}{n_{0i}} \frac{J_0(k_y \rho_i)}{k_z v_z + \omega_{Fi} - \omega} d^3v \right] = 0 \quad (1.69)$$

where $\omega_{Fi} \propto \nabla \ln B$ appears in the velocity integral since the forces related to the curvature and gradient of \mathbf{B} are velocity dependent.

The dispersion relation for the toroidal-ITG has to be numerically solved in order to obtain reliable results. This is due to the fact that, for the ions, no approximation can be made about $k_y \rho_i$ (because of the size of their gyro-orbit) and $\omega/(k_z v_{th,i})$ (to treat thermal hot ions) in order to easily treat the velocity integral. The growth rate γ as a function of $k_y \rho_i$ is a bell shaped curve with a maximum at $k_y \rho_i \approx 0.5$ (see chapter 2).

However, the fluid limit ($k_y \rho_i \ll 1$), with the ions treated as a cold fluid ($\omega/(k_z v_{th,i}) \gg 1$), provides a useful way to study the qualitative behaviour of this instability. In particular, the dispersion relation becomes [14]

$$1 - \left(1 - \frac{\omega_{Ti}}{\omega} \right) \left[\left(\frac{k_z c_s}{\omega} \right)^2 + \frac{T_{0e} \bar{\omega}_{Fi}}{T_{0i} \omega} \right] = 0 \quad (1.70)$$

where $\bar{\omega}_{Fi}$ is the ω_{Fi} averaged over the Maxwellian distribution. This equation is the modification of Eq. (1.66) in the presence of a non uniform magnetic field. In fact it provides an instability also if $k_z = 0$, i.e. in the case of purely perpendicular propagation of the wave. Assuming $|\omega| \ll |\omega_{Ti}|$ the solution is given by

$$\omega = \pm \left(-\frac{T_{0e}}{T_{0i}} \omega_{Ti} \bar{\omega}_{Fi} \right)^{1/2} \propto (-\nabla \ln T_{0i} \cdot \nabla \ln B)^{1/2} . \quad (1.71)$$

The necessary condition to provide an unstable mode is that the gradient of the magnetic field has to be in the same direction of the ion temperature gradient. In the opposite case the mode is stable. This shows the interchange-like character of the toroidal-ITG instability. Therefore, in a tokamak, there are regions of stability (favourable curvature) and region

in which the toroidal-ITG can go unstable (unfavourable curvature). The favourable curvature is in the inner, high magnetic field region of the torus, while the unfavourable curvature is the outer, low field region of the torus.

1.6 The gyro-kinetic model

The purpose of this thesis is the study of microscopic scale turbulence in plasmas magnetically confined in tokamaks. In this case the evolution of the fields perturbations is characterized by specific spatial and time scales, which makes the kinetic theory much more suitable to the description of the problem than the fluid theory. The application of this space-time ordering to the general kinetic plasma theory leads to the gyro-kinetic equation. This is the equation generally used to describe magnetically confined plasma microturbulence. It will be used throughout the rest of this thesis.

In this section we present the system of equations necessary for the gyro-kinetic treatment of a collisionless plasma. Start from the the plasma kinetic theory, i.e. the Vlasov-Maxwell equations system, then we apply the gyro-kinetic ordering to this equations in the case of a tokamak plasma.

1.6.1 The gyro-kinetic ordering

The purpose of gyro-kinetic theory is to model microturbulence in magnetically confined plasmas. In particular it is build to describe drift waves instability (see section 1.5) due to turbulent phenomena occurring in the plasma at small scales compared to the tokamak size. The properties of drift wave turbulence and particles motion in tokamak plasmas, make possible to treat the problem through an asymptotic expansion in small parameters, which are naturally defined by an analysis of the typical scales involved. In particular, the fundamental principle of gyro-kinetics is the removal of the fast cyclotron timescale, since the phenomena of interest are characterised by frequencies much smaller than the cyclotron frequency. This is expressed in the time scale ordering parameter

$$\epsilon_\omega \approx \frac{\omega}{\omega_c} \ll 1 \quad (1.72)$$

where ω_c refers to both ion and electron cyclotron frequency. The spatial variation of the background quantities (magnetic field B , temperature T and density n) are expressed in terms of logarithmic gradient length scales $1/L_G = |\nabla G|/|G| = \nabla \ln G|$ (where G indicates a generic background quantity) of the order of the device size R (with R major radius of the tokamak), i.e.

$$L_G \approx R. \quad (1.73)$$

The gyro-radius is much smaller than the device size, but much bigger than the Debye length, these properties are expressed as

$$\epsilon_B \approx \frac{\rho}{R} \ll 1 \quad \text{with} \quad \rho \gg \lambda_D \quad (1.74)$$

where ρ and λ_D refer to both ion and electron Larmor radius and Debye length respectively. Fluctuations of the fields are allowed to vary on the scale of the gyro-radius in the direction perpendicular to the magnetic field (this is the main difference between gyro-kinetic and drift-kinetic theory), this concept is expressed in the form

$$\epsilon_{\perp} \approx k_{\perp} \rho \approx 1, \quad (1.75)$$

however, the amplitude of the fluctuations (δG) is assumed to be small compared to the background equilibrium quantities (G), this property defines the small parameter

$$\epsilon_{\delta} \approx \left| \frac{\delta G}{G} \right| \ll 1. \quad (1.76)$$

In this thesis, only the case of tokamak with large aspect ratio is treated, i.e. tokamak with $R/r \gg 1$ where r is the minor radius of the tokamak (radius of the poloidal cross section). Assuming a maximum ordering, allowing to treat all effects on equal footing, the simplest ordering $\epsilon_{\omega} \approx \epsilon_B \approx \epsilon_{\delta}$ can be employed, and the asymptotic expansion is performed only in terms of the normalized gyro-radius

$$\rho_* = \frac{\rho}{R}. \quad (1.77)$$

The ordering assumption about the amplitude of the fluctuations given in Eq. (1.76) can be exploited employing the δf -approximation formalism (it will be used in this thesis), which consists in writing the total single particle distribution function as $f_{tot} = F + f$ where F is the background equilibrium distribution and f is the perturbation. These are related by the ordering

$$f \approx \rho_* F. \quad (1.78)$$

The particles motion along the field lines is characterised by velocities v_{\parallel} of the order of the thermal velocity $v_{th} = \sqrt{2T/m}$. Thus, the fluctuations vary over spatial length much larger than the Larmor radius along the field lines ($k_{\parallel} \rho \ll 1$). Using Eq. (1.75), the parallel and perpendicular dynamics are ordered as

$$\frac{k_{\parallel}}{k_{\perp}} \approx \rho_* \quad (1.79)$$

which is equivalent to ordering the gradients, along (∇_{\parallel}) and perpendicular (∇_{\perp}) to the magnetic field, of the perturbed distribution function as

$$\nabla_{\parallel} f \approx \rho_* \nabla_{\perp} f. \quad (1.80)$$

Eq. (1.74) states that the perturbed distribution varies, in the perpendicular direction, on length scales of order ρ compared to the background distribution ($L_{\perp f} \approx \rho_* L_{\perp F}$), therefore

$$\nabla_{\perp} f \approx \nabla_{\perp} F, \quad (1.81)$$

instead, the length scales of F and f are of the same order along the field lines ($L_{\parallel F} \approx L_{\parallel f}$), thus their parallel derivatives are ordered as

$$\nabla_{\parallel} f \approx \rho_* \nabla_{\parallel} F. \quad (1.82)$$

Concerning the velocity space derivative the δf -approximation implies

$$\frac{\partial f}{\partial v_{\parallel}} \approx \rho_* \frac{\partial F}{\partial v_{\parallel}} \quad (1.83)$$

and the derivative towards μ does not appear since $d\mu/dt = 0$.

The equations will be formulated in the comoving system of a toroidally rotating plasma, the transformation to the comoving frame introduces a background centrifugal potential Φ . Similarly, the ordering for the background (Φ) and perturbed (ϕ) electrostatic potential is

$$\phi \approx \rho_* \Phi \quad \nabla_{\perp} \phi \approx \nabla_{\perp} \Phi \quad \nabla_{\parallel} \phi \approx \rho_* \nabla_{\parallel} \Phi \quad (1.84)$$

with

$$\Phi \approx T/e \quad \phi \approx \rho_* T/e \quad (1.85)$$

where these last ordering relations are due to the linearization of the electron Boltzmann response.

1.6.2 The local limit approximation

The separation of spatial scales presented above, allows to evaluate the equations in the local limit approximation [15] (note that only in the δf -approximation this limit can be applied, since only in this case the ordering relations hold).

The local limit approximation consists in simulating only a small region of the tokamak, in particular the domain is considered to be a thin tube containing a field line winding around a flux surface (in fact, it also called flux-tube approximation). Using the ordering expressed in Eq. (1.74), indicating with l_{\perp} the perpendicular extent of the simulated domain, the local limit approximation is formulated as the ordering relations

$$l_{\perp} \ll R \quad l_{\perp} \gg \rho \quad (1.86)$$

i.e. l_{\perp} is considered to be much smaller than the device size, but much bigger than the turbulence typical length scale.

The operative meaning of this local limit is that background quantities and their gradients are evaluated at the flux surface considered, thus they are considered to be constant over the perpendicular extent of the domain. The background gradients are therefore kept as linear drive terms. The physics due to profile variation is not included in this approximation, since parameters for only a single flux surface are used.

The main effect of the local limit approximation is that the local turbulence is homogeneous in the perpendicular plane, allowing periodic boundary conditions and Fourier decomposition to be used in the perpendicular directions, and an obvious simplification of globally varying quantities. The equations in the rest of this thesis will be formulated in the local limit approximation.

1.6.3 The gyro-kinetic equations

The equations here presented take into account eventual plasma rotation, and are formulated in the comoving frame rotating with the plasma, in toroidal geometry. The detailed derivation can be found in [4, 11].

The gyro-kinetic ordering allows to replace the particle distribution function $f_\alpha(\mathbf{x}, \mathbf{v}, t)$ by a guiding center distribution function $f_{\alpha,gc}(\mathbf{X}, v_\perp, v_\parallel, t)$, where \mathbf{X} is the position of the guiding center, v_\perp and v_\parallel are velocity coordinates perpendicular and parallel to the magnetic field. For guiding centers, the phase space has only five dimensions, since the guiding center velocities are defined by two velocity coordinates, the volume element in phase space is then given by

$$d\mathbf{x} d\mathbf{v} = d\mathbf{X} 2\pi v_\perp dv_\perp dv_\parallel = d\mathbf{X} 2\pi(m_\alpha/B)d\mu dv_\parallel \quad (1.87)$$

where the expression for the magnetic moment $\mu = m_\alpha v_\perp^2 / (2B)$ has been used in the last equality. This is a common choice in gyro-kinetic theory, since the magnetic moment is a relevant physical quantity which is conserved during the particle motion.

From now on, we will always refer to guiding center distribution functions, therefore the 'gc' subscript will be omitted.

The guiding center equations of motion

The guiding center equations of motion in the rotating frame can be obtained with the procedure shown in section 1.3 and more generally within the Lagrangian framework. They are given by

$$\begin{aligned} \frac{d\mathbf{X}}{dt} &= v_\parallel \mathbf{b} + \mathbf{v}_D + \mathbf{v}_\chi \\ mv_\parallel \frac{dv_\parallel}{dt} &= \frac{d\mathbf{X}}{dt} \cdot [Z\mathbf{E} - \mu\nabla B + m\Omega^2 R\nabla R] \\ \frac{d\mu}{dt} &= 0 \end{aligned} \quad (1.88)$$

where Z is the particle charge, R the local major radius, Ω the frame rotation frequency, \mathbf{E} is the gyro-averaged perturbed electric field plus the inertial electric field (background electric field due to the transformation to the rotating frame)

$$\mathbf{E} = -\nabla\chi - \nabla\Phi \quad (1.89)$$

with $\chi = \langle\phi\rangle$ the gyro-averaged electrostatic potential. The velocity \mathbf{v}_χ is the gyro-averaged $\mathbf{E} \times \mathbf{B}$ drift velocity, i.e.

$$\mathbf{v}_\chi = \frac{\mathbf{B} \times \nabla\chi}{B^2} . \quad (1.90)$$

The drifts due to the inhomogeneous magnetic field and inertial terms can be written in the form [4, 11]

$$\begin{aligned} \mathbf{v}_D = & \frac{1}{Z} \left(\frac{mv_\parallel^2}{B} + \mu \right) \frac{\mathbf{B} \times \nabla B}{B^2} + \frac{mv_\parallel^2}{2ZB} \beta' \mathbf{b} \times \nabla\psi \\ & + \frac{2mv_\parallel}{ZB} \boldsymbol{\Omega}_\perp + \frac{1}{ZB} \mathbf{b} \times \nabla\mathcal{E}_\Omega \end{aligned} \quad (1.91)$$

where ψ is the radial coordinate (i.e. the flux surface label, already defined in Eq. (1.28)), $\boldsymbol{\Omega}_\perp$ is the angular (toroidal) rotation vector perpendicular to the magnetic field. The first term on the right is the combination of the grad-B and curvature drift in the low β approximation, whereas the second term, involving

$$\beta' = \frac{2\mu_0}{B^2} \frac{\partial p}{\partial\psi} \quad (1.92)$$

is the correction to the curvature drift due to the modification of the equilibrium associated with the pressure gradient. The penultimate term is the Coriolis drift [16]. The last term combines the centrifugal drift and background potential in the (species dependent) centrifugal energy

$$\mathcal{E}_\Omega = Z\Phi - \frac{1}{2}m\Omega^2(R^2 - R_0^2) \quad (1.93)$$

where R_0 is the radius of the magnetic axis.

The gyro-kinetic Vlasov-Maxwell equations

The results presented in this section can be found in [5]. The Vlasov equation for the total one particle distribution function in guiding center coordinates is given by

$$\frac{\partial f_{tot}}{\partial t} + \frac{d\mathbf{X}}{dt} \cdot \nabla f_{tot} + \frac{dv_\parallel}{dt} \frac{\partial f_{tot}}{\partial v_\parallel} = 0 . \quad (1.94)$$

Employing the δf -approximation, as already mentioned, the distribution function is written as $f_{tot} = F + f$ with F a background equilibrium distribution and f a perturbation of order ρ_* to the equilibrium. The Vlasov

equation can be therefore expanded order by order in ρ_* to obtain the equations for the equilibrium and the perturbation. For the purpose of this thesis, an expansion to first order in ρ_* is necessary (with the exception of the polarisation which enters in the field equations).

The equilibrium equation (zeroth order in ρ_*) for F is given by

$$v_{\parallel} \mathbf{b} \cdot \nabla F - \frac{1}{m} \mathbf{b} \cdot [Z \nabla \Phi + \mu \nabla B - m \Omega^2 R \nabla R] \frac{\partial F}{\partial v_{\parallel}} = 0 \quad (1.95)$$

solution of this equation gives the background equilibrium distribution as a Maxwellian written in the form

$$F = F_M = \frac{n_{R_0}}{(2\pi T/m)^{3/2}} \exp \left[-\frac{m(v_{\parallel} - u_{\parallel})^2/2 + \mu B + \mathcal{E}_{\Omega}}{T} \right] \quad (1.96)$$

where n_{R_0} is an integration constant chosen to be the density at $R = R_0$, $u_{\parallel} = (RB_t/B)[\omega_{\phi}(\psi) - \Omega]$, with B_t toroidal component of the magnetic field, is the radial dependent mean parallel velocity flow relative to the comoving frame. The equations are formulated with $\Omega = \omega_{\phi}$ at the flux surface considered. Therefore $u_{\parallel} = 0$ however, it is kept in writing the Maxwellian since it has a finite radial gradient which will appear in the equations as $\nabla \omega_{\phi}$.

The equation for f (first order in ρ_*) can then be written in the form

$$\frac{\partial f}{\partial t} + (v_{\parallel} \mathbf{b} + \mathbf{v}_D + \mathbf{v}_{\chi}) \cdot \nabla f + \frac{\mathbf{b}}{m} \cdot (\mu \nabla B + \nabla \mathcal{E}_{\Omega}) \frac{\partial f}{\partial v_{\parallel}} = S \quad (1.97)$$

where S is determined by the form of F , in particular we have

$$S = -(\mathbf{v}_{\chi} + \mathbf{v}_D) \cdot \nabla_p F_M - \frac{Z}{T} F_M [v_{\parallel} \mathbf{b} + \mathbf{v}_D] \cdot \nabla \chi \quad (1.98)$$

with

$$\begin{aligned} \nabla_p F_M = & \left[\frac{\nabla n_0}{n_0} + \left(\frac{mv_{\parallel}^2/2 + \mu B + \mathcal{E}_{\Omega}}{T} - \frac{3}{2} \right) \frac{\nabla T}{T} \right. \\ & \left. + \left(\frac{mv_{\parallel} RB_t}{TB} + \frac{m\Omega}{T} (R^2 - R_0^2) \right) \nabla \omega_{\phi} \right] F_M . \end{aligned} \quad (1.99)$$

Note that in Eq. (1.97), because of the ordering Eq. (1.83), the parallel velocity nonlinearity (combinations of the electrostatic field perturbation and the velocity space derivative of the perturbed distribution) is neglected.

The electric and magnetic fields have to be calculated self-consistently from the Maxwell equations. In the case treated here, i.e. the electrostatic limit in the low β approximation, the magnetic field is a background equilibrium quantity (no magnetic field perturbations), therefore only the Poisson

equation is needed. The ordering relation relating the gyro-radius and the Debye length given in Eq. (1.74) allows to replace the Poisson equation with the quasi-neutrality condition

$$\sum_s Z_s n_s(\mathbf{x}) = 0 \quad (1.100)$$

where the sum runs over the species in the plasma. This equation is valid for all cases in which the scale lengths are larger than the Debye length. The quasi-neutrality equation always replaces the Poisson equation as an approximation, i.e. when using the quasi-neutrality equation one can no longer use the Poisson equation to calculate the field. In fact, given a zero charge density, the solution of the Poisson equation would not give the consistent electric field produced by the plasma particles.

The replacement of the Poisson equation with the quasi-neutrality condition simplifies the calculation (there is no need to solve a partial differential equation), however care has to be taken in treating Eq. (1.100). Note that \mathbf{x} is not the guiding centers position, but is the actual particles position in physical phase space. The difference between the actual density and the density of guiding centers at a given point is due to the average variation in the electrostatic potential over a gyro-orbit. This can also be understood as the consequence of the polarisation drift averaged over the gyro-orbit time scale. In the context of a variational principle derivation of the fields equation [11], one sees that the polarization term is due to higher order (ρ_*^2) field terms, which have to be included in the Hamiltonian in order to guarantee energy consistency. The final form of Eq. (1.100) is given by

$$\sum_s \int d^3\mathbf{v} \left[Z_s G(f_s) + \frac{Z_s^2 F_M}{T_s} (G^2(\phi) - \phi) \right] = 0 \quad (1.101)$$

where G indicates the gyro-average operator ($G(\phi) = \langle \phi \rangle$).

1.6.4 The GKW code

The GKW (Gyro-Kinetics at Warwick) code [4, 5, 6] is a code for the simulation of microinstabilities and turbulence in a magnetically confined plasma. It solves the gyro-kinetic equations presented above on a fixed grid in the 5-dimensional space using a combination of finite difference and pseudo spectral methods. The code is coupled to the MHD equilibrium solver CHEASE [17] for the calculation of the magnetic field configuration.

Normalizations

All quantities in the code are normalised. The velocity will be normalised by the thermal velocity of each species. Quantities like the electrostatic

potential, which is species independent, are normalized by a reference temperature.

We define a reference mass m_{ref} , a reference thermal velocity v_{thref} , a reference density n_{ref} , a reference temperature T_{ref} , a reference magnetic field B_{ref} evaluated on the magnetic axis, and a reference major radius R_{ref} . These are related by

$$T_{\text{ref}} = \frac{1}{2} m_{\text{ref}} v_{\text{thref}}^2 \quad \rho_{\text{ref}} = \frac{m_{\text{ref}} v_{\text{thref}}}{e B_{\text{ref}}} . \quad (1.102)$$

Furthermore we define a normalised Larmor radius as

$$\rho_* = \rho_{\text{ref}} / R_{\text{ref}} . \quad (1.103)$$

The reference values are used to define, for each species, a dimensionless mass m_R , thermal velocity v_R , density n_R , temperature T_R , and centrifugal energy \mathcal{E}_R

$$\begin{aligned} m_R &= \frac{m}{m_{\text{ref}}} & v_R &= \frac{v_{\text{th}}}{v_{\text{thref}}} & n_R &= \frac{n_{R0}}{n_{\text{ref}}} \\ T_R &= \frac{T}{T_{\text{ref}}} & \mathcal{E}_R &= \frac{\mathcal{E}_\Omega}{T_R T_{\text{ref}}} . \end{aligned} \quad (1.104)$$

The fields are normalised using the reference values as

$$\phi = \rho_* \frac{T_{\text{ref}}}{e} \phi_N \quad \chi = \rho_* \frac{T_{\text{ref}}}{e} \chi_N \quad \Phi = \frac{T_{\text{ref}}}{e} \Phi_N . \quad (1.105)$$

The index N refers to a normalised quantity. Factors of ρ_* have been added in the definitions of the normalised perturbed fields, such that the normalised quantities are of order 1 in ρ_* .

Time t , magnetic field B , angular rotation frequency Ω , and the major radius R , are made normalised as

$$\begin{aligned} t &= R_{\text{ref}} t_N / v_{\text{thref}} & B &= B_{\text{ref}} B_N \\ \Omega &= v_{\text{thref}} \Omega_N / R_{\text{ref}} & R &= R_{\text{ref}} R_N . \end{aligned} \quad (1.106)$$

For the velocity space coordinates it is

$$v_{\parallel} = v_{\parallel N} v_{\text{th}} \quad \mu = \frac{m v_{\text{th}}^2}{B_{\text{ref}}} \mu_N . \quad (1.107)$$

The distribution functions are normalised according to

$$f = \rho_* \frac{n_{R0}}{v_{\text{th}}^3} f_N \quad F_M = \frac{n_{R0}}{v_{\text{th}}^3} F_{MN} . \quad (1.108)$$

For the gradient of density, temperature and plasma rotation the normalisations are

$$\begin{aligned} \frac{1}{L_{n,N}} = \frac{R_{\text{ref}}}{L_n} = -\frac{1}{n_{R_0}} \frac{\partial n_{R_0}}{\partial \psi} \quad \frac{1}{L_{T,N}} = \frac{R_{\text{ref}}}{L_T} = -\frac{1}{T} \frac{\partial T}{\partial \psi} \\ u'_N = -\frac{R_{\text{ref}}}{v_{\text{thref}}} \frac{\partial \omega_\phi}{\partial \psi}. \end{aligned} \quad (1.109)$$

The radial coordinate ψ is normalised as

$$\psi = \frac{R_{\text{max}} - R_{\text{min}}}{2R_{\text{ref}}}, \quad (1.110)$$

where R_{max} (R_{min}) is the maximum (minimum) major radius of the flux surface. All gradients are normalised using the major radius R_{ref} , i.e.

$$\nabla = \frac{1}{R_{\text{ref}}} \nabla_N. \quad (1.111)$$

The poloidal flux Ψ is normalised according to

$$\Psi = R_{\text{ref}}^2 B_{\text{ref}} \Psi_N. \quad (1.112)$$

Although β is dimensionless, in the code, a different dimensionless beta (β_N) is defined in the form

$$\beta_N = \frac{n_{\text{ref}} T_{\text{ref}}}{B_{\text{ref}}^2 / 2\mu_0}. \quad (1.113)$$

The wave vectors introduced in the spectral representation arise from the perpendicular gradient of a fluctuating quantity and are therefore normalised to ρ_{ref} as

$$k = \frac{k_N}{\rho_{\text{ref}}}. \quad (1.114)$$

In all the following sections we will use only the normalised quantities, the index N is then dropped.

Field aligned Hamada coordinates

The equations in GKW are formulated in a particular coordinates system called field aligned Hamada coordinates. Quantities like the potential In the following, the transformation from an orthogonal coordinate system to the Hamada coordinates is discussed.

We indicate cartesian coordinates with latin indices so $\{x^i\} = (x, y, z)$ and the metric tensor can be written as

$$g_{ij} = \text{diag}(1, 1, 1). \quad (1.115)$$

We refer to other coordinate systems with greek indices. The element of length ds^2 is an invariant, so we have

$$ds^2 = g_{ij}dx^i dx^j = g_{\alpha\beta}dx^\alpha dx^\beta \quad (1.116)$$

from which we get the metric tensor in a generic coordinate system

$$g_{\alpha\beta} = g_{ij} \frac{\partial x^i}{\partial x^\alpha} \frac{\partial x^j}{\partial x^\beta} = \frac{\partial x^i}{\partial x^\alpha} \frac{\partial x_i}{\partial x^\beta}, \quad (1.117)$$

and its inverse

$$g^{\alpha\beta} = \frac{\partial x^\alpha}{\partial x^i} \frac{\partial x^\beta}{\partial x_i}. \quad (1.118)$$

The contravariant components of a vector \mathbf{v} are written as

$$v^\alpha = \mathbf{v} \cdot \nabla x^\alpha \quad (1.119)$$

which under a change of coordinates $\{x^\alpha\} \rightarrow \{z^\alpha\}$ transform as

$$v_z^\alpha = \frac{\partial z^\alpha}{\partial x^\beta} v_x^\beta = \Lambda^\alpha_\beta v_x^\beta \quad (1.120)$$

where the lower indices of the vector components refer to the coordinate systems.

We start with an arbitrarily shaped, but toroidally symmetric geometry. We assume that we have an orthogonal coordinate system $\{x^\alpha\} = (\psi, \theta, \phi)$, where ψ is the radial coordinate, i.e.

$$\mathbf{B} \cdot \nabla \psi = 0, \quad (1.121)$$

and so from (1.119) we get

$$B^\psi = 0, \quad (1.122)$$

θ is the poloidal angle (upward on the outboard midplane) and ϕ is the toroidal angle (clockwise when viewed from above).

We require a coordinate system which is advantageous to turbulence study, which will exploit that parallel and perpendicular dynamics are decoupled in the gyro-kinetic equation, so that when we build the gridpoints for the numerical calculations we can use long scale distances along the magnetic field direction and short scale distances in the direction perpendicular to the magnetic field.

We have to perform a coordinate transformation

$$\{x^\alpha\} = (\psi, \theta, \phi) \rightarrow \{z^\alpha\} = (\psi, s, \zeta), \quad (1.123)$$

that will make the field lines straight in the new coordinates and that will align one of the coordinates (s) with the magnetic field. Toroidal symmetry

has to be evident in the new coordinate system so there must be one ignorable coordinate (ζ) associated with the toroidal angle such that if a function is independent of ϕ will be independent of ζ .

To perform the transformation (1.123) we have to go through two subsequent transformations. The first is given by

$$\{x^\alpha\} = (\psi, \theta, \phi) \rightarrow \{y^\alpha\} = (\psi, s, \gamma) , \quad (1.124)$$

where

$$s = s(\psi, \theta) \quad \gamma = \gamma(\psi, \theta, \phi) , \quad (1.125)$$

note that γ is an ignorable coordinate: inverting the transformation we have $\theta = \theta(\psi, s)$ and so $f(\psi, \theta) \rightarrow f(\psi, s)$.

We choose the contravariant components of the magnetic field in the coordinate system $\{y^\alpha\}$ to be flux functions, i.e.

$$B^s = B^s(\psi) \quad B^\gamma = B^\gamma(\psi) , \quad (1.126)$$

so from the field line equation it follows that on a field line we have

$$\frac{d\gamma}{ds} = \frac{B^\gamma}{B^s} = q(\psi) = \text{const} , \quad (1.127)$$

where $q(\psi)$ is the safety factor. The equation (1.127) means that in the coordinate system $\{y^\alpha\}$ we have straight field lines, these coordinates are known as Hamada coordinates. Note that the magnetic field components are flux functions so they don't change over a flux surface, but the magnetic field strength depends on the poloidal angle, infact we have

$$B^2 = g_{\alpha\beta} B^\alpha B^\beta , \quad (1.128)$$

where $g_{\alpha\beta}$ is not a flux function and so

$$B^2 = B^2(\psi, \theta) . \quad (1.129)$$

The explicit expression of the transformation (1.125) is given by

$$\begin{aligned} s(\psi, \theta) &= \int_0^\theta \frac{d\theta'}{\mathbf{B} \cdot \nabla\theta'} \Big/ \oint \frac{d\theta'}{\mathbf{B} \cdot \nabla\theta'} \\ \gamma(\psi, \theta, \phi) &= \frac{\phi}{2\pi} + \frac{F}{2\pi} \int_0^\theta \frac{d\theta'}{\mathbf{B} \cdot \nabla\theta'} \left[\left\{ \frac{1}{R^2} \right\} - \frac{1}{R^2} \right] , \end{aligned} \quad (1.130)$$

where $s \in [-1/2, 1/2]$ corresponds to one poloidal turn, $\gamma \in [0, 1]$ corresponds to one toroidal turn, $F = RB_t$ with R local major radius and B_t toroidal component of the magnetic field, and $\{\cdot\}$ is the flux surface average that for a generic function $g = g(\psi, \theta)$ is given by

$$\{g\} = \lim_{\delta\psi \rightarrow 0} \frac{1}{V} \int_V d^3\mathbf{x} g = \oint ds g , \quad (1.131)$$

where $\delta\psi$ and V are the 'radial' distance and the volume between two flux surfaces, and the last integral is to be taken at constant ψ .

We perform now the second transformation

$$\{y^\alpha\} = (\psi, s, \gamma) \rightarrow \{z^\alpha\} = (\psi, s, \zeta) , \quad (1.132)$$

where

$$\zeta = \zeta(\psi, s, \gamma) , \quad (1.133)$$

note that ζ as γ is an ignorable coordinate. We choose to align the coordinate s with the magnetic field, so we demand that

$$\mathbf{B} \cdot \nabla = B^s \frac{\partial}{\partial s} + B^\zeta \frac{\partial}{\partial \zeta} = B^s \frac{\partial}{\partial s} , \quad (1.134)$$

which corresponds to the choice

$$B^\zeta = 0 . \quad (1.135)$$

The latter condition can be formulated as

$$B_z^\zeta = \Lambda^\zeta_\beta B_y^\beta = \frac{\partial \zeta}{\partial s} B_y^s + \frac{\partial \zeta}{\partial \gamma} B_y^\gamma = \mathbf{B} \cdot \nabla \zeta = 0 , \quad (1.136)$$

where we have used (1.120) for the transformation (1.132). It should be found that (1.136) is satisfied for the simple linear transformation

$$\zeta = qs - \gamma , \quad (1.137)$$

where q is given by (1.127).

From the field line equation and using (1.135) it follows that on a field line we have

$$\frac{d\zeta}{ds} = \frac{B^\zeta}{B^s} = 0 , \quad (1.138)$$

which means that in the coordinate system $\{z^\alpha\}$ we have straight field lines over which ζ is constant, these are the field aligned Hamada coordinates.

The ballooning representation

The GKW code can solve the gyro-kinetic equations in the local limit (see section 1.6.2) in which only a small region is simulated (flux tube approximation). The natural technique for problems with disparate length scales is the eikonal or WKB analysis. In the case of the analytic linear treatment of a single mode, such as drift wave, which has large extension $k_\parallel \ll k_\perp$ along the magnetic field line is often used the *ballooning representation*. The combination of field aligned coordinates, spectral representation and parallel boundary condition (Eq. (3.53) of [11]) used in GKW give a formulation equivalent to the ballooning representation. In this formalism the

toroidal perturbed solutions of the gyro-kinetic equation are represented in an eikonal basis $f_n^{(0)}$ which contains any rapid spatial variation perpendicular to the field. By assumption, an eikonal must satisfy $\mathbf{B} \cdot \nabla f_n^{(0)} = 0$. In toroidal coordinates (ψ, θ, ϕ) and large aspect ratio ($r/R \ll 1$), assuming solution of the form $f_n^{(0)} = l(\theta) \exp[in\phi]$ and applying the condition of toroidal periodicity leads to the eikonal basis

$$f_n^{(0)} = \exp \{in [\phi - q(\theta + \theta_0)]\} \quad (1.139)$$

where n is an integer representing the toroidal mode number and θ_0 is a constant of integration representing the poloidal angle at which the mode is at its maximum. Since all perpendicular variation are contained in $f_n^{(0)}$, a perpendicular wave vector $\mathbf{k}_{\perp,n}$ may be defined by analogy with the Fourier basis to satisfy $\nabla f_n^{(0)} = i\mathbf{k}_{\perp,n} f_n^{(0)}$. Hence from (1.139) one finds

$$\mathbf{k}_{\perp,n} = k_{\theta,n} \mathbf{e}_\theta + k_{\psi,n} \mathbf{e}_\psi = -\frac{nq}{\psi} [\psi \nabla \theta + \hat{s} \nabla \psi (\theta - \theta_0)] \quad (1.140)$$

since $|\nabla \phi| = 1/R$, $|\nabla \theta| = 1/r$ and the definition of the magnetic shear $\hat{s} = (\psi/q) \partial q / \partial \psi$ has been used. From (1.140) one finds

$$k_{\theta,n} = -\frac{nq}{r} \quad k_{\psi,n}(\theta) = \hat{s}\theta k_{\theta,n} + k_{\psi_0,n} \quad (1.141)$$

where $k_{\psi_0,n} = \hat{s}\theta_0 nq/r$ is the radial wavenumber at $\theta = \theta_0$. The shear in the magnetic field creates a rotation in the perpendicular structure of the mode. The ballooning representation can be thought of as a *ballooning transform* analogous to the Fourier transform which can represent an arbitrary function in a nonlinear system. The ballooning representation can also be extended to treat radial profile variations. The global solutions are linear combinations of the local ballooning modes.

The non-spectral representation

The work presented in this thesis is focused on the transition from a local description towards a global description of a tokamak plasma. The latter refers to simulation of large region of the tokamak, which therefore need to include profiles effect, i.e. variation of the physical quantities in the plane perpendicular to the magnetic field. In particular, since the geometry is considered to be axisymmetric, global effects are due to the introduction of radial profiles. In order to describe this kind of scenario, it is strictly necessary not to use Fourier decomposition when representing the radial dependence of the quantities of interest (in fact, this is the case of the local limit approximation, in which background quantities are kept constant over the radial domain and the turbulence is homogeneous in the perpendicular plane). Instead, a finite differences method must necessarily be applied

(these are the quasi-local simulations mentioned in the first section of this chapter). The GW code allows for this treatment. In the rest of this thesis, this version of the code will be referred to as the 'non-spectral representation'.

Chapter 2

ITG instability at sub-Larmor radius scales with non-zero ballooning angle

Linear gyro-kinetic stability calculations predict unstable toroidal Ion Temperature Gradient (ITG) modes with normalised poloidal wave vectors well above one ($k_\theta \rho_i > 1$) for standard tokamak parameters with adiabatic electron response. These modes have a maximum amplitude at a poloidal angle θ that is shifted away from the low field side ($\theta \neq 0$). In this chapter the physical mechanism is clarified through the use of a fluid model. It is shown that the shift of the mode away from the low field side reduces the effective drift frequency which allows for the instability to develop. Numerical tests using the gyro-kinetic model confirm this physical mechanism. Furthermore it is shown that modes localized away from the low field side can be important also for $k_\theta \rho_i < 1$ close to the threshold of the ITG. In fact, modes with maximum amplitude at $\theta \neq 0$ can exist for normalised temperature gradient lengths below the threshold of the ITG obtained for the case with the maximum at $\theta = 0$.

2.1 Introduction

The growth rate of the ion temperature gradient mode (ITG) as a function of the normalised poloidal wave vector $k_\theta \rho_i$, has been reported many times in the literature, see for instance [18], as a bell shaped curve with a single maximum. Here, k_θ is the poloidal component of the wave vector and $\rho_i = m_i v_{thi} / ZeB = \sqrt{2m_i T_i} / ZeB$ is the ion Larmor radius, with m_i the ion mass, v_{thi} the ion thermal velocity, Z the charge number, e the elementary charge,

B the magnetic field strength, and T_i the ion temperature.

In this chapter we report on collisionless ITG instabilities with $k_\theta \rho_i > 1$ and adiabatic electrons. It will be shown that these instabilities can exist for relevant tokamak parameters. The physical mechanism of these instabilities will be shown to be related to the reduction of the effective drift frequency through the shift of the mode away from the low field side position. This mechanism is different from those previously reported [19, 20, 21, 22, 23] with $k_\theta \rho_i > 1$, which are unstable only in a slab or for weak toroidicity.

This chapter is structured as follows: Section 2.2 introduces the high k_θ ITG through numerical simulation based on the gyro-kinetic model, Section 2.3 discusses the physics of the instability through the use of a simple fluid model. Section 2.4 discusses the relation with previously published work, and finally Section 2.5 gives the conclusions.

2.2 High k_θ ITG

In this chapter all simulations are performed using the local limit or flux tube approximation [15]. This limit considers a radial domain around a local flux surface that is sufficiently small such that all plasma as well as all geometry parameters can be taken to be uniform in the radial direction. The local limit allows for a spectral approach in the radial direction, and is equivalent to the ballooning transform [24] (the use of ballooning transform below is referred as the "spectral case") when only terms of lowest significant order in the normalized Larmor radius are considered. The ballooning transform, however, is often utilised in a restrictive manner, by choosing the radial wave vector zero at the low field side. A choice motivated by the observation that this usually yields the most unstable mode. An example of a calculation using this restrictive form of ballooning transform, obtained with the gyrokinetic code GKW [4, 5, 6], is given in Fig. 2.1 by the dash-dotted (blue 'x') curve that has a single maximum. The parameters of this, and all other simulations in this chapter, are those of the Waltz standard case [25]: ion temperature gradient length $R/L_T = 9.0$, density gradient length $R/L_N = 3.0$, electron and ion temperature $T_e = T_i$, safety factor $q = 2$, magnetic shear $\hat{s} = 1$, and inverse aspect ratio $\epsilon = 0.166$. The simulations use circular geometry [26] retaining finite ϵ effects, and the flux tube approximation is always applied.

However, GKW simulations with the radial direction described using finite differences (simulations that use finite difference in the radial direction below are referred to as the "non-spectral case") show a surprisingly different behaviour for $k_\theta \rho_i > 0.6$, displaying a spectrum with two maxima and having unstable modes with $k_\theta \rho_i$ well above one, as is shown by the full (black) line of Fig. 2.1. The dashed line (red circles) in this figure is obtained by choosing in the spectral runs the radial wave vector at the low field side

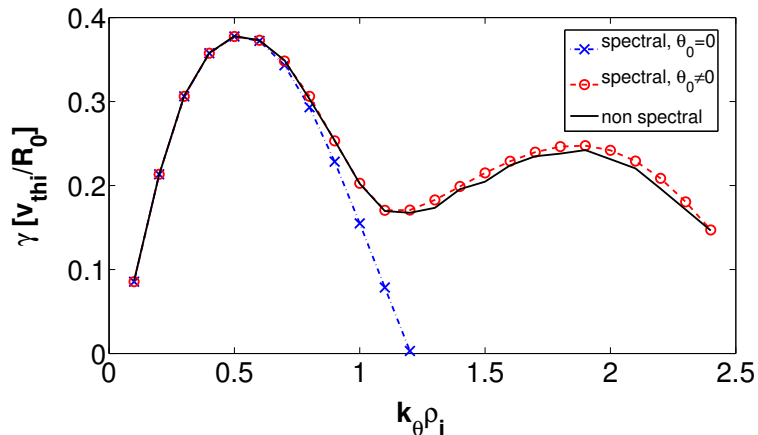


Figure 2.1: Growth rate (γ in units v_{thi}/R_0 where R_0 is the major radius of the magnetic axis) as a function of $k_\theta \rho_i$. The dash-dotted (blue 'x') line is the spectral case with $\theta_0 = 0$, the solid (black) line is the non-spectral case, and the dashed (red circles) line is the maximum growth rate obtained when varying θ_0 in the spectral case.

that maximises the growth rate. This radial wave vector happens to be not always zero. This will be explained in the following.

The essential difference between these two simulations is the number of radial modes that are kept. There are many more radial modes in the non-spectral case compared to the spectral one, in which the radial wave vector (k_r) is set by the condition of the field alignment of the mode [24]

$$k_r = \hat{s}\theta k_\theta , \quad (2.1)$$

which is zero at the low field side position (poloidal angle $\theta = 0$). This suggests that the unstable modes for $k_\theta \rho_i > 1$ have a finite radial wave vector at the low field side position. It is well known that a finite radial wave vector can be introduced in the ballooning transform through the introduction of the angle, θ_0 , such that

$$k_r = \hat{s}(\theta - \theta_0)k_\theta . \quad (2.2)$$

The growth rate as a function of θ_0 for various values of $k_\theta \rho_i$ is shown in Fig. 2.2. For $k_\theta \rho_i > 0.6$ the most unstable mode has a finite θ_0 and the mode is shifted away from the low field side, as shown in Fig. 2.3, which displays the eigenfunction along the magnetic field for $k_\theta \rho_i = 1.5$ and $\theta_0 = 1.2$. There is no preferred sign for θ_0 and the mode with $\theta_0 = -1.2$ is equally unstable but shifted in the negative θ direction. Taking the maximum growth rate (by varying θ_0) for each $k_\theta \rho_i$ from the spectral simulations yields the dashed (red circles) curve in Fig. 2.1. There is the expected agreement between the spectral and the non-spectral cases.

In order to get further insight into the high k_θ ITGs several parameter scans have been performed. These are done by varying one parameter while

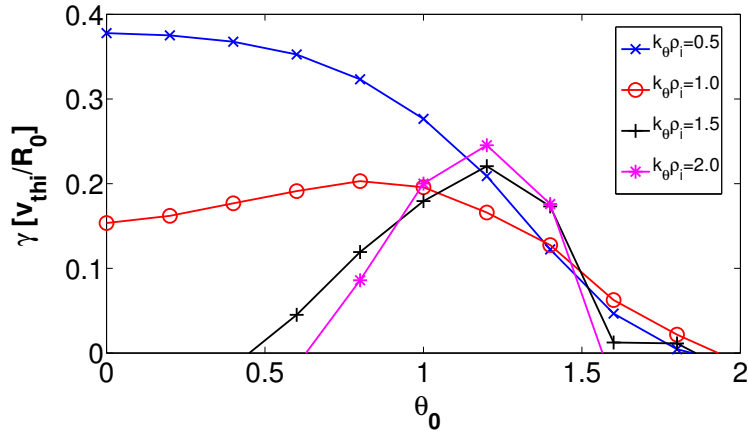


Figure 2.2: Growth rates of the spectral case (γ in units v_{thi}/R_0) as a function of θ_0 for four representative values of $k_\theta \rho_i$. The curves are denoted as follows: $k_\theta \rho_i = 0.5$ (blue 'x') crosses, $k_\theta \rho_i = 1.0$ (red circles) circles, $k_\theta \rho_i = 1.5$ (black '+') pluses, $k_\theta \rho_i = 2.0$ (magenta stars)

keeping all the other parameters fixed to the standard case. The results of the R/L_T , q and \hat{s} scans are shown in Figs. 2.4 and 2.5. All calculations are performed using the non-spectral setup with $k_\theta \rho_i = 1.9$. For comparison, the results for $k_\theta \rho_i = 0.5$ are also shown. Fig. 2.4 shows that the growth rate of the high k_θ ITG increases with R/L_T very similar to the $k_\theta \rho_i = 0.5$ mode. The mode has a higher threshold in R/L_T though it is more stable over the entire scan. In the same figure the dependence on the safety factor is also shown. A larger safety factor increases the connection length between the low and high field side increasing the time in which a perturbation propagates along the magnetic field line from the unfavourable curvature to the favourable curvature region. Therefore, increasing the safety factor has a destabilizing effect. This is the case for $k_\theta \rho_i = 0.5$, but to a much larger extent for the high k_θ ITG. The localisation of the mode at $\theta_0 \neq 0$ makes the requirement of a sufficient long field line length harder to satisfy.

Fig. 2.5 gives the value of the growth rate as a function of the magnetic shear. The growth rate curve has two maxima for $k_\theta \rho_i = 1.9$, and it can be verified from the figure of the frequency (right panel in Fig. 2.5) that these maxima belong to two different modes. For low magnetic shear the mode is found to reach its maximum amplitude at the low field side (standard ITG with $\theta_0 = 0$). Indeed the frequency of this mode is high, and its growth rate is rather small. For high magnetic shear the mode is shifted away from the low field side (maximum amplitude at $\theta_0 = 1.2$). A high growth rate is obtained only at sufficiently large shear. A high shear reduces the width in θ of the eigenmode and is therefore beneficial for the $\theta_0 \neq 0$ modes. As already pointed out, a large width in θ would mean that the mode has a

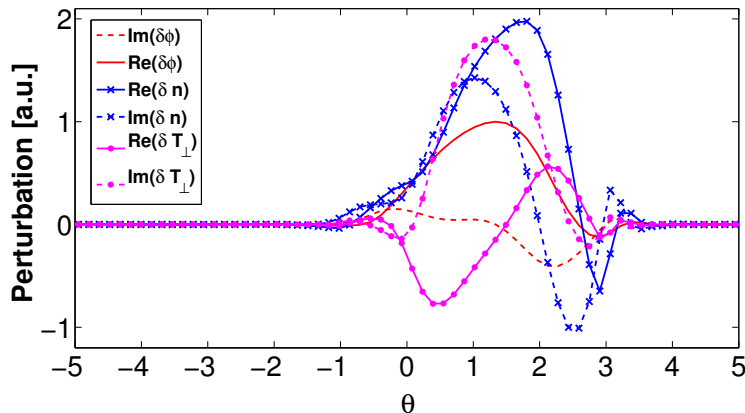


Figure 2.3: Eigenfunction in arbitrary units as a function of the poloidal angle θ . The figure is obtained from a spectral run with $k_\theta \rho_i = 1.5$ and $\theta_0 = 1.2$. Solid lines give the real, whereas dashed lines give the imaginary part. The (red) lines without symbols is the potential perturbation ($\delta\phi$), the (blue) lines with the symbol 'x' the density perturbation (δn), and the (magenta) lines with the closed circles is the perpendicular temperature perturbation (δT_\perp).

significant amplitude in the favourable curvature region, which is stabilizing. At constant R (drifts roughly constant), the dependence of the growth rate on the inverse aspect ratio ϵ (not shown) is found to be relatively weak.

2.3 Physical mechanism

An understanding of the physics of the high k_θ ITGs can be obtained by considering a simple fluid model. Here, the equations and normalisation given in section 1.6 are used, and the reader is referred to [5] for details on the derivation. The gyro-kinetic equation, neglecting the parallel derivatives can be written in the form (see Eq. (1.97)):

$$\frac{\partial f}{\partial t} + \mathbf{v}_D \cdot \nabla f = -\mathbf{v}_E \cdot \nabla_p F_M - \mathbf{v}_D \cdot \frac{Ze\nabla\langle\phi\rangle}{T} F_M \quad (2.3)$$

where \mathbf{v}_D is the drift due to the magnetic field inhomogeneity, \mathbf{v}_E is the perturbed $E \times B$ velocity, f the perturbed distribution function, ϕ the perturbed electrostatic potential, F_M is the Maxwell distribution Eq. (1.96), and ∇_p is defined through Eq. (1.99). In comparison to Ref. [5] the plasma rotation will be neglected, but it will not be assumed that the mode is localised on the low field side. Assuming a concentric circular magnetic equilibrium and small inverse aspect ratio we have

$$\mathbf{v}_D \cdot \nabla = iv_D k_\theta \cos \theta + iv_D k_r \sin \theta = ik_\theta v_D K \quad (2.4)$$

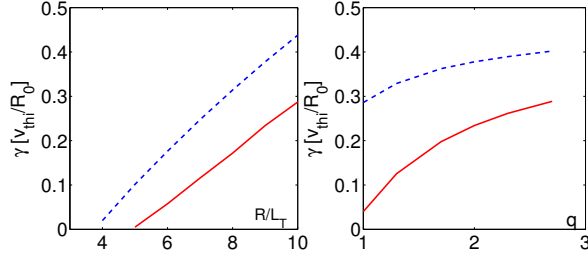


Figure 2.4: The growth rate as a function of R/L_T (left) and the safety factor q (right) for the non-spectral case. The (red) full line gives the result for $k_\theta \rho_i = 1.9$, while the (blue) dashed line gives the result for $k_\theta \rho_i = 0.5$.

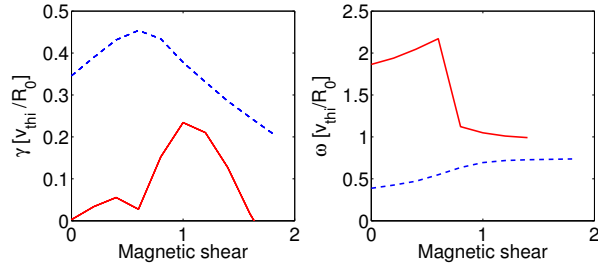


Figure 2.5: The growth rate (left) and frequency (right) as a function of the magnetic shear for the non-spectral case. The (red) full line gives the result for $k_\theta \rho_i = 1.9$, while the (blue) dashed line gives the result for $k_\theta \rho_i = 0.5$.

where θ is the poloidal angle, and k_θ (k_r) is the poloidal (radial) wave vector. In the equation above K is introduced to shorten the mathematics. Using Eq. (2.2) one obtains

$$K = \cos \theta + \hat{s}(\theta - \theta_0) \sin \theta . \quad (2.5)$$

K measures the dependence of the convective derivative ($\mathbf{v}_D \cdot \nabla$) on the poloidal angle.

Starting from Eq. (2.3) one can follow the same procedure as outlined in Ref. [5] to obtain the equations for the perturbed density (\tilde{n}) normalised to the background density, and perturbed temperature (\tilde{T}) normalised to the background temperature. For singly charged ions, neglecting the plasma rotation the expressions are

$$\omega \tilde{n} + 2K \tilde{n} + 2K \tilde{T} = \langle \tilde{\phi} \rangle \left(\frac{R}{L_N} - 2K \right) \quad (2.6)$$

$$\omega \tilde{T} + \frac{4}{3} K \tilde{n} + \frac{14}{3} K \tilde{T} = \langle \tilde{\phi} \rangle \left(\frac{R}{L_T} - \frac{4}{3} K \right) \quad (2.7)$$

where ω is the frequency normalised to the drift frequency $\omega_D = -k_\theta T/eBR$, and $\tilde{\phi}$ here is the perturbed electrostatic potential normalised with e/T . Note that all terms that are due to the drift are proportional to K . We will therefore refer to $\omega_D^* = \omega_D K$ as the effective drift frequency.

The angle brackets in the equation above denote the gyro-average, or FLR effects, which will be modelled using the approximation

$$\langle \tilde{\phi} \rangle = \frac{\tilde{\phi}}{1 + (k_\perp \rho_i)^2/2} = F\tilde{\phi} \quad (2.8)$$

where F has been introduced to shorten the notation. Finally, the gyrokinetic Poisson equation is solved assuming adiabatic electrons

$$\tilde{n} = \left(1 + \frac{1}{2}k_\perp^2 \rho_i^2\right) \tilde{\phi} = G\tilde{\phi} \quad (2.9)$$

where the term proportional to k_\perp^2 is due to the polarization.

From the equations above, a dispersion relation can be derived of the form:

$$A \left(\frac{\omega}{K}\right)^2 + B \frac{\omega}{K} + C = 0 \quad (2.10)$$

where

$$A = G \quad (2.11)$$

$$B = \frac{20}{3}G + 2F - \frac{F}{K} \frac{R}{L_N} \quad (2.12)$$

$$C = \frac{20}{3}(F + G) + 2\frac{F}{K} \frac{R}{L_T} - \frac{14}{3} \frac{F}{K} \frac{R}{L_N} \quad (2.13)$$

The growth rate (γ) normalised to $|\omega_D|$ can be readily calculated

$$\gamma = \frac{\sqrt{2K}}{G} \sqrt{\frac{R}{L_T} - K \frac{R}{L_{Tcrit}}} \quad (2.14)$$

where the critical gradient is given by

$$\frac{R}{L_{Tcrit}} = \frac{1}{8}B^2 - \frac{10}{3}(1 + G^2) + \frac{7}{3} \frac{1}{K} \frac{R}{L_N} \quad (2.15)$$

and we have used $FG = 1$.

Fig. 2.6 shows the growth rate, normalised to $|\omega_D|$, of the fluid model as a function of θ for three values of $\theta_0 = 0, 0.5, 1.0$. The left panel shows the results for $k_\theta \rho_i = 0.5$, whereas the right panel shows the results for $k_\theta \rho_i = 1.3$. It can be seen that for $k_\theta \rho_i = 0.5$ the mode has a maximum growth rate for $\theta = 0$, whereas for $k_\theta \rho_i = 1.3$ the mode with $\theta_0 = 0$ is stable and the most unstable mode occurs in the case $\theta_0 = 1.0$ with maximum at $\theta \approx \theta_0$.

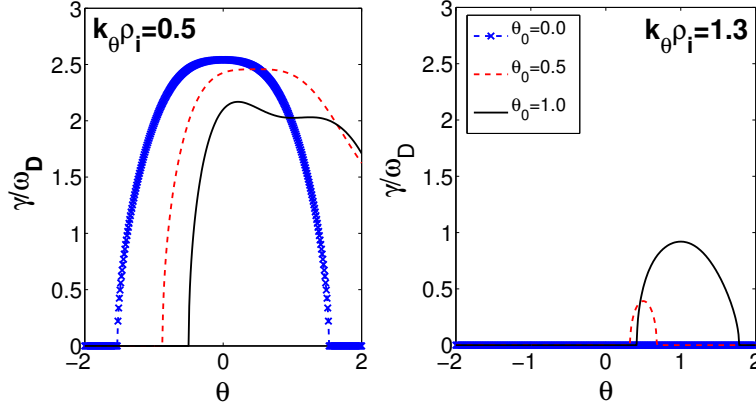


Figure 2.6: Growth rates of the fluid model as a function of θ for $\theta_0 = 0$ (blue dashed 'x'), $\theta_0 = 0.5$ (red dashed) and $\theta_0 = 1.0$ (black solid). The left panel gives the growth rates for $k_\theta \rho_i = 0.5$, whereas the right panel gives the results for $k_\theta \rho_i = 1.3$. The values of θ_0 as well as the curve labels are the same for both panels.

The figure of the growth rate shows that the largest growth rate at high $k_\theta \rho_i$ is obtained for $\theta \approx \theta_0$, i.e. for $k_r \approx 0$. Therefore, from now on the local growth rate of the fluid model at the location $\theta = \theta_0$ (at this location $k_r = 0$) is considered. The value of k_r does not increase the FLR and polarization stabilisation of the mode. Next, we clarify why the mode is strongly stabilised for $\theta_0 = 0$ and has its maximum growth rate for $\theta_0 \neq 0$. For $\theta \approx \theta_0$, $k_r = 0$ and $K = \cos \theta_0$. Therefore $K = 1$ at the low field side position ($\theta_0 = 0$) and decreases for $\theta_0 \neq 0$. Eq. (2.14) gives the dependence of the growth rate on K . If K , rather than θ_0 , is treated as a free parameter, and the density gradient is chosen to be zero for simplicity $R/L_N = 0$, then a maximum in the growth rate is obtained for

$$K_M = \frac{1}{2} \frac{R/L_T}{R/L_{Tcrit}} . \quad (2.16)$$

i.e. when $R/L_T > 2R/L_{Tcrit}$ a maximum growth rate is obtained for the low field side position whereas for $R/L_T < 2R/L_{Tcrit}$ the maximum growth rate will be obtained for $\theta_0 \neq 0$. As $k_\theta \rho_i$ is increased for fixed R/L_T , R/L_{Tcrit} increases, K_M decreases, and the mode shifts away from the low field side. The dependence of γ on K is shown in Fig. 2.7 for various values of $k_\theta \rho_i$. It can be seen that for $k_\theta \rho_i = 0.5$ the low field side position is the position for which the maximum is reached, while it is shifted away from the low field side for $k_\theta \rho_i > 1$.

The physical reason for a maximum in K can be understood as follows. The ITG generates ion temperature perturbations due to the perturbed ExB velocity in the background gradients (the term proportional to R/L_T on the

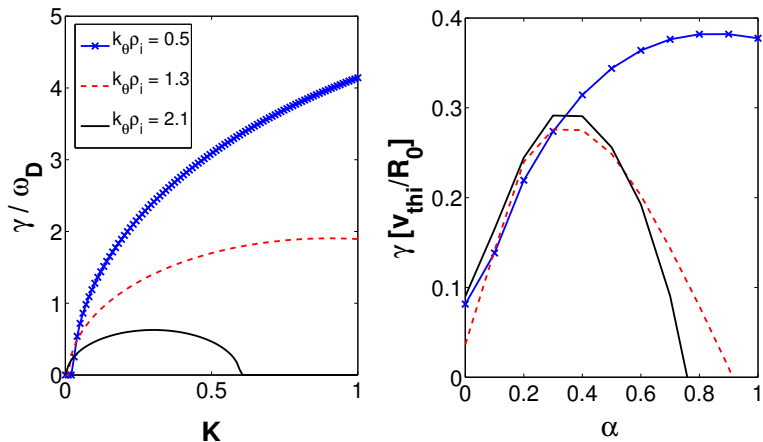


Figure 2.7: Left panel: Growth rates (normalised to $|\omega_D|$) of the fluid model as a function of K for $k_\theta \rho_i = 0.5$ (blue solid 'x'), $k_\theta \rho_i = 1.3$ (red dashed), and $k_\theta \rho_i = 2.1$ (black solid). Right panel: Growth rates (normalised to v_{thi}/R_0) of spectral gyro-kinetic simulations with $\theta_0 = 0$, with the drift multiplied with a constant α . The values of $k_\theta \rho_i$ as well as the curve labels are the same as that of the fluid model in the left panel.

right hand side of Eq. (2.7)). Since the drift (\mathbf{v}_D) is a function of the particle energy, the temperature perturbations generate density perturbations through the convection (the term $2KT$ on the left hand side of Eq. (2.6)). These ion density perturbations then lead to the generation of the electric field (Eq. (2.9)) which is responsible for the perturbed ExB velocity. For $K = 0$, the convection due to the drift is zero and the mode is stable. One might therefore expect that a higher K leads to a more unstable mode, and to some extent this is indeed the case, as it is clear from the $\sqrt{2K}$ in the expression for γ in Eq. (2.14). However, the Eqs. (2.6,2.7) also contain terms that have a stabilising effect: the change in kinetic energy of the ions due to the drift motion in the perturbed potential (the term $-4K/3\langle\phi\rangle$ on the right hand side of Eq. (2.7)), the temperature perturbations that are generated by the perturbed density perturbations (the term $4Kn/3$ on the left hand side of Eq. (2.7)), and the fact that density and temperature perturbations have a tendency to propagate with different phase velocities (more physics explanations using diagrams can be found in [11]). These stabilising terms are responsible for the threshold of the mode, and are all proportional to K . When the threshold is increased by FLR and polarization effects, and is close to R/L_T , the largest growth rate is obtained for $K < 1$, i.e. a mode shifted away from the low field side.

The fluid model is, of course, a strong simplification compared with the full gyro-kinetic model. The fluid model not only suggests that all instabilities close to the threshold would have their maximum growth rate away from the low field side, it also finds no threshold for the ITG, since for any finite

R/L_T , K can be chosen small enough that an instability arises. In particular the parallel dynamics (Landau damping) contained in the gyro-kinetic model must be considered. This stabilising mechanism is independent of K and can be expected to stabilise any instability for which K is too small. Nevertheless, if the explanation based on the fluid model is correct, its predictions should be qualitatively reproducible by the gyro-kinetic simulations. We discuss two tests below.

First, we calculate the growth rate from the fluid model for different values of $k_\theta \rho_i$, treating K as a free parameter rather than θ_0 (as we did in the derivation of Eq. (2.16)). The outcome for the Waltz standard case parameters is shown in the left panel of Fig. 2.7. Indeed the fluid model reproduces qualitatively the same result given by the gyro-kinetic simulations, as can be seen comparing Figs. 2.7 and 2.2. The fluid model suggests that the reduction of the effective drift frequency leads to an increase in the growth rate. To verify if the same physics mechanism is present also in the gyro-kinetic simulations, we can artificially multiply the drift velocity with a factor α ($0 \leq \alpha \leq 1$), in spectral simulations with $\theta_0 = 0$. This reduces the drift frequency and is as if we introduce the factor K of the fluid model into the gyro-kinetic simulations (with $\alpha = K$). The right panel of Fig. 2.7 shows the growth rates of the gyro-kinetic simulations as a function of α for the same values of $k_\theta \rho_i$ as the fluid model (shown in the left panel). The scan in α is performed in the spectral case with $\theta_0 = 0$. In this case there is no shift of the mode away from the low field side. For those modes that have a maximum growth rate when the mode is shifted away from the low field side, one expects the maximum growth rate for $\theta_0 = 0$ to be obtained for $\alpha < 1$, if the physics mechanism discussed above is correct. Indeed, the gyro-kinetic simulations at high $k_\theta \rho_i$ are stable for $\alpha = 1$ and have a maximum in the growth rate for $\alpha < 1$, qualitatively reproducing the fluid model.

Second, as discussed above, the mechanism is not limited to $k_\theta \rho_i > 1$. Close to the threshold, the most unstable mode can be expected to be shifted away from the low field side (provided the Landau damping is small enough). Fig. 2.8 shows the growth rate as a function of θ_0 of the Waltz standard case with $k_\theta \rho_i = 0.5$ for several values of R/L_T close to the threshold of the mode. Although the effect is small, the largest growth rate is obtained for $\theta_0 \neq 0$. In fact, for $R/L_T = 3.7$, an unstable mode exists for $\theta_0 \neq 0$ whereas the mode at $\theta_0 = 0$ is stable, i.e. a mode shifted away from the low field side exists for a temperature gradient length below the threshold of the ITG obtained for $\theta_0 = 0$. Both tests give confidence that the physical mechanism found through the analytic fluid model is indeed the reason for the observed behaviour of the gyro-kinetic simulations.

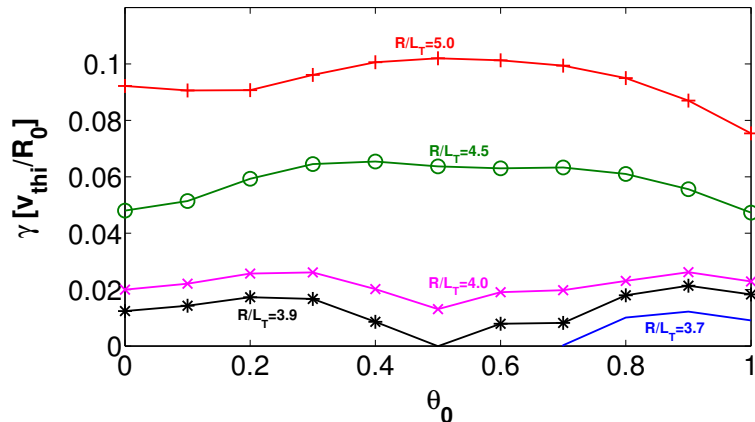


Figure 2.8: Growth rates as a function of θ_0 (spectral case) for the Waltz standard case with $k_\theta \rho_i = 0.5$, and $R/L_T = 3.7$ (blue no symbols), $R/L_T = 3.9$ (black stars), $R/L_T = 4.0$ (magenta 'x'), $R/L_T = 4.5$ (green open circles), and $R/L_T = 5.0$ (red '+').

2.4 Comparison with previous work

Ion temperature gradient instabilities at sub-Larmor radius scales have previously been reported in the literature [19, 20, 21, 22, 23]. These modes have been found in slab geometry, as well as in the case of weak toroidicity. The latter condition translates to a density gradient $R/L_N > 6$ for the instability to occur [20, 23]. Such a high gradient is not usually obtained in tokamak plasmas under normal operation. In contrast, the high $k_\theta \rho_i$ ITG described in this chapter occurs for a wide range of R/L_N as shown in Fig. 2.9, and is unstable for $R/L_N = 0$.

There are similarities between previous work and ours. In Refs. [19, 20] it is stressed that the non adiabatic response of the ions at $k_\theta \rho_i > 1$ is essential for the instability to occur. A similar statement can be made for the modes discussed in this chapter. However, the essential ingredient discussed in this chapter, the shift of the mode away from the low field side, reducing the effective drift frequency, is a distinct mechanism from that of the works published to date. In particular, an inspection of the equations in Refs. [19, 20, 22] shows that all these references assume $\theta_0 = 0$. We would like to point out that there are many numerical models [19, 20, 22, 23, 25, 27, 28, 29] that include the necessary physics to generate these shifted modes, and double humped structures in growth rate vs. k_θ have been observed on several occasions, even though the physics mechanism was not completely clarified.

2.5 Conclusion

In this chapter we have shown that:

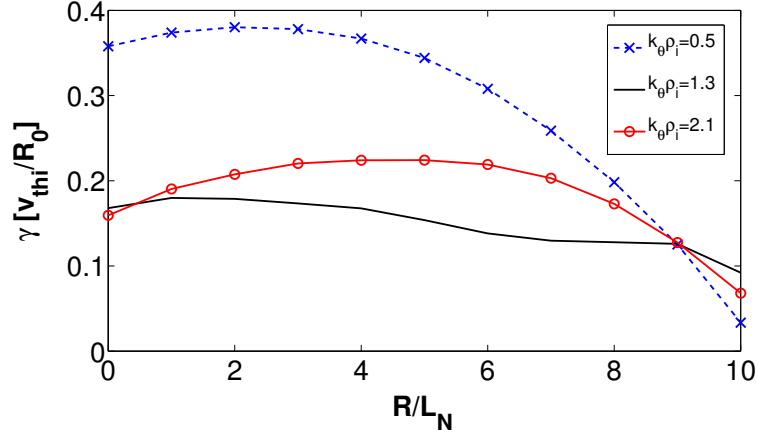


Figure 2.9: Growth rates as a function of R/L_N (non-spectral case) for $k_{\theta}\rho_i = 0.5$ (blue dashed 'x'), $k_{\theta}\rho_i = 1.3$ (black solid), and $k_{\theta}\rho_i = 2.1$ (red open circles).

- The ITG with adiabatic electrons for standard tokamak parameters can be unstable for $k_{\theta}\rho_i$ substantially larger than one.
- Essential for the instability at the parameters studied in this chapter is a reduction of the effective drift frequency through the shift of the mode away from the low field side.
- An enhancement of the growth rate through the reduction of the effective drift frequency can be important for $k_{\theta}\rho_i < 1$, in particular close to the mode threshold.
- Unstable modes with $\theta_0 \neq 0$ can exist for ion temperature gradient lengths below the threshold of the mode obtained with $\theta_0 = 0$.

The existence of these modes might set additional requirements on resolution in nonlinear runs, and might play a role in small scale zonal flow generation.

Chapter 3

On the radial propagation of turbulence in gyro-kinetic toroidal systems

In this chapter a conservation equation is derived for the radially dependent entropy in toroidal geometry using the local approximation of the gyro-kinetic equation. This naturally leads to an operative definition for the turbulence intensity. It is shown that the conservation equation can be split into two contributions, one describing the dynamics of the zonal modes and one for the non-zonal modes. In essence this chapter provides an operative tool for both analytic as well as numeric studies of the radial propagation of turbulence in tokamak plasmas.

3.1 Introduction

A detailed understanding of turbulent transport in magnetically confined plasmas is essential for the development of nuclear fusion devices. One of the key questions regards the relation between local and global model descriptions of plasma turbulence. A fundamental issue of the latter research area is understanding the role of the transport of turbulence intensity (turbulence spreading) that occurs in the global model, but is lacking in any local description. Several authors have considered this problem in the past. In [30] a fluid model is used to show that mode coupling provides an efficient mechanism for the radial propagation of turbulence in tokamaks. Furthermore, a conservation equation, for the evolution of the local intensity I of the turbulence, is given in [31] in the form of a Fisher-Kolmogorov equation [32, 33] with an inhomogeneous diffusion coefficient. In the case of weak turbulence (see [34]) it takes the form

$$\frac{\partial I}{\partial t} - \frac{\partial}{\partial \psi} \left[D(I) \frac{\partial I}{\partial \psi} \right] = \gamma I - k_{\perp}^2 I^2 . \quad (3.1)$$

An argument on the dynamics of turbulence spreading, which gives validity to this equation, can be found in [35, 36]. In the following we give a brief description of the terms that appear in the equation. The second term on the left hand side describes the spatial scattering of turbulence energy induced by non-linear coupling. The local turbulent diffusion coefficient $D(I) = D_0 I$ is considered to be proportional to the intensity itself. This as a key hypothesis of previous models, but which has to be derived from first principles. Infact, Eq. (3.1) physical interpretation relies on the flux term expression entirely. The local growth rate of the intensity is γ . The non-linear saturation of the turbulence is modelled by the non-linear damping term $-k_\perp^2 I^2$, where k_\perp is a suitably chosen scale of the turbulent fluctuations. The variable ψ is the radial coordinate, and t is the time.

Eq. (3.1) has been largely used by these and other authors (see for example [51] and [38]) to tackle the problem of turbulence spreading. It provides a very useful model for the discussion of turbulence spreading, but it is affected by some deficiencies. Although physically motivated, it is not derived from first principles. Indeed, the evolution of the local turbulence intensity defined as the squared modulus of the electrostatic potential can be shown not to satisfy a conservation equation of the form given. Furthermore the scaling of the diffusion coefficient $D = D_0 I$ itself cannot be derived. Therefore, numerical calculations can not be directly interpreted in terms of the dynamics described by this equation. Another point of concern is that there is no clear separation between turbulent and zonal intensity. With the latter we refer to the potential perturbation connected with the zonal ($n = 0$ toroidal) mode. It is not obvious if the turbulent intensity should contain (or not contain) the zonal contribution. The points raised above provide a motivation to investigate the possibility of deriving analytically a conservation equation of the form given by Eq. (3.1). In this chapter we undertake this task starting from the gyro-kinetic framework. The goal is to give a solid foundation to the discussion of turbulence spreading, and to derive analytic expressions for the form of the turbulent flux of turbulence intensity.

Our starting point is the choice of a quantity describing the intensity of the turbulence. A reasonable candidate is the entropy of the system, since the entropy is a measure of the departure from equilibrium, and the entropy satisfies a proper conservation equation. The idea of using the entropy to define the intensity of the turbulence has been already suggested in the literature, for instance in [39] where a balance equation for the entropy density is given starting from the drift kinetic equation in cylindrical geometry. Entropy conservation in gyro-kinetic toroidal system has already been extensively treated in the literature (see for instance [40, 41, 42, 43, 44, 45, 46]). In particular in this chapter we perform a calculation close to the one given in [45, 46] (which was performed for the case of the local limit approximation [15], considering the total entropy of the system, i.e. integrated over the entire computational domain), but we exclude the integral over the ra-

dial coordinate in order to explicitly keep track of the radial dependence of the perturbations. This procedure leads to an equation for the evolution of the radially dependent entropy of the system considered. The form of the conservation equation for the entropy leads naturally to an operative definition for the intensity of the turbulence and its conservation equation. Further analysis allow this equation to be split in two separate equations, one describing the dynamics of the turbulence intensity in the zonal ($n = 0$ toroidal) mode and the other the turbulence intensity in the perturbations (non-zonal $n \neq 0$ toroidal modes). The symmetry and simplicity of the resulting system of equations give a genuine insight into the connection between the dynamics of zonal and non-zonal modes.

3.2 Turbulence intensity balance in gyro-kinetic theory

In this section we derive the conservation equation for the radially dependent turbulence intensity of a collisionless plasma with no rotation, in the electrostatic case, for general toroidal geometry. The calculation is performed in the local limit approximation [15], in particular we consider the case in which background quantities do not vary across the perpendicular (to the magnetic field) extent of the domain, applying periodic boundary conditions in the binormal direction, excluding the integral over the radial coordinate. This choice, although it does not describe the most general case, allows to study the behaviour of radial inhomogeneities in the perturbations of the system.

We need an operative definition for the intensity of the turbulence, i.e. we look for a quantity which is radially dependent and satisfies a conservation equation in the form of Eq. (3.1), so that numerical results from gyro-kinetic simulations can then be properly interpreted in terms of the dynamics described by this equation. As already pointed out in the introduction, a natural candidate is the entropy of the system. We define the radially dependent entropy of the particles of the sp -species as

$$\epsilon_{sp} = - \int dx dv f_{sp}^{tot} \ln \frac{f_{sp}^{tot}}{F_M}, \quad (3.2)$$

the radially dependent entropy of all particles is obviously obtained taking the sum over all species. In Eq. (3.2) we have $dx dv = 2\pi(B/m_{sp})J ds d\zeta dv_{\parallel} d\mu$ with $J = \sqrt{g}$ the Jacobian of the transformation (g being the determinant of the metric tensor, m_{sp} the mass of the sp -species and B the background magnetic field strength) and $f_{sp}^{tot} = F_M + f_{sp}$ is the total distribution of the sp -species written as a sum of F_M , the equilibrium Maxwell distribution as given in Eq. (1.96), and a small perturbation f_{sp} of order ρ_* to the equilibrium (where $\rho_* = \rho/R$ is the normalized reference Larmor radius, with R

the tokamak reference major radius and $\rho = \sqrt{2T/m}/\omega_c$ where m is the reference mass, ω_c is the reference cyclotron frequency, T is the reference temperature). We use gyro-center field aligned Hamada coordinates $(\mathbf{X}, v_{\parallel}, \mu)$, $\mathbf{X} = (\psi, s, \zeta)$ being the gyro-center position (with ψ, s and ζ respectively radial, field line and binormal coordinates), v_{\parallel} the parallel (to the magnetic field) velocity, and μ the magnetic moment $\mu = m_{sp}v_{\perp}^2/(2B)$ where v_{\perp} is the velocity component perpendicular to the equilibrium magnetic field. We choose the Maxwell distribution F_M as the reference distribution in the definition of the entropy to make the maximum entropy state correspond to the physical equilibrium distribution (ϵ_{sp} has a maximum when $f_{sp} = 0$). It is important to stress again that in contrast to [46] here the integral is performed over the phase space excluding the radial coordinate ψ in order to explicitly keep track of the radial dependence of the perturbations.

We make a Taylor expansion of Eq. (3.2) to the second order in ρ_* then the following approximation holds

$$\epsilon_{sp} \approx - \int dx dv \left(f_{sp} + \frac{f_{sp}^2}{2F_M} \right), \quad (3.3)$$

note that the first term does not vanish in this case since the integral is not performed over the entire phase space. We build the equation which describes the time evolution of ϵ_{sp} using the gyro-kinetic equation given in Eq. (1.97), considering the case of a plasma as described at the beginning of this section. The time derivative of the first term in Eq. (3.3) simply gives

$$\frac{\partial n_{sp}}{\partial t} + \frac{\partial \Gamma_{n_{sp}}}{\partial \psi} = 0, \quad (3.4)$$

i.e. the continuity equation for the mass density, here ψ is the radial coordinate, t is the time $n_{sp} = \int dx dv f_{sp}$ is the radially dependent perturbed particle density of the sp -species and $\Gamma_{n_{sp}}$ its relative radial flux given by

$$\Gamma_{n_{sp}} = \int dx dv \left[\left(f_{sp} + \frac{Z_{sp}}{T_{sp}} F_M \chi \right) v_D^{\psi} + f_{sp} v_E^{\psi} \right], \quad (3.5)$$

where Z_{sp} and T_{sp} are respectively the electric charge and the temperature of the sp -species, $\chi = G(\phi)$ is the gyro-averaged perturbed electrostatic potential (G is the gyro-average operator and ϕ the perturbed electrostatic potential), v_E^{ψ} is the radial component of the perturbed gyro-averaged $\mathbf{E} \times \mathbf{B}$ velocity and v_D^{ψ} is the radial component of the drift velocity. The time derivative of the second term in Eq. (3.3) can be rewritten in the form

$$\int dx dv \frac{\partial}{\partial t} \left(\frac{f_{sp}^2}{2F_M} \right) = \int dx dv \left(\frac{f_{sp}}{F_M} \frac{\partial f_{sp}}{\partial t} \right), \quad (3.6)$$

therefore we find

$$\begin{aligned}
& \int dx dv \left[\frac{\partial}{\partial t} \left(\frac{f_{sp}^2}{2F_M} \right) + \frac{Z_{sp}}{T_{sp}} \chi \frac{\partial f_{sp}}{\partial t} \right] = \\
& = - \int dx dv \frac{\partial}{\partial \psi} \left[\left(\frac{f_{sp}^2}{2F_M} + \frac{Z_{sp}}{T_{sp}} \chi f_{sp} \right) v_E^\psi \right. \\
& \quad \left. + \left(\frac{f_{sp}^2}{2F_M} + \frac{Z_{sp}^2}{2T_{sp}^2} F_M \chi^2 \right) v_D^\psi \right] \\
& \quad + \int dx \left[\left(\frac{1}{L_n} - \frac{3}{2} \frac{1}{L_T} \right) J_{sp} + \frac{1}{L_T} K_{sp} \right] ,
\end{aligned} \tag{3.7}$$

where $1/L_n$ and $1/L_T$ are the inverse density and temperature background gradient lengths, J_{sp} and K_{sp} are given by

$$\begin{aligned}
J_{sp} &= \int dv \left[h_{sp} \left(v_D^\psi + v_E^\psi \right) \right] \\
K_{sp} &= \int dv \left[\frac{m_{sp} v^2}{2} h_{sp} \left(v_D^\psi + v_E^\psi \right) \right] ,
\end{aligned} \tag{3.8}$$

where $h_{sp} = f_{sp} + (Z_{sp}/T_{sp})\chi F_M$ is the sp -species non-adiabatic gyro-center response, m_{sp} the mass of the sp -species and $v^2 = v_{\parallel}^2 + v_{\perp}^2$ with v_{\parallel} and v_{\perp} velocity space coordinates as defined at the beginning of this section.

Eq. (3.7) does not quite show the features of a proper conservation equation in the form of Eq. (3.1), the problem is clearly the second term in the first line which requires particular attention. In the following we discuss how to deal with it. When integrating over the entire phase space a proper scalar product between functions of the gyro-center coordinates can be defined, therefore the following relation holds exactly

$$\int d\psi dx dv [G(s)t] = \int d\psi dx dv [sG(t)] , \tag{3.9}$$

where s and t are any functions of the gyro-center coordinates and the hermiticity of the gyro-average operator $G = G^\dagger$ (with G^\dagger adjoint gyro-average operator) has been used because of the local limit approximation (this identity is the analogous to Eq. (28) in [46]). In our case Eq. (3.9) can not be directly applied since the integration over the radial coordinate is not performed, but using periodic boundary conditions we can write

$$\int dx dv [G(s)t] = \int dx dv [sG(t)] + \frac{\partial}{\partial \psi} (\Gamma_{GA}) , \tag{3.10}$$

with Γ_{GA} a periodic function of the radial coordinate only; its physical meaning will be soon clarified.

We now manipulate the second term in the first line of Eq. (3.7) according to Eq. (3.10), then we use the quasineutrality condition, Eq. (1.101), written in the form

$$\sum_{sp} \int dv \left[Z_{sp} G(f_{sp}) + \frac{Z_{sp}^2 F_M}{T_{sp}} (G(\chi) - \phi) \right] = 0, \quad (3.11)$$

and combining eqs. (3.5) and (3.7) we can write

$$\frac{\partial}{\partial t}(\epsilon + w) + \frac{\partial}{\partial \psi}(\Gamma + \Gamma_{GA}) + C = 0, \quad (3.12)$$

where we have defined

$$\begin{aligned} \epsilon &= \sum_{sp} \epsilon_{sp} \\ w &= \sum_{sp} w_{sp} = \sum_{sp} \int dx dv \frac{Z_{sp}^2 F_M}{2T_{sp}^2} (\chi^2 - \phi^2) \\ \Gamma &= - \sum_{sp} \left\{ \Gamma_{n_{sp}} + \int dx dv \left[\left(\frac{f_{sp}^2}{2F_M} + \frac{Z_{sp}}{T_{sp}} \chi f_{sp} \right) v_E^\psi \right. \right. \\ &\quad \left. \left. + \left(\frac{f_{sp}^2}{2F_M} + \frac{Z_{sp}^2}{2T_{sp}^2} F_M \chi^2 \right) v_D^\psi \right] \right\} \\ C &= \sum_{sp} \int dx \left[\left(\frac{1}{L_n} - \frac{3}{2} \frac{1}{L_T} \right) J_{sp} + \frac{1}{L_T} K_{sp} \right], \end{aligned} \quad (3.13)$$

while Γ_{GA} is the term arising from leaving out the integration over ψ when performing the operation in Eq. (3.10) with the gyro-average operator. It is interesting to notice that because of Eq. (3.11) it is not possible to write a conservation equation for the entropy of one species ($\epsilon_{sp} + w_{sp}$). The conserved quantity is the entropy of the whole system.

Since Eq. (3.12) appears in the proper form of a conservation equation we can read out of it the physical meaning of each single term: $\epsilon + w$ is the radially dependent entropy of the system, with ϵ entropy in the particles and w the contribution of the electrostatic field to the entropy of the system; $\Gamma + \Gamma_{GA}$ is the radial flux of entropy, this means that the physical effect of Eq. (3.10) is giving rise to an additional contribution to the radial flux, the last term C represents sources and sinks as fluxes in the background gradients.

The contribution of Γ_{GA} can be shown to be of higher order in the Larmor radius compared to Γ as follows: by approximating the gyro-average operator as

$$G \approx 1 - \frac{1}{4} \rho_*^2 \Delta, \quad (3.14)$$

where Δ is the normalized Laplacian operator, and applying for each species the gyrokinetic ordering

$$\frac{f_{sp}}{F_M} \approx \frac{Z_{sp}\phi}{T_{sp}} \approx \rho_* , \quad (3.15)$$

it is straightforward to show that

$$\Gamma_{GA} \approx \rho_* \Gamma . \quad (3.16)$$

We can therefore neglect the contribution of Γ_{GA} to the total flux of entropy. Furthermore our purpose is to find a balance equation whose form can be directly related to Eq. (3.1) in the context of gyro-kinetic theory, thus we quantitatively miss a small part of the radial flux but it does not qualitatively destroy the form of the balance equation.

From now on, for simplicity in the notation, we omit the sum over the species and we get rid of the sp -index, however each quantity in the equations has to be understood as related to a particular species and the physical equations are obtained performing the sum over all species in the system.

We consider Eq. (3.12) and subtract from it the continuity equation for the mass density (3.5), neglecting the contribution of Γ_{GA} we are left with a conservation equation of the form

$$\frac{\partial I}{\partial t} + \frac{\partial \Gamma_I}{\partial \psi} = C , \quad (3.17)$$

for the quantity

$$I = \int dx dv \left[\frac{f^2}{2F_M} + \frac{Z^2 F_M}{2T^2} (\phi^2 - \chi^2) \right] , \quad (3.18)$$

where Γ_I is given by

$$\Gamma_I = \int dx dv \left[\left(\frac{f^2}{2F_M} + \frac{Z}{T} \chi f \right) v_E^\psi + \left(\frac{f^2}{2F_M} + \frac{Z^2}{2T^2} F_M \chi^2 \right) v_D^\psi \right] , \quad (3.19)$$

and C given in Eq. (3.13). It is clear that Eq. (3.17) has the same form as Eq. (3.1), i.e. term by term starting from the left we have the time derivative of I , the radial derivative of its radial flux and the source terms. Furthermore, the quantity in Eq. (4.3) is quadratic in the perturbation. For these reasons we choose I as definition for the intensity of the turbulence.

Although the intensity I satisfies a conservation equation, it still contains both zonal ($n = 0$) and non-zonal contributions. The intensity I does not provide a meaningful definition of the turbulence intensity simply because it does not depend on turbulent fluctuations only. The entropy depends on

the temperature, and the intensity I is, therefore, affected by the evolution of the temperature profile, preventing the separation of turbulence intensity and temperature profile evolution. In order to describe the turbulence intensity in terms of fluctuating quantities only, the possibility of separating the evolution of the zonal and the non-zonal part of I is investigated. Surprisingly, it turns out that it is possible to split the evolution equation of I into two separate conservation equations, one describing the dynamics of the zonal part, and one describing the non-zonal part. Below this splitting is discussed in detail.

The binormal coordinate ζ is an ignorable coordinate, therefore it can be treated spectrally. Using the Parseval's theorem the integral over ζ can be replaced by a sum over the toroidal modes (n), then the definition of the turbulence intensity given in Eq. (4.3) is

$$I = \int d\sigma \sum_n \left[\frac{|f_n|^2}{2F_M} + \frac{Z^2 F_M}{2T^2} (|\phi_n|^2 - |\chi_n|^2) \right], \quad (3.20)$$

where the sum runs over all integers $n \in (-\infty, +\infty)$, $d\sigma = 2\pi(B/m_{sp})Jdsdv_{\parallel}d\mu$ is a short-hand notation for the reduced infinitesimal volume of integration and all quantities with the subscript 'n' are defined by their Fourier transform in the binormal direction, i.e. for a generic function t of the coordinates we have

$$t(\psi, \zeta, s) = \sum_n t_n(\psi, s) e^{ik_n \zeta} \quad k_n = \frac{2\pi n}{L_\zeta}, \quad (3.21)$$

with L_ζ length of the ζ domain in real space, then the quantity $|t_n|^2 = t_n t_n^*$ is the square modulus of the complex Fourier amplitude t_n with the star indicating the complex conjugate.

We split the case of the zonal modes and all other perturbations writing the turbulence intensity in the form $I = I_{ZM} + I_P$ with

$$\begin{aligned} I_{ZM} &= \int d\sigma \left[\frac{|f_0|^2}{2F_M} + \frac{Z^2 F_M}{2T^2} (|\phi_0|^2 - |\chi_0|^2) \right] \\ I_P &= \int d\sigma \sum_{n \neq 0} \left[\frac{|f_n|^2}{2F_M} + \frac{Z^2 F_M}{2T^2} (|\phi_n|^2 - |\chi_n|^2) \right]. \end{aligned} \quad (3.22)$$

The turbulence intensity flux Γ_I can be written in the spectral representation for ζ using the Parseval's theorem together with the convolution theorem, we obtain

$$\begin{aligned} \Gamma_I &= \int d\sigma \sum_{n,m} \left[\left(\frac{f_m}{2F_M} + \frac{Z}{T} \chi_m \right) f_{n-m} \alpha_n^* \right. \\ &\quad \left. + \left(\frac{|f_n|^2}{2F_M} + \frac{Z^2}{2T^2} F_M |\chi_n|^2 \right) v_D^\psi \right], \end{aligned} \quad (3.23)$$

where we have renamed the Fourier transform in the binormal direction of the $\mathbf{E} \times \mathbf{B}$ velocity as $\alpha_n = (v_E^\psi)_n$ in order to lighten the notation. Unrolling now the sums over n and m in Eq. (3.23) and using the identities

$$\alpha_0 = 0 \quad \int d\sigma \sum_n \chi_n \alpha_n^* = 0, \quad (3.24)$$

which hold due to the fact that $\alpha_n \propto ik_n \chi_n$, one can see that the flux Γ_I can be split similarly to the turbulence intensity in the form $\Gamma_I = \Gamma_{I_{ZM}} + \Gamma_{I_P}$ where

$$\begin{aligned} \Gamma_{I_{ZM}} &= \int d\sigma \left[\sum_n \left(\frac{h_0}{F_M} f_n \alpha_n^* \right) \right. \\ &\quad \left. + \left(\frac{|f_0|^2}{2F_M} + \frac{Z^2}{2T^2} F_M |\chi_0|^2 \right) v_D^\psi \right] \\ \Gamma_{I_P} &= \int d\sigma \sum_{m \neq 0} \left\{ \sum_{n \neq m} \left[\left(\frac{f_m}{2F_M} + \frac{Z}{T} \chi_m \right) f_{n-m} \alpha_n^* \right] \right. \\ &\quad \left. + \left(\frac{|f_m|^2}{2F_M} + \frac{Z^2}{2T^2} F_M |\chi_m|^2 \right) v_D^\psi \right\}, \end{aligned} \quad (3.25)$$

where $h_0 = f_0 + (Z/T)\chi_0 F_M$ is the zonal modes component of the non-adiabatic gyro-center response.

Eq. (3.25) can be considered the main result of this work, in fact it is shown for the first time that the turbulence intensity flux can be split in two terms, one of which (the second one) does not contain any contribution from the zonal modes.

The physical meaning of this property can be understood as follow: considering the relation

$$\int dx dv \left(\frac{f_0}{F_M} \frac{\partial f}{\partial t} \right) = \int d\sigma \frac{\partial}{\partial t} \left(\frac{f_0^2}{2F_M} \right), \quad (3.26)$$

it is clear that multiplying the gyro-kinetic equation by f_0/F_M and integrating over the entire phase space apart from the radial direction, one can find a separate conservation equation for the intensity in the zonal modes I_{ZM} . In fact, applying this procedure we obtain

$$\frac{\partial I_{ZM}}{\partial t} + \frac{\partial \Gamma_{I_{ZM}}}{\partial \psi} = C_{ZM}, \quad (3.27)$$

where C_{ZM} is a source term written as

$$\begin{aligned} C_{ZM} &= \int d\sigma \left[\frac{1}{F_M} \frac{\partial h_0}{\partial \psi} \sum_n (f_n \alpha_n^*) \right. \\ &\quad \left. + \left(\frac{1}{L_n} - \frac{3}{2} \frac{1}{L_T} + \frac{mv^2}{2} \frac{1}{L_T} \right) h_0 v_D^\psi \right], \end{aligned} \quad (3.28)$$

i.e. it is given by the flux in the gradient of the zonal perturbation plus a part arising from the drift term. It provides the source for the zonal turbulence intensity.

It is remarkable that the first term in Eq. (3.25) is exactly the turbulence intensity flux connected with the zonal modes, i.e. Eq. (3.27) shows that the zonal modes give a specific separate contribution to the turbulence intensity flux. Therefore we can now subtract Eq. (3.27) from Eq. (3.17) and obtain a conservation equation for the turbulence intensity in the perturbations I_P , i.e.

$$\frac{\partial I_P}{\partial t} + \frac{\partial \Gamma_{I_P}}{\partial \psi} = C - C_{ZM} . \quad (3.29)$$

This equation shows that the zonal modes enter the equation for I_P only as a modification of the source term: C_{ZM} can be interpreted as a correction to the source term of Eq. (3.17) which together with the flux in the background gradient provides the total source for the non-zonal turbulence intensity.

3.3 Conclusion

We have shown that starting from the conservation equation for the entropy, it is possible to write two separate conservation equations: Eq. (3.27) describes the evolution of the turbulence intensity in the zonal modes (I_{ZM}) and Eq. (3.29) the turbulence intensity in all the other perturbations (I_P). The turbulence flux connected to I_P , as shown in Eq. (3.25), does not receive any contribution from the zonal modes. Eq. (3.29) shows that the zonal modes contribute to the conservation equation for I_P as a correction to the source term given by the flux in the gradient of the zonal perturbation.

The turbulence flux non linearity due to the $\mathbf{E} \times \mathbf{B}$ velocity is found to be cubic in the perturbation amplitude while the one in the drift velocity is quadratic. Many works in the literature are based on the assumption that the turbulence flux can be expressed as a quadratic non linearity in turbulence intensity (therefore 4th order, or quartic, in field amplitude), leading to Eq. (3.1), or similar formulations. The reason is that many authors use a closure scheme. In fact this leads to an approximate expression for the turbulence flux, whereas the conservation equation derived above is exact.

This treatment gives an operative tool to actually measure the flux of turbulence in gyro-kinetic numerical calculations and can therefore be used to quantitatively study the problem of the radial propagation of turbulence in tokamak plasmas.

Chapter 4

Turbulence spreading in gyro-kinetic theory

Turbulence spreading has been proposed as the mechanism responsible for the transition from Bohm to gyro-Bohm scaling of the heat conductivity observed in gyro-kinetic simulations. In this chapter a new operative definition for the turbulence intensity is given. In contrast to previous definitions the new definition satisfies a Fisher-Kolmogorov-Petrovskii-Piskunov (FK) type equation. Furthermore, explicit expressions for the turbulence intensity and the turbulence intensity flux, that allow direct numerical evaluation, are derived. A carefully designed numerical experiment for the case of a tokamak is performed. The effective turbulence diffusion coefficient is measured to be smaller than the heat conduction coefficient and the turbulence spreading length is found to be of the order of the turbulence correlation length. The results show that turbulence spreading can play a role in the non-local flux gradient relation, or in the scaling of transport coefficients with the normalized Larmor radius, only over length scale of the order of the turbulence correlation length. The chapter then discusses the turbulence convection through the drift connected with the magnetic field inhomogeneities. The convective flux integrates to zero under the flux surface average unless there is an up-down asymmetry in the turbulence intensity. The latter asymmetry can be generated through a radial inhomogeneity or plasma rotation. It is shown that the turbulence convection can lead to a spreading of the order of the correlation length under some circumstances.

4.1 Introduction

A detailed description of anomalous transport in magnetically confined plasmas is essential for the development of nuclear fusion devices. A fundamental issue is the scaling of turbulent transport with respect to the size of the reactor. In this regard it is important to understand to what extent

the transport is determined by non-local effects. Here and throughout the rest of this chapter non-local refers to situations in which the fluxes do not depend just on the local gradients.

In [47] transport scaling with respect to device size is examined using particles simulations for electrostatic toroidal ion temperature gradient (ITG) driven turbulence [34]. It is shown that the local ion heat conductivity (χ) exhibits Bohm-like scaling (χ is proportional to the Bohm diffusion coefficient χ_B) in the case of nowadays tokamak size (in agreement with the results of experiments performed on DIII-D reported in [48]), while a gradual transition to gyro-Bohm scaling (χ is proportional to $\chi_{GB} = \rho_* \chi_B$, where $\rho_* = \rho/R$ is the ion Larmor radius normalized by the tokamak major radius, the ion Larmor radius been given by $\rho = \sqrt{2T/m}/\omega_c$ where m is the ion mass, ω_c is the ion cyclotron frequency, T is the ion temperature) is predicted as the device size is increased. The authors interpret this behaviour using the physics mechanism discussed in [49] as a consequence of non-local effects. Turbulence spreading, i.e. the turbulent transport of turbulent fluctuations, is then proposed as a plausible non-local mechanism responsible for this size scaling transition.

The connection between non-locality and turbulence spreading can be understood as follow: because turbulent eddies driven by a gradient in density or temperature at a particular location can be transported and generate a particle or heat flux at a different location, turbulence spreading introduces a non-locality in the flux gradient relations.

The question of non-locality of turbulence through turbulence spreading has been firstly addressed in [30], where a fluid model is used to show that mode coupling provides an efficient mechanism for the radial propagation of turbulence in tokamaks. During the last decade, turbulence spreading has been analytically described [31, 35, 36] applying an ad hoc conservation equation for the evolution of the local intensity of the turbulence I , defined as the squared modulus of the electrostatic potential $I \propto |\phi|^2$, given in the form of a Fisher-Kolmogorov (FK) equation [32, 33] with inhomogeneous diffusion coefficient, i.e.

$$\frac{\partial I}{\partial t} - \frac{\partial}{\partial \psi} \left[D \frac{\partial I}{\partial \psi} \right] = \gamma I - k_{\perp}^2 I^2, \quad (4.1)$$

where the diffusion coefficient (D) is assumed to be proportional to the intensity itself (i.e. $D = D_0 I$) and the typical growth rate for the intensity (γ) as well as the dissipation coefficient (k_{\perp}^2) are taken to be constants, t is the time and ψ the radial coordinate.

Although physically motivated, the FK equation proposed to describe turbulence spreading is not derived from first principles in gyro-kinetic theory. Indeed, $I \propto |\phi|^2$ can be shown not to satisfy a conservation equation of the form given by Eq. (4.1). No explicit expression for the transport flux of turbulence (given by $D(\partial I/\partial \psi)$ in the equation above) exists, and this flux

can therefore not be directly calculated in numerical simulations of plasma turbulence. Another point of concern is that there is no clear separation between the zonal mode and the small scale turbulence.

In the absence of an explicit expression for the turbulent flux, numerical experiments have focussed on the spreading of turbulence into a stable region, i.e. a region for which $\gamma \leq 0$. The intensity $I \propto |\phi|^2$ then decays with a typical length scale $\lambda = \sqrt{k_{\perp}^2/D_0}$, and this length scale can be measured directly. In [47, 50, 31] a typical length scale of $24\rho_s$ has been reported ($\rho = \sqrt{2}\rho_s$), while in [51] a somewhat smaller length of $10\rho_s$ (according to the authors: "possibly overestimated") is given. In this respect it has to be mentioned that turbulence spreading is difficult to measure, since it is difficult to separate its effect from the effect due to temperature profile evolution. They are interlinked because a convection of turbulence into a region with a different temperature gradient will always be accompanied by a modification of the temperature profile. This modification will then affect the turbulence intensity through a change in the local drive (γ), rather than through a non-local effect [38, 53]. In [47, 50, 31] the temperature profile evolution is not discussed. In [51], to prevent significant temperature profile evolution, the authors use a local heat source. The strength of the source is chosen to be sufficiently small such that it does not affect too much the turbulent state. Even in this case, as pointed out by the authors, the measurement is affected by observed small deviations from the original profile. The study of turbulence spreading is further complicated by the fact that the radial scale reported is not particularly large. In non-linear simulations the mode with the highest intensity is often found to have a poloidal wave vector $k_{\theta}\rho \approx 0.1 - 0.2$. This corresponds to an eddy size of $10 - 24\rho$ in the poloidal direction, i.e. the scale sizes involved in turbulence spreading are similar to those of the turbulence itself.

In this chapter we present a systematic analysis of turbulence spreading. A new definition of turbulence intensity related to the entropy is introduced that does satisfy a FK equation of the form of Eq. (4.1). The derived evolution equation contains an explicit expression for the turbulence intensity flux. A numerical experiment is then introduced in which the turbulence intensity flux is measured in a fully developed turbulent state, thereby determining the effective diffusion coefficient (D) for the first time. This diffusion coefficient is compared with the heat conduction coefficient. Furthermore, measuring the typical decay time (τ) of the turbulence, a scale length is obtained through $\lambda = \sqrt{2D\tau}$.

In contrast to the studies mentioned above, this treatment eliminates any spurious effects of profile relaxation and, therefore, allows a unambiguous determination of turbulence spreading. Furthermore, this new approach is more flexible and allows for the study of the influence of plasma parameters, and zonal flow dynamics on turbulence spreading. In essence we

perform a numerical experiment that contains enough physics to study the mechanisms at work. In addition, the turbulence convection through the drift connected with the magnetic field inhomogeneities is also discussed.

4.2 Analytical analysis of turbulence spreading

In the previous chapter, the balance equation for the turbulence intensity has been derived. Its generalization to a plasma with a background toroidal rotation is

$$\frac{\partial I}{\partial t} + \frac{\partial \Gamma_I}{\partial \psi} = C, \quad (4.2)$$

for the quantity

$$I = \int dx dv \left[\frac{f^2}{2F_M} + \frac{Z^2 F_M}{2T^2} (\phi^2 - \eta^2) \right], \quad (4.3)$$

with relative flux Γ_I given by

$$\Gamma_I = \int dx dv \left[\left(\frac{f^2}{2F_M} + \frac{Z}{T} \eta f \right) v_E^\psi + \left(\frac{f^2}{2F_M} + \frac{Z^2}{2T^2} F_M \eta^2 \right) v_D^\psi \right], \quad (4.4)$$

where $\eta = G(\phi)$ is the gyro-averaged electrostatic potential (in comparison to the previous chapter the symbol η has been introduced to avoid later confusion with the heat diffusion coefficient). v_E^ψ is the radial component of the perturbed $\mathbf{E} \times \mathbf{B}$ velocity, given in Eq. (1.90) and v_D^ψ is the radial component of the drift velocity, given in Eq. (1.91). The source term C is given by

$$C = \sum_{sp} \int dx \left[\left(\frac{1}{L_n} + \left(\mathcal{E}_\Omega - \frac{3}{2} \right) \frac{1}{L_T} \right) J_{sp} + \frac{1}{L_T} K_{sp} + \frac{m\Omega}{T} (R^2 - R_0^2) \nabla \omega_\phi J_{sp} + \nabla \omega_\phi \Pi_{sp} \right], \quad (4.5)$$

where $1/L_n$ and $1/L_T$ are the inverse density and temperature background gradient lengths. The quantities J_{sp} , K_{sp} and Π_{sp} are given by

$$\begin{aligned} J_{sp} &= \int dv \left[h_{sp} \left(v_D^\psi + v_E^\psi \right) \right] \\ K_{sp} &= \int dv \left[\frac{m_{sp} v^2}{2} h_{sp} \left(v_D^\psi + v_E^\psi \right) \right] \\ \Pi_{sp} &= \int dv \left[\frac{R B_t}{B} v_\parallel h_{sp} \left(v_D^\psi + v_E^\psi \right) \right], \end{aligned} \quad (4.6)$$

with $h_{sp} = f_{sp} + (Z_{sp}/T_{sp})\eta F_M$ the sp -species non-adiabatic gyro-center response, $v^2 = v_{\parallel}^2 + v_{\perp}^2$ with v_{\parallel} and v_{\perp} velocity space coordinates, and B_t is toroidal component of the magnetic field. The centrifugal energy \mathcal{E}_{Ω} is

$$\mathcal{E}_{\Omega} = Z\Phi - \frac{1}{2}m\Omega^2(R^2 - R_0^2) \quad (4.7)$$

where R_0 is the radius of the magnetic axis, Ω is the frame toroidal rotation frequency and Φ is the background centrifugal potential. The frequency ω_{ϕ} is the toroidal rotation frequency in the comoving frame (which is zero at the radial location considered), but has a finite radial gradient which enters the equations as $\nabla\omega_{\phi}$.

It is shown (see chapter 3 and [52]) that Eq. (4.2) can be split into a system of two separate conservation equations, one describing the dynamics of the zonal modes and one for the non-zonal modes, Eqs. (3.22)-(3.29). The splitting of the intensity into I_P and I_{ZM} is important since the toroidally symmetric $n = 0$ zonal mode can contain non fluctuating modifications to the equilibrium. This is, for instance, the case in the numerical experiment discussed in the next section. Therefore, the zonal contribution to the entropy is not necessarily related with the turbulence. It is, furthermore, noted that the physics of avalanches which is connected with profile effects will enter through the zonal mode. For these reasons the turbulence intensity is defined as I_P , i.e. the intensity in all but the zonal mode. The turbulent transport of turbulence is studied through a transport of the turbulence intensity I_P . Finally, we stress here, to avoid confusion, that zonal mode here refers to the zonal entropy, not to the more familiar zonal flow which is related with the electro-static potential only.

The $\mathbf{E} \times \mathbf{B}$ and drift velocity contributions to the fluxes can be treated separately, i.e. we can write

$$\begin{aligned} \Gamma_{ZM} &= \Gamma_{ZM,E \times B} + \Gamma_{ZM,drift} \\ \Gamma_P &= \Gamma_{P,E \times B} + \Gamma_{P,drift} \end{aligned} \quad (4.8)$$

with

$$\begin{aligned} \Gamma_{ZM,E \times B} &= \int d\sigma \sum_n \left(\frac{h_0}{F_M} f_n \alpha_n^* \right) \\ \Gamma_{ZM,drift} &= \int d\sigma \left(\frac{|f_0|^2}{2F_M} + \frac{Z^2}{2T^2} F_M |\eta_0|^2 \right) v_D^{\psi} \\ \Gamma_{P,E \times B} &= \int d\sigma \sum_{\substack{n \neq m \\ m \neq 0}} \left(\frac{f_m}{2F_M} + \frac{Z}{T} \eta_m \right) f_{n-m} \alpha_n^* \\ \Gamma_{P,drift} &= \int d\sigma \sum_{m \neq 0} \left(\frac{|f_m|^2}{2F_M} + \frac{Z^2}{2T^2} F_M |\eta_m|^2 \right) v_D^{\psi} . \end{aligned} \quad (4.9)$$

The $\mathbf{E} \times \mathbf{B}$ contribution to the flux of I_P ($\Gamma_{P,ExB}$) is the one of interest concerning the treatment of turbulence spreading, describing the transport of turbulence due to the fluctuating $\mathbf{E} \times \mathbf{B}$ velocity field. The flux connected with the drift is proportional to the product of the intensity and the drift velocity, it represents a convection of the intensity by the turbulence independent drift velocity. For an up-down symmetric equilibrium the radial component of the drift velocity is anti-symmetric with respect to reflection in the mid-plane. The flux surface average of the flux is then zero, provided the turbulence intensity is symmetric under reflection. The latter symmetry of the intensity is obtained in homogeneous flux tube simulations of up-down symmetric equilibria provided there is no plasma rotation [54, 55]

In the next section we show the results of a numerical experiment in which the turbulence intensity (3.22) and its relative flux (3.25) are measured. As a last remark we point out that in the numerics an additional dissipation damping term, which enters on the right hand side of the gyro-kinetic equation without changing the form of the balance equation (4.2), is added in order to stabilize the numerical scheme [46].

4.3 Turbulence spreading measurement

The aim of the experiment is to study the nature and the effect of turbulence spreading in a fully developed turbulent state in which an equilibrium with the zonal flows is achieved. In this section, two measurements are presented.

We perform the numerical calculations using the gyro-kinetic code GKW [4, 5, 6] with the radial direction described using finite differences, and the flux-tube approximation with radial periodic boundary conditions (see chapter 2 and [56] for linear benchmarks).

All simulations presented in this chapter use the following parameters: temperature gradient length $R/L_T = 9.0$, density gradient length $R/L_N = 2.2$, electron and ion temperature $T_e = T_i$, safety factor $q = 1.4$, magnetic shear $\hat{s} = 0.78$, and inverse aspect ratio $\epsilon = 0.19$. The box size in radial and binormal direction is indicated as (L_ψ, L_ζ) defined in units of the normalized ion Larmor radius, in particular we have $(L_\psi, L_\zeta)/\rho_* = (192, 192)$ with $N = 43$ toroidal modes and $0 \leq k_\zeta \rho_* \leq 1.37$. We use $n_\psi = L_\psi/\rho_*$ radial grid points, so that $\Delta\psi = \rho_*$. The resolution in the field-line direction is $n_s = 16$ grid points per poloidal turn. The velocity space grid is given by $n_{v_\parallel} = 32$ and $n_\mu = 8$.

The simulations use circular geometry, no collisions, no rotation and adiabatic electrons. We use the following normalizations: length is normalized to the tokamak major radius R , time is normalized to the ratio R/v_{th} , with v_{th} the ion thermal velocity.

The numerical experiment is specifically designed with the purpose of controlling the behaviour of the turbulence intensity and temperature pro-

file. A heating (cooling) source is used to introduce a small perturbation in the temperature and turbulence intensity. The induced perturbation is then the only radial inhomogeneity in the system, and provides a minimum model to study the effect of turbulence spreading. This choice has the advantage that no other radial inhomogeneities (profiles, geometry) interfere with the measurements.

We set up a simulation with all background parameters constant, and we introduce on the right hand side of the gyro-kinetic equation a radially dependent source of the form

$$S = S_0 \left[\left(\frac{v^2}{v_{th}^2} - \frac{3}{2} \right) F_M \right] \cos \left(\frac{2\pi}{L_\psi} \psi \right), \quad (4.10)$$

which enters as an additional source term in the right hand side of the balance equation of the zonal mode, without changing its form. The evolution equation of the turbulence intensity I_P is unchanged. The source controls the evolution of the temperature perturbation. It can be directly checked from its definition that the source S is built such that it does not act as a particle and momentum source, but only as a heat source.

The GKW code uses the δf -approximation (it neglects the parallel velocity non linearity, which is a valid assumption in the case of a flux-tube), therefore in our case care has to be taken in the choice of the source amplitude such that this approximation is not violated. In all simulations presented in this chapter it has been verified that the temperature perturbation connected with the source has the same amplitude as the temperature fluctuations due to the turbulence (for the particular set of plasma parameter chosen, this is the case for $S_0 \leq 0.1$), ensuring the validity of the δf -approximation.

We let the system evolve until it reaches a stationary state as it is shown in Fig. 4.1 by the radially integrated entropy balance and in Fig. 4.2 where the time evolution of the intensity in the perturbations and in the zonal modes (respectively I_P and I_{ZM} from Eq. (3.22)) is given. It is clear that the intensity I_{ZM} needs much more time than I_P to reach the stationary state.

The main interesting quantities are the temperature perturbation (δT), the zonal intensity (I_{ZM}) and the turbulent intensity (I_P). The equations for the time evolution of I_{ZM} and I_P have been given in the previous section. The δT time evolution is given by

$$\frac{3}{2} \frac{\partial(\delta T)}{\partial t} + \frac{\partial \Gamma_H}{\partial \psi} = \int d\sigma \left(\frac{1}{2} m v^2 S \right), \quad (4.11)$$

with δT and the resulting heat flux Γ_H , induced by the action of the background temperature gradient (R/L_T) and the heating source (S) that we

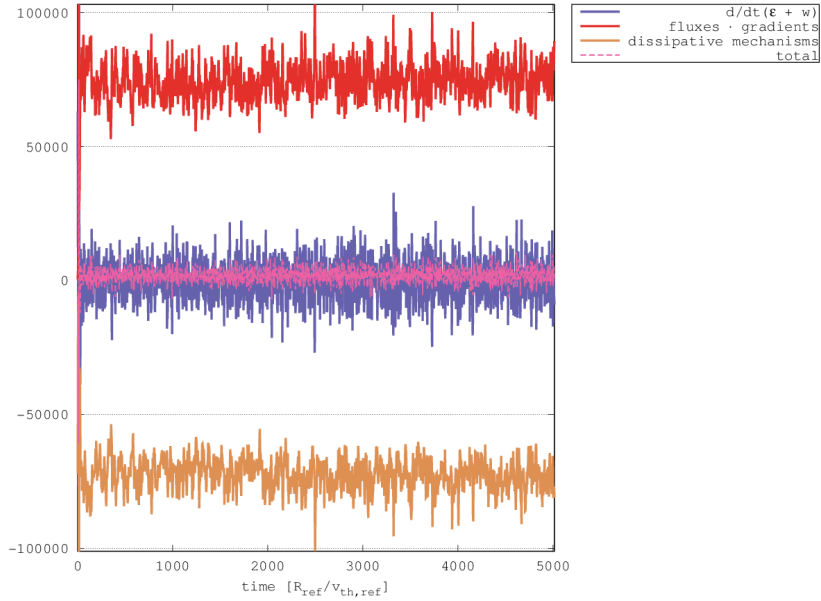


Figure 4.1: (Colour on-line) Entropy balance. The purple (time derivative of the total entropy), red (fluxes in the gradients, i.e. the source term) and orange (dissipation) lines sum up to zero to give the total (pink dashed line) balance.

have introduced, respectively given by

$$\begin{aligned}\delta T &= \frac{2}{3} \int d\sigma \left(\frac{1}{2} m v^2 f_0 \right) \\ \Gamma_H &= \int d\sigma \sum_{n=-N}^N \left[\frac{1}{2} m v^2 f_n \alpha_n^* \right],\end{aligned}\tag{4.12}$$

where all the quantities have already been defined.

In order to study the radial dependence of the quantities involved (turbulence intensity, temperature and relative fluxes) we calculate their radial profile by averaging over the stationary state time interval, i.e. we define for a general quantity F its time average as

$$\langle F \rangle = \frac{1}{t_f - t_i} \sum_{t=t_i}^{t_f} F_t,\tag{4.13}$$

where t_i and t_f are the instants which delimit the stationary state time interval (typically $t_i = 10^3$ and $t_f = 10^4 R/v_{th}$). In the following, we separately analyse the temperature perturbation (δT), the zonal intensity (I_{ZM}) and the turbulent intensity (I_P).

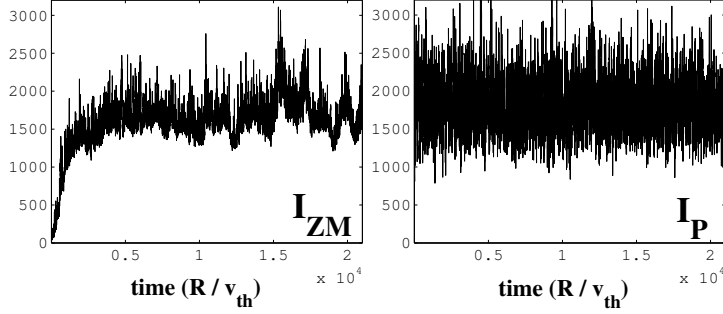


Figure 4.2: Time evolution of the zonal (I_{ZM}) and turbulence intensity (I_P).

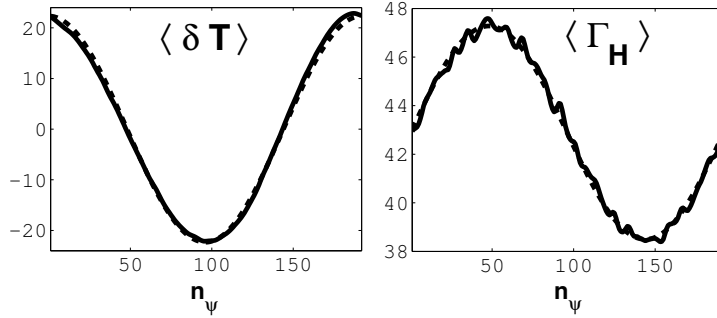


Figure 4.3: Radial profiles of the temperature perturbation (δT) and the heat flux (Γ_H) averaged over the stationary state time interval. The bold lines are the result of the numerical calculation, the dashed lines are given by the main Fourier components of the respective signal ($\langle \delta T \rangle$ has a dominant cosine component and $\langle \Gamma_H \rangle$ a dominant sine component).

Start with the temperature perturbation (δT). The time averaged radial profiles of δT and Γ_H are shown in Fig. 4.3. Then, it is clear that the dependence of $\langle \Gamma_H \rangle$ on the temperature gradient can be written as

$$\langle \Gamma_H \rangle \approx \chi_i \frac{R}{L_T} - \chi \frac{\partial \langle \delta T \rangle}{\partial \psi}, \quad (4.14)$$

where $\langle \Gamma_H \rangle$ is expressed as a Taylor expansion in the temperature gradient, with

$$\chi_i \approx 4.8 \quad \chi \approx 6.0 \quad (\rho^2 v_{th}/R). \quad (4.15)$$

The heat transport is therefore very well described as a diffusion process, driven by the temperature gradient.

Fig. 4.4 shows the time averaged radial profiles of the zonal intensity (I_{ZM}) and the $\mathbf{E} \times \mathbf{B}$ contribution to the zonal flux ($\Gamma_{ZM, E \times B}$). It follows that $\langle \Gamma_{ZM, E \times B} \rangle$ is not simply given by the gradient of $\langle I_{ZM} \rangle$.

In order to understand the zonal intensity behaviour, we notice that Eq. (4.12) and Eq. (3.22) show that δT is proportional to f_0 and I_{ZM} is proportional to f_0^2 (neglecting the field part, which is observed to be only

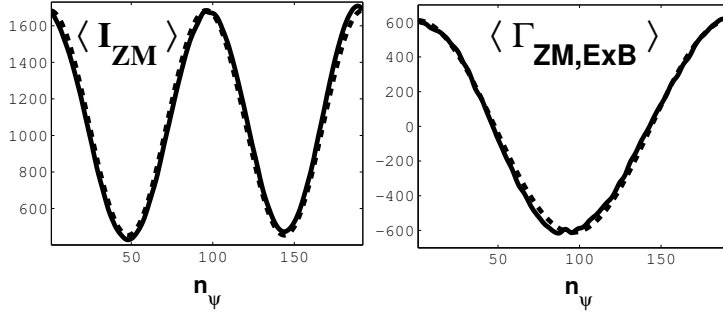


Figure 4.4: Radial profiles of the zonal intensity (I_{ZM}) and the $\mathbf{E} \times \mathbf{B}$ contribution to the zonal flux ($\Gamma_{ZM, E \times B}$) averaged over the stationary state time interval. The bold lines are the result of the numerical calculation, the dashed lines are given by the main Fourier components of the respective signal ($\langle I_{ZM} \rangle$ has a dominant double cosine component and $\langle \Gamma_{ZM, E \times B} \rangle$ a dominant cosine component).

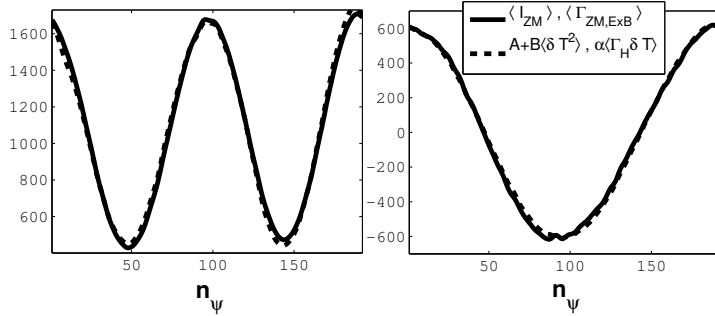


Figure 4.5: Left panel: Comparison between $\langle I_{ZM} \rangle$ (bold line) and $\langle \delta T^2 \rangle$ (dashed line) as stated in Eq. (4.16). Right panel: Comparison between $\langle \Gamma_{ZM} \rangle$ (bold line) and $\langle \Gamma_H \delta T \rangle$ (dashed line) as stated in Eq. (4.17) (in this case $A \approx 344$, $B \approx 2.5$ and $\alpha \approx 0.64$).

a small contribution as shown also in [46]). Therefore δT and I_{ZM} can be related as

$$I_{ZM} \approx (\delta T)^2 \quad \rightarrow \quad \frac{\partial I_{ZM}}{\partial t} \approx \delta T \frac{\partial(\delta T)}{\partial t} . \quad (4.16)$$

The evolution of the temperature perturbation is governed by Eq. (4.11), therefore substituting Eq. (4.11) in Eq. (4.16) one finds a relation of the form

$$\Gamma_{ZM, E \times B} \approx \delta T \Gamma_H . \quad (4.17)$$

The behaviour of the zonal intensity is therefore dominated by the temperature evolution: Fig. 4.5 shows the validity of Eq. (4.16) (left panel) and Eq. (4.17) (right panel). The factors of proportionality depend on the plasma parameters, indeed Eq. (4.16) is not an exact relation, but the qualitative behaviour is always reproduced in all cases that have been considered. We believe that this simple model contains the main physics ingredients to explain the zonal intensity evolution, i.e. I_{ZM} represents the temperature

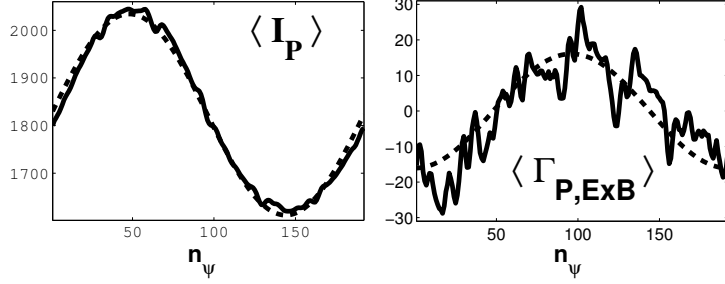


Figure 4.6: Radial profiles of the turbulent intensity (I_P) and the $\mathbf{E} \times \mathbf{B}$ contribution to the turbulent flux ($\Gamma_{P,ExB}$) averaged over the stationary state time interval. The bold lines are the result of the numerical calculation, the dashed lines are given by the main Fourier components of the respective signal ($\langle I_P \rangle$ has a dominant sine component, $\langle \Gamma_{P,ExB} \rangle$ has a dominant cosine component).

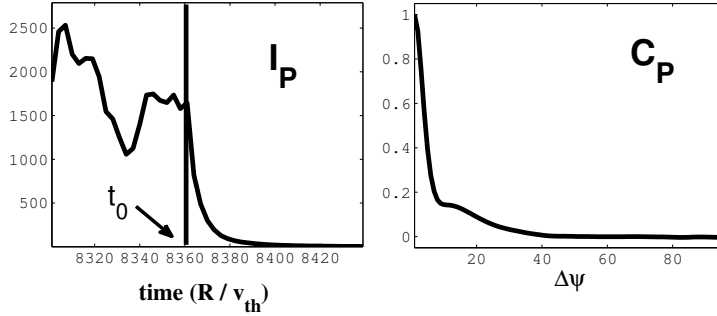


Figure 4.7: Left-panel: Time-decay of the turbulent intensity (I_P) after switching off temperature gradient and heating source ($t_0 = 8360$ is the instant at which I_P starts decaying). Right-panel: Turbulence radial correlation function as given in Eq. (4.22).

contribution to the entropy of the system and Eq (4.17) shows how the heat diffusion process contributes to the turbulence flux. Therefore the zonal intensity I_{ZM} is not the quantity of interest when measuring turbulence spreading. Furthermore, this observation shows the importance and the necessity of splitting the zonal and the turbulent modes dynamics to properly treat turbulence spreading.

Consider now Fig. 4.6. The time averaged radial profile of the turbulent intensity $\langle I_P \rangle$ shows a radial sine dependence, resembling the fact that turbulent modes are driven by the temperature gradient. The $\mathbf{E} \times \mathbf{B}$ contribution to the turbulent flux $\langle \Gamma_{P,ExB} \rangle$ shows a cosine dependence, therefore it can be described as a diffusion process in the form

$$\langle \Gamma_{P,ExB} \rangle \approx -D \frac{\partial \langle I_P \rangle}{\partial \psi} \quad \rightarrow \quad D = 2.2 \pm 0.8, \quad (4.18)$$

with the effective turbulence diffusion coefficient D expressed in unit of $\rho^2 v_{th}/R$. The error bar is obtained measuring D on different selections

of time intervals chosen within the stationary state time interval. Notice that $D < \chi$, meaning that the heat conduction process is faster than the turbulence spreading. The explicit dependence of D on $\langle I_P \rangle$ (i.e. $D = D_0 \langle I_P \rangle$) as stated in Eq. (4.1)), although consistent with the numerical results, can not be obtained due to the the signal to noise ratio. In order to estimate the turbulence spreading length, defined as $\lambda = \sqrt{2D\tau}$, one needs now to measure the turbulence life-time τ . Once the stationary state has been reached the system is let to evolve from that point by switching off temperature gradient and heating source, then τ is obtained from the measure of the time needed for the turbulence to decay. The left-panel of Fig 4.7 shows the time decay of I_P . Modeling the decay of I_P simply as

$$\frac{\partial I_P}{\partial t} \approx -\frac{I_P}{\tau} \quad \rightarrow \quad I_P \approx I_P(t_0) \exp\left(-\frac{t-t_0}{\tau}\right), \quad (4.19)$$

where the time t and the life-time τ are normalized with the ratio v_{th}/R and t_0 is the instant at which I_P starts decaying. The curve is fitted with the exponential given in Eq. (4.19). The normalized turbulence life-time numerical value is

$$\tau \approx 5.5 (R/v_{th}). \quad (4.20)$$

The turbulence spreading length is then

$$\lambda_{max} \approx 4.9\rho \approx 6.9\rho_s. \quad (4.21)$$

A comparison of λ with the correlation length of the turbulence is needed in order to determine to which extent turbulence spreading can affect non-local phenomena. The right-panel of Fig. 4.7 shows the correlation function of the gyro-averaged perturbed electrostatic potential excluding the zonal mode contribution, i.e.

$$C_P(\Delta\psi) = \frac{\int \eta_P(\psi, \zeta, s) \eta_P(\psi + \Delta\psi, \zeta, s) J d\psi ds d\zeta}{\int |\eta_P(\psi, \zeta, s)|^2 J d\psi ds d\zeta} \quad (4.22)$$

with η_P the perturbed electrostatic potential given by

$$\eta_P(\psi, \zeta, s) = \sum_{n \neq 0} \eta_n(\psi, s) e^{ik_n \zeta} \quad k_n = \frac{2\pi n}{L_\zeta}, \quad (4.23)$$

with L_ζ length of the ζ domain in real space, and $\Delta\psi$ is the radial distance at which the correlation function is evaluated. A decaying exponential fit of C_P gives the correlation length

$$C_P \approx \exp(-\Delta\psi/L_c) \quad \rightarrow \quad L_c \approx 4.2\rho \approx 6\rho_s. \quad (4.24)$$

Therefore the turbulence spreading length is estimated to be extrimely close to the turbulence correlation length.

4.4 Turbulence convection measurement

Below the drift contribution to the turbulence flux is analyzed in the case with the radially inhomogeneous heat source and in the case of a plasma with a background toroidal rotation.

4.4.1 Radially inhomogeneous heat source

Since the case of circular geometry is considered, the projection of the field lines on the poloidal plane are circles. The dependence of the radial component of the drift velocity on the poloidal angle is anti-symmetric in the poloidal angle θ

$$v_D^\psi(\theta) \propto \sin \theta . \quad (4.25)$$

and the flux surface average is

$$\{G\} = \oint ds G(s) = \oint (1 + \epsilon \cos \theta) G(\theta) d\theta \quad (4.26)$$

The drift contribution to the turbulence flux is given in Eq. (4.9) and it can be generally written in the form $\Gamma_{drift} = \int d\sigma (F v_D^\psi)$. It is then expected to be zero, since the functions

$$\begin{aligned} F_{ZM}(s) &= \int d\sigma' \left(\frac{|f_0|^2}{2F_M} + \frac{Z^2}{2T^2} F_M |\eta_0|^2 \right) \\ F_P(s) &= \int d\sigma' \sum_{m \neq 0} \left(\frac{|f_m|^2}{2F_M} + \frac{Z^2}{2T^2} F_M |\eta_m|^2 \right) \end{aligned} \quad (4.27)$$

are expected to be symmetric with respect to the s coordinate ($d\sigma' = 2\pi(B/m_{sp})Jd\psi dv_{\parallel} d\mu$). However, Fig. 4.8 shows a non zero contribution of the drift term to the turbulence flux. Therefore, the functions in Eq. (4.27) must have a non zero antisymmetric part along the s direction. Indeed, Fig. 4.9 shows that this is the case. It is noted that the anti-symmetric part is small compared with the symmetric part. We conclude that the drift contributes to the turbulence flux through a symmetry breaking mechanism, in particular a deviation from the up-down (in the poloidal plane) symmetry is observed.

For homogeneous turbulence in the up-down symmetric equilibrium used in this chapter, the turbulence intensity can be shown to be up-down symmetric when taking long time averages. The symmetry breaking is, therefore, connected with the radially inhomogeneous heat source that is applied in the simulations. One of the mechanisms that can break the symmetry is the radial gradient of the turbulence intensity. Assuming that the anti-symmetric part of the turbulence intensity is proportional to the radial gradient of the

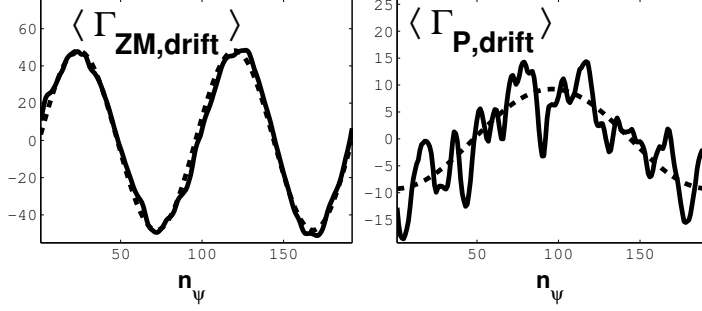


Figure 4.8: (Case with the radially inhomogenous heat source) Radial profiles of the drift contribution to the turbulence flux, zonal ($\Gamma_{ZM,drift}$) and turbulent ($\Gamma_{P,drift}$) part, averaged over the stationary state time interval. The bold lines are the result of the numerical calculation, the dashed lines are given by the main Fourier components of the respective signal ($\langle \Gamma_{ZM,drift} \rangle$ has a dominant double sine component, $\langle \Gamma_{P,drift} \rangle$ a dominant cosine component).

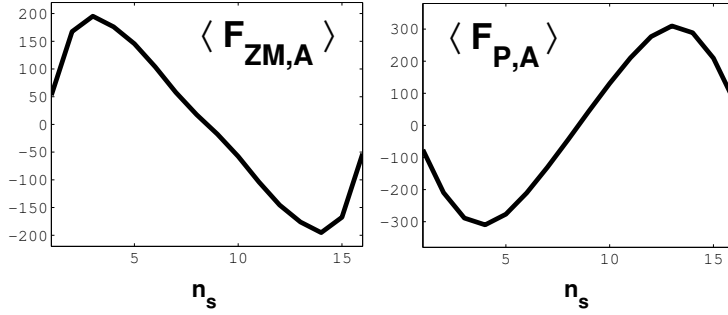


Figure 4.9: (Case with the radially inhomogenous heat source) Field line (s) profile of $\langle F_{ZM,A} \rangle$ and $\langle F_{P,A} \rangle$, i.e. respectively the antisymmetric part of the functions F_{ZM} and F_P given in Eq. (4.27), averaged over the stationary state time interval, showing a left-right asymmetry (up-down in the poloidal plane, the middle of the s domain corresponding to the low field side $\theta = 0$). It is noted that the anti-symmetric part is small compared with the symmetric part.

intensity one arrives at the following relations for the fluxes

$$\begin{aligned} \Gamma_{ZM,drift} &\approx -\gamma_{ZM} \frac{\partial \langle I_{ZM} \rangle}{\partial \psi} & \gamma_{ZM} &= 1.2 \pm 0.1 \\ \Gamma_{P,drift} &\approx -\gamma_P \frac{\partial \langle I_P \rangle}{\partial \psi} & \gamma_P &= 1.3 \pm 0.2, \end{aligned} \quad (4.28)$$

where γ_{ZM} and γ_P are determined from the numerical simulations. They have the dimension of a diffusion coefficient and are expressed in units of $\rho^2 v_{th}/R$. The values of the diffusion coefficients for the zonal mode and turbulence intensity are equal within the error bars. They have a sizeable magnitude but are smaller than the heat diffusion coefficient. Therefore, in this case the convection generates a flux proportional to the intensity

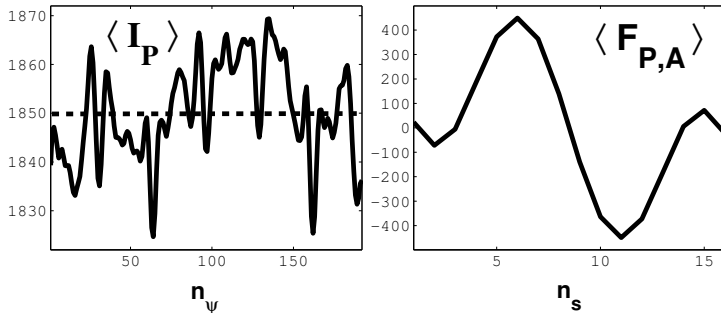


Figure 4.10: (Case with the background toroidal rotation) Left panel: Radial profile of turbulent intensity (I_P) averaged over the stationary state time interval. Right panel: Field line (s) profile of $\langle F_{P,A} \rangle$, i.e. the antisymmetric part of the function F_P given in Eq. (4.27), averaged over the stationary state time interval, showing a left-right asymmetry (up-down in the poloidal plane, the middle of the s domain corresponding to the low field side $\theta = 0$). It is noted that the anti-symmetric part is small compared with the symmetric part.

gradient and acts as a diffusion. A typical length (λ_{drift}) can be associated to this mechanism as

$$\lambda_{drift} = \sqrt{2\gamma P\tau} \approx 3.9\rho \approx 5.5\rho_s, \quad (4.29)$$

which is approximately equal to the correlation length.

As last remark, we point out that the results about the turbulence spreading mechanism are reproduced by all sets of plasma parameters investigated. The intensity flux generated by the fluctuating $E \times B$ velocity is effectively zero in all cases. On the other hand, the behaviour of the turbulence flux due to the drift is not observed to give a consistent picture for all simulations with some simulations being not fully understood, showing negative diffusion coefficient. The drift contribution to the flux is consistently observed to be related to the symmetry properties of the system, but the introduction of any kind of inhomogeneity can produce a symmetry breaking mechanism, which gives rise to a non zero flux. The impact of the inhomogeneity can depend on the particular choice of plasma parameters and influence the drift flux in different way. In the next paragraph, we present a further example which shows this mechanism at work.

4.4.2 Background toroidal rotation

In order to corroborate the hypothesis formulated in the previous paragraph, i.e. a non zero contribution of the drift to the turbulence flux is due to a symmetry breaking mechanism, we perform a second numerical experiment. We consider a radially homogenous plasma (no heating source), but we force an up-down asymmetry in the system, by introducing a background toroidal rotation. We choose the rotation velocity to be of magnitude equal to twenty percent of the sound speed.

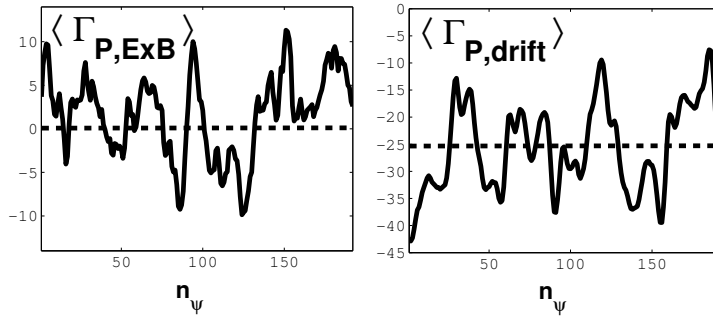


Figure 4.11: (Case with the background toroidal rotation) Radial profiles of the turbulent $E \times B$ (left panel) and drift (right panel) contribution to the turbulence flux averaged over the stationary state time interval. The bold lines are the result of the numerical calculation, the dashed lines indicate the mean values over the radial domain.

The numerical results concerning the turbulent intensity I_P are shown in Figs. 4.10 and 4.11. The turbulence is homogeneous over the radial domain, meaning that there is no intensity gradient in this case, and the only source of asymmetry in the system is the imposed background toroidal velocity. The system develops an up-down asymmetry, as shown by the the s profile of $F_{P,A}$, i.e. the antisymmetric part of the function F_P given in Eq. (4.27). The $E \times B$ term $\langle \Gamma_{P,E \times B} \rangle$ does not give a net contribution to the turbulence flux, it oscillates around zero. The drift term $\langle \Gamma_{P,drift} \rangle$ gives a net contribution to the turbulence flux, which can be modeled as a pinch effect in the form

$$\langle \Gamma_{P,drift} \rangle \approx v_p \langle I_P \rangle \quad v_p \approx -0.014, \quad (4.30)$$

with the pinch velocity v_p expressed in unit of $\rho v_{th}/R$.

We conclude that the nature of the turbulence flux is predominantly convective being connected with the drift contribution. The drift velocity contribution $\langle \Gamma_{P,drift} \rangle$ is different from zero because of the up-down symmetry breaking mechanism, due to the introduction of a non zero background toroidal velocity. In this case, the behaviour of the turbulence flux is a pinch effect, showing that the spreading of turbulence, in general, is not strictly diffusive.

4.5 Conclusion

The problem of turbulence spreading has been studied analytically and numerically in the framework of gyro-kinetic theory for a toroidal system. The main points can be summarized as follows:

1. The conservation equation for the radially dependent entropy in gyro-kinetic toroidal system is analytically derived for a collisionless plasma, with a background toroidal rotation, in the electrostatic limit, keeping

all background quantities constant throughout the perpendicular (to the magnetic field) domain (flux-tube approximation) and applying periodic radial boundary conditions. The properties of this equation lead to the definition of the turbulence intensity of the system and its conservation equation. The developed formalism contains explicit expressions for the turbulence intensity and turbulence flux. The turbulence flux consists of two parts: one due to the the $E \times B$ velocity, the other due to the drift velocity. The $E \times B$ velocity is considered the one connected to the turbulence spreading mechanism (transport of turbulence due to the fluctuating $E \times B$ velocity field). The drift contribution represents a convection of turbulence and is connected to the geometry of the system. The explicit expression for the turbulence flux allows to determine the turbulence diffusion coefficient directly through numerical simulation for the first time.

2. Numerical experiments are performed to study the physical nature and the effects of turbulence spreading in a fully developed turbulent state in which an equilibrium with the zonal flows is achieved. The first experiment is specifically designed with the purpose of controlling the behaviour of the temperature profile through the introduction of the radially inhomogeneous heating source into the gyro-kinetic equation. The model is build such that it contains the physics proposed in the literature to explain the turbulence spreading phenomena, i.e. although the simulations presented are performed in the flux-tube approximation, the introduction of the radially inhomogeneous heating source generates a small radial perturbation in the temperature and in the turbulence intensity such that a non-zero radial turbulence intensity gradient is present. The model contains therefore sufficient physics to determine the turbulence diffusion but, on the other hand, eliminates any spurious effects of profile and geometry inhomogeneity. The second experiment aims at the measurement of the turbulence flux in the case of a rotating plasma.
3. The heat flux is very well described as a diffusion process. The zonal intensity is totally dominated by the temperature perturbation. It represents the temprature contribution to the entropy of the system. The turbulent intensity is driven by the temperature gradient. The $E \times B$ and drift velocity contribution to the turbulence flux are separately analysed.

The $E \times B$ contribution to the turbulent intensity flux is measured. It is found that the turbulence spreading mechanism is well described as a diffusion process. The numerical experiments yield a turbulence spreading coefficient smaller than the heat conduction coefficient, and a turbulence spreading length of the order of the turbulence correlation

length. The results show that turbulence spreading can play a role in the non-local flux gradient relation, or in the scaling of transport coefficients with the normalized Larmor radius, only over length scale of the order of the turbulence correlation length.

The non zero drift velocity contribution to the turbulence flux is ascribed to a symmetry breaking mechanism due to the introduction of any inhomogeneities in the system.

In the case of the radially inhomogeneous heating source, where the symmetry is broken by the presence of a non zero radial turbulence intensity gradient, the observed phenomenon can be treated as a diffusion-like process. The diffusion coefficient turns out to be much smaller than the heat diffusion coefficient. This means that the temperature perturbation profile evolves considerably quicker than the turbulence intensity one. The typical length scale of this mechanism (over the time-decay of the turbulence) is found to be of the same magnitude of the correlation length of the turbulence.

Forcing an up-down asymmetry in the system through the introduction of a background toroidal rotation, the only non zero contribution to the turbulent flux is again given by the convective contribution to the turbulence flux. This fact corroborates the conjecture that the turbulent flux is generated through a symmetry breaking mechanism. In this case the flux of turbulence intensity is represented by a pinch velocity.

Chapter 5

Conclusion and outlook

In this thesis, physical phenomena connected with the global description of turbulence in tokamak plasma have been analysed. Quasi-local simulations of electrostatic Ion Temperature Gradient (ITG) modes instabilities, i.e. electrostatic microinstabilities driven in the plasma by the presence of an ion temperature gradient, have been performed. Quasi-local refers to the case in which background quantities are assumed constant throughout the simulation domain, but inhomogeneities in the profiles of the turbulent quantities are taken into account. The work consists of two main parts.

In the first part of the thesis (chapter 2), the electrostatic linear ITG modes growth rate (γ) spectrum is numerically calculated. It is observed that γ as a function of the poloidal wave vector (k_θ) is given by a double-humped curve. In particular unstable toroidal ITG modes with normalised poloidal wave vectors well above one ($k_\theta \rho_i > 1$) for standard tokamak parameters with adiabatic electron response are predicted. It is observed that these modes have a maximum amplitude at a poloidal angle θ that is shifted away from the low field side ($\theta \neq 0$). The physical mechanism responsible for this behaviour is clarified through the use of a fluid model. It is shown that the shift of the mode away from the low field side reduces the effective drift frequency which allows for the instability to develop. Numerical tests using the gyro-kinetic model confirm this physical mechanism. Furthermore it is shown that modes localized away from the low field side can be important also for $k_\theta \rho_i < 1$ close to the threshold of the ITG. In fact, modes with maximum amplitude at $\theta \neq 0$ can exist for normalised temperature gradient lengths below the threshold of the ITG obtained for the case with the maximum at $\theta = 0$.

The second part of the thesis (chapters 3 and 4) is dedicated to the study of Turbulence Spreading (TS), i.e. the turbulent transport of turbulence.

Gyro-kinetic simulations predict that, when increasing the size of the reactor, the heat conduction coefficient (χ) undergoes a scaling transition from Bohm ($\chi \propto \chi_B$, with χ_B the Bohm diffusion coefficient) to gyro-Bohm

($\chi \propto \rho_* \chi_B$, with ρ_* the normalized Larmor radius $\rho_* = \rho/R$ where ρ is the ion Larmor radius and R is the tokamak size). This transition is ascribed to non-local phenomena. Non-local refers to situations in which the fluxes do not depend just on the local gradients. TS has been proposed as the mechanism responsible for this transition. Up to now, TS has been analytically described applying an ad hoc conservation equation for the evolution of the local intensity of the turbulence, defined as the squared modulus of the electrostatic potential, given in the form of a Fisher-Kolmogorov (FK) equation with inhomogeneous diffusion coefficient. Although physically motivated, the FK equation proposed to describe TS is not derived from first principles. No explicit expression for the transport flux of turbulence exists, and this flux can therefore not be directly calculated in numerical simulations of plasma turbulence.

In chapter 3 a conservation equation is derived for the radially dependent entropy in toroidal geometry using the local approximation of the gyrokinetic equation. This naturally leads to an operative definition for the turbulence intensity. It is shown that the conservation equation can be split into two contributions, one describing the dynamics of the zonal modes ($n = 0$ toroidal) and one for the non-zonal modes ($n \neq 0$). Chapter 3 provides an operative tool for both analytic as well as numeric studies of the radial propagation of turbulence in tokamak plasmas. In contrast to previous definitions the new definition satisfies a FK type equation. Furthermore, explicit expressions for the turbulence intensity and the turbulence intensity flux, that allow direct numerical evaluation, are derived.

In chapter 4 the generalization to a plasma with a background toroidal rotation is presented. Then a carefully designed numerical experiment is used to determine the turbulence diffusion coefficient for the first time. This is found to be smaller than the heat conduction coefficient, and a spreading length of the order of the turbulence correlation length. The results show that turbulence spreading can play a role in the non-local flux gradient relation, or in the scaling of transport coefficients with the normalized Larmor radius, only over length scale of the order of the turbulence correlation length. The chapter then discusses the turbulence convection through the drift connected with the magnetic field inhomogeneities. The convective flux integrates to zero under the flux surface average unless there is an up-down (in the poloidal plane) asymmetry in the turbulence intensity. The latter asymmetry can be generated through a radial inhomogeneity or plasma rotation. It is shown that the turbulence convection can lead to a spreading of the order of the correlation length under some circumstances.

The main result of this thesis is that TS is an unrealistic candidate for the explanation of relevant (i.e. concerning distances much bigger than the turbulence correlation length) non-local phenomena, unlike previously suggested. Therefore any non-local effect must be due to other mechanisms. For example, a major role could be played by avalanches, appearing through

profile effects, which are therefore affected by the zonal modes dynamics (excluded in our numerical treatment). These could be studied in more detail. An interesting follow up project would be the investigation if the formalism developed in this thesis can be applied to the description of avalanches.

Although TS is found to be a small effect, the results presented suffer of the enormous computational cost needed, it is not unimportant to extend the study to different conditions (for example kinetic electrons, electromagnetic, collisional plasma).

The symmetry breaking process could be worked out in more details, investigating the possibility of constructing an analytic model of the convective flux of turbulence intensity (I) in the form of ∇I , which gives the diffusion equation. The analytic equation could be used to extrapolate the behaviour in the case of different plasma parameters. An expression for the diffusion coefficient would offer the possibility of comparison with gyrokinetic numerical calculations.

The extension of the theory to the full- f treatment, i.e. not employing the δf -approximation, and to the global case, i.e. dropping the constriction of periodic boundary conditions in the radial domain, would enable the application of our treatment to the most general cases.

Bibliography

- [1] D. Meade, Nucl. Fusion **50**, 014004 (2010)
- [2] W. Horton, Turbulent Transport in Magnetized Plasmas, World Scientific Publishing (2012)
- [3] K. Ida *et al.*, Nucl. Fusion **55**, 013022 (2015)
- [4] A.G. Peeters, Y. Camenen, F.J. Casson, W.A. Hornsby, A.P. Snodin, D. Strintzi and G. Szepesi, Comp. Phys. Comm. **180**, 2650 (2009)
- [5] A.G. Peeters, D. Strintzi, C. Angioni, et al., Phys. Plasmas **16**, 042310 (2009)
- [6] A.G. Peeters, D. Strintzi, Phys. Plasmas **11**, 3748 (2004)
- [7] J. Wesson, Tokamaks, Clarendon press (2004)
- [8] R.J. Goldston and P.H. Rutherford, Introduction to Plasma Physics, IOP Publishing (1995)
- [9] Y. Hu, Notes on tokamak equilibrium, Institute of Plasma Physics, Chinese Academy of Sciences (2015)
- [10] L. Lao *et al.*, Nucl. Fusion **25**, 1611 (1985)
- [11] F.J. Casson, PhD Thesis, University of Warwick (2011)
- [12] L.D. Landau and E.M. Lifshitz, Statistical Physics, Elsevier Ltd. (1980)
- [13] N.A. Krall and A.W. Trivelpiece, Principles of Plasma Physics, McGraw-Hill, Inc. (1973)
- [14] S. Brunner, Waves and Instabilities in Inhomogeneous Plasmas, CRPP-PPB, CH-1015 Lausanne, Switzerland
- [15] M. A. Beer, S. C. Cowley, and G. W. Hammett, Phys. Plasmas **2**, 2687 (1995)
- [16] A.G. Peeters, C. Angioni, D. Strintzi, Phys. Rev. Lett. **98**, 265003 (2007)

- [17] H. Lütjens, A. Bondeson and O. Sauter, *Comput. Phys. Commun.* **97**, 219 (1996)
- [18] A.M. Dimits, G. Bateman, M.A. Beer, B.I. Cohen, W. Dorland, G.W. Hammett, C. Kim, J.E. Kinsey, M. Kotschenreuther, A.H. Kritz, L.L. Lao, J. Mandrekas, W.M. Nevins, S.E. Parker, A.J. Redd, D.E. Shumaker, R. Sydora, J. Weiland, *Physics of Plasmas* **7**, 969 (2000)
- [19] A.I. Smolyakov, M. Yagi, and Y. Kishimoto, *Phys. Rev. Lett.* **89**, 125005 (2002)
- [20] A. Hirose, M. Elia, A.I. Smolyakov, and M. Yagi, *Phys. Plasmas* **9**, 1659 (2002)
- [21] Z. Gao, H. Sanuki, K. Itoh, and J.Q. Dong, *Phys. Plasmas* **10**, 2831 (2003)
- [22] Z. Gao, H. Sanuki, K. Itoh, and J.Q. Dong, *Phys. Plasmas* **12**, 022502 (2005)
- [23] J. Chowdhury, R. Ganesh, J. Vaclavik, S. Brunner, L. Villard, P. Angelino, *Phys. Plasmas* **16**, 082511 (2009)
- [24] J.W. Connor, R.J. Hastie, J.B. Taylor, *Phys. Rev. Lett.* **40**, 396 (1978)
- [25] R.E. Waltz, G.D. Kerbel, J. Milovich, *Phys. Plasmas* **1**, 2229 (1994)
- [26] X. Lapillone, S. Brunner, T. Dannert, S. Jolliet and A. Marinoni et al., *Physics of Plasmas* **16**, num. 3 (2009)
- [27] J. Chowdhury, S. Brunner, R. Ganesh, X. Lapillonne, L. Villard, and F. Jenko *Phys. Plasmas* **19**, 102508 (2012)
- [28] D. Told et al., *Phys. Plasmas* **15**, 102306 (2008)
- [29] A. Mishchenko, R. Hatzky and A. Koenies, *Theory of Fusion Plasmas, Joint Varenna-Lausanne International Workshop, AIP Conference Proceedings* **871**, 395 (2006)
- [30] X. Garbet, L. Laurent, A. Samain and J. Chinardet, *Nuclear Fusion* **34**, No. 7 (1994)
- [31] T.S. Hahm, P.H. Diamond, Z. Lin, K. Itoh and S-I. Itoh, *Plasma Phys. Control. Fusion* **46**, A323 (2004)
- [32] R.A Fisher, *Ann. Eugenics* **7**, 335 (1937)
- [33] A.N. Kolmogorov *et al*, *Bull. Univ. Moscow, Ser. Internat., Sect. A* **1**, 1 (1937)

- [34] W. Horton, Rev. Mod. Phys. **71**, 735 (1999)
- [35] Ö.D. Gürcan, P.H. Diamond, T.S. Hahm, and Z. Lin, Phys. Plasmas **12**, 032303 (2005)
- [36] Ö.D. Gürcan, P.H. Diamond, T.S. Hahm, Phys. Plasmas **13**, 052306 (2006)
- [37] R.E. Waltz, Phys. Plasmas **12**, 072303 (2005)
- [38] Z.H. Wang, P.H. Diamond, Ö.D. Gürcan, X. Garbet and X.G. Wang, Nucl. Fusion **51**, 073009 (2011)
- [39] Ö.D. Gürcan *et al*, Nucl. Fusion **53**, 073029 (2013)
- [40] A.H. Boozer, Phys. Fluids **B 4**, 2845 (1992)
- [41] J. A. Krommes and G. Hu, Phys. Fluids **B 5**, 3908 (1993)
- [42] J. A. Krommes and G. Hu, Physics of Plasmas **1**, 3211 (1994)
- [43] H. Sugama and W. Horton, Phys. Plasmas **4**, 405 (1997)
- [44] H. Sugama and W. Horton, Phys. Plasmas **5**, 2560 (1998)
- [45] T.H. Watanabe and H. Sugama, Nucl. Fusion **46**, 24 (2006)
- [46] J. Candy and R. E. Waltz, Phys. Plasmas **13**, 032310 (2006)
- [47] Z. Lin, S.Ethier, T. S. Hahm and W. M. Tang, Phys. Rev. Lett. **88**, 195004 (2002)
- [48] G. McKee *et al.*, Nucl. Fusion **41**, 1235 (2002)
- [49] X. Garbet and R. E. Waltz, Phys. Plasmas **3**, 1898 (1996)
- [50] Z. Lin, T.S. Hahm, Phys. Plasmas, **11**, 1099 (2004)
- [51] R.E. Waltz, Phys. Plasmas **12**, 072303 (2005)
- [52] P. Migliano *et al*, arXiv:1408.1345 [physics.plasm-ph], accepted for publication in PPCF (2015)
- [53] X. Garbet *et al*, Physics of Plasmas **14**, 122305 (2007)
- [54] A. G. Peeters, C. Angioni and the ASDEX Upgrade Team, Phys. Plasmas **12**, 072515 (2005)
- [55] F. I. Parra, M. Barnes and A. G. Peeters, Phys. Plasmas **18**, 062501 (2011)
- [56] P. Migliano, Y. Camenen, F.J. Casson, W.A. Hornsby and A.G. Peeters, Phys. Plasmas **20**, 022101 (2013)